Sede Amministrativa: Università degli Studi di Padova

Dipartimento di Ingegneria Civile, Edile e Ambientale

DOTTORATO DI RICERCA IN

SCIENZE DELL'INGEGNERIA CIVILE E AMBIENTALE

CICLO XXVI

Dispersion in Alluvial River

Direttore della scuola: Ch.mo Prof. Stefano Lanzoni

Supervisore: Ch.mo Prof. Stefano Lanzoni

Dottoranda: Amena Ferdousi

Gennaio 2014

Acknowledgments

I am heartily thankful to my supervisor, Prof. Stefano Lanzoni, who continuously guided me with his enthusiasm, his inspiration, time, ideas and his great effort to explain things clearly and simply. Throughout my thesis period, he provided encouragement, sound advice, good teaching, good company, and lots of good ideas.

I would like to thanks all my colleagues for theier heartiest assistance in all stage.

I owe my deepest gratitude to my husband for his sacrifice, encouragement and support.

Lastly, and most importantly, I wish to thank my parents. They raised me, supported me, taught me, and loved me. To them I dedicate this thesis.

Contents

Abstract

River pollution is the contamination of river water by pollutant being discharged directly or indirectly on it. Depending on the degree of pollutant concentration, subsequent negative environmental effects such as oxygen depletion and severe reductions in water quality may occur which affect the whole environment. River pollution can then cause a serious threat for fresh water and as well as the entire living creatures. Dispersion in natural stream is the ability of a stream to dilute soluble pollutants. Different types of pollution, such as accidental spill of toxic chemicals, industrial waste, intermittent discharge from combined sewer overflows and temperature variations produced by thermal outflows, may generate a cloud whose longitudinal spreading strongly affects the pollutant concentration dynamics. Pollutants discharging form a point source is easier to control where as pollutant discharging from non point sources are hardly controllable and may represent severe threat to the river ecosystem. The longitudinal dispersion coefficient is used to describe the change in characteristics of a solute cloud from an initial state of high concentration and low spatial variance to a downstream state of lower concentration and higher spatial variance. Therefore, in order to correctly estimate the degree of pollution within a stream and ensure an efficient and informed management of riverine environments, a reliable estimation of the dispersion within the stream is a crucial concern.

The objective of my research is to develop a mathematical model for determining

the dispersion in alluvial river. In order to achieve the goal, a model has been developed which provides an analytical relation for the prediction of the dispersion coefficient in natural streams, given the planimetric configuration of the river and the relevant hydrodynamic and morphodynamic parameters (i.e., width to depth ratio, the sediment grain size, scaled with the flow depth, the Shields stress).

One of the most striking features of alluvial rivers is their tendency to develop regular meandering plan forms. Their geometry is in fact characterized by a sequence of symmetrical curves which amplify over time due to erosion processes at the outer bank and deposition at the inner bank. This planimetric pattern affects both the hydrodynamics of the river and the distribution of bed elevations, as well as its hydraulic response, as the average bed slope is progressively reduced along with the flow cross sections. The flow filed that establishes in meandering rivers has clearly a great relevance on the behavior of the pollutant cloud and hence on the dispersion that drives its microscopic evolution.

To develop a dispersion coefficient predicting model, the analytical models of flow field establishing in the cross section of a straight river [Tubino ans Colombini, 1992] and of a meandering river [Frascati and Lanzoni, 2013] are developed. The two dimensional mass balance equation governing the dynamics of a pollutant is then solved using asymptotic expression and Morse and Feshbach [1953] formalism. Finally, using the two dimensional spatial distributions of the concentration, the flow depth and the velocity, the dispersion coefficient are obtained. For straight rivers the cross-sectional velocity and the theoretically predicted dispersion coefficients with the field data collected by Godfrey and Frederick (1970) in two rivers (Clinch River, Copper Creek). The comparison is reasonably good. The performance of the model is also tested with reference to the predictions provided by the model proposed by Deng (2001). The resultant model is found to give prediction closer to 80% of the experimental data, a much better performance agreement with respect to the model

of Deng (2001). The results of the model developed to estimate the dispersion coefficients in meandering river, have been compared with the experimental data available in experimental and referring to six different rivers. Also in this case the agreement between the dispersion coefficient predicted theoretically and those calculated on the basis of tracer tests is quite good and better than that ensured by the other theoretical and empirical predictors available in literature.

Sommario

Lo studio della dinamica di un inquinante convenzionale (e.g., BOD) all'interno di un corso d'acqua naturale richiede la conoscenza del campo di moto e della batimetria che si realizzano nel corso d'acqua stesso, delle modalità di immissione (continua o localizzata, accidentale o sistematica) e delle reazioni chimiche a cui l'inquinante è soggetto. L'obiettivo della presente tesi è quello di caratterizzare la distribuzione spazio-temporale della nuvola di inquinante, in modo da poter valutare i carichi inquinanti e controllare il soddisfacimento, o meno, dei requisiti di legge.

In particolare, l'attenzione è stata concentrata sul comportamento dell'inquinante nel cosiddetto campo lontano, ovvero a una distanza dalla sorgente tale per cui l'inquinante si è mescolato verticalmente e trasversalmente, distribuendosi quasi uniformemente sulla sezione. In tali condizioni, ai fini applicativi è sufficiente studiare il comportamento della concentrazione media sulla sezione. Tale comportamento è retto dalla classica equazione dell'avvezione-dispersione la cui soluzione, nel caso di immissione istantanea e localizzata di una determinata massa di sostanza inquinante e tratto di corso d'acqua omogeneo, è data dal classico andamento Gaussiano.

La stima del coefficiente di dispersione da utilizzare nella suddetta equazione risulta di fondamentale importanza per una corretta previsione del comportamento spazio-temporale dell'inquinante. La struttura di tale coefficiente, d'altra parte, è strettamente legata al campo di moto che si realizza in un alveo naturale e, in particolare, alle deviazioni rispetto ai valori medi sulla sezione della velocità e della

concentrazione.

Utilizzando le attuali conoscenza relative al campo di moto in alvei a fondo mobile, nella presente tesi viene derivata una soluzione analitica del coefficiente di dispersione dipendente da parametri in ingresso quali il rapporto larghezza-profondità desumibile dalla geometria della sezione, il diametro dei sedimenti, normalizzato con la profondità della corrente, la pendenza del corso d'acqua.

Il problema è inizialmente affrontato nel caso di alveo rettilineo e sezione in equilibrio con il trasporto in cui il fondo varia gradualmente in direzione trasversale. Risulta così possibile suddividere la generica sezione in una zona centrale, dove la profondità della corrente si mantiene approssimativamente costante, e due regioni di sponda, nelle quali la profondità si riduce gradualmente a zero. Il campo di moto calcolato tendendo conto di questa lenta variazione trasversale del fondo (che consente di semplificare opportunamente l'equazione della quantità di moto), raccordato con quello che si realizza nella regione centrale, unitamente all'equazione del bilancio di massa dell'inquinante, consentono di determinare analiticamente il coefficiente di dispersione.

Il passo successivo è stato quello di considerare in caso di alvei alluvionali ad andamento meandriforme. Si tratta di una tipologia di configurazione planimetrica molto comune in natura, caratterizzata da una sequenza più o meno regolare di curve alternate. Sfruttando il fatto che molto spesso la curvatura dell'asse del canale è debole, risulta possibile ottenere una soluzione analitica del campo di moto e della topografia del fondo. Tale soluzione, associata all'equazione del bilancio di massa dell'inquinante riscritta in coordinate curvilinee, opportunamente semplificata sfruttando l'ipotesi di deboli curvature, consente di determinare analiticamente il coefficiente di dispersione.

Le stime del coefficiente di dispersione ottenute nei casi di alveo rettilineo e ad andamento meandriforme, sono state infine confrontate con i dati di campo reperibili

in letteratura, ottenuti tramite campagne di misura con traccianti. Per entrambe le configurazioni planimetriche analizzate(rettilinea e meandriforme), l'accordo tra coefficienti osservati in campo e i risultati delle previsioni teoriche appare generalmente buono e, comunque, decisamente migliore di quello offerto dalle varie formulazioni semi-empiriche e teoriche attualmente disponibili in letteratura.

Chapter 1

Introduction

1.1   Motivation

River pollution is the contamination of river water by pollutant discharged directly or indirectly on it. River pollution is a serious problem for the entire riverine ecosystem. Depending on the degree of pollutant concentration, subsequent negative environmental effects such as oxygen depletion and severe reductions in water quality may occur, affecting fish, population and other species. Generally pollutants discharged form a point source are easier to control then diffused pollution which often causes a sever threat to the river ecosystem. Different types of pollution such as accidental spill of toxic chemicals, industrial waste, intermittent discharge from combined sewer overflows may generate a cloud whose longitudinal spreading strongly affects the pollutant concentration dynamics. The longitudinal dispersion coefficient is used to describe the change in characteristics of a solute cloud from an initial state of high concentration and low spatial variance to a downstream state of lower concentration and higher spatial variance. On the other hand within portable water network it is important to qualify the changing characteristics of solute as they travel the network [Hart et al., 2013].

Estimating accurate value of the longitudinal dispersion coefficient is required in several applied hydraulic problems such as environmental engineering, river engineering, intake design and risk assessment of injection of pollutant and contaminants into river stream [Seo and Baek, 2004].

The reliable estimation of longitudinal dispersion coefficient is important for devising water diversion strategies, designing treatment plants, intakes and outfalls, and studying environmental impact due to injection of polluting effluents into streams [Ho et al., 2002].

To forecast and control the solubility of any accidental spill in any river channel the longitudinal dispersion coefficient is the key coefficient.

Objective of this research is to develop a mathematical model to determine the longitudinal dispersion coefficient in alluvial rivers considering the morphological parameters in input.

1.2   State of the Art

The first attempt to quantify the effects of river morphology (i.e., bends) on longitudinal dispersion goes back to the seminal work of Fischer [1969]. The dispersion coefficient turns out to be given by a triple integral given depending on the deviations local value of the depth averaged longitudinal velocity from the cross sectionally averaged value. Nearly contemporaneously, Sooky [1969] attempted to obtain the longitudinal dispersion coefficient using the transverse velocity distribution, taken to be a combination of the logarithmic velocity profile and a linear function. Since then, various approaches have been proposed to estimate longitudinal dispersion of solutes in natural streams, as described by Fischer et al. [1979]. Although velocity measurements at a number of cross sections and concentration monitoring carried out at suitably placed stations can provide reliable predictions of dispersion processes, these data are not easily available in most cases, owing to the costs associated with

measurements or to the large spatial scales implied by a given study [Rutherford, 1994]. In order to fit the velocity data measured in both the Sacramento River and the Old River in the U.S., [1997] Bogle suggested an empirical equation based on a quartic function. Deng et al. [2001] also proposed a transverse velocity distribution as a power-law function, to determine the longitudinal dispersion coefficient in Fischers expressed triple integral expression [Deng et al., 2001].

Widely used solution procedures for determining longitudinal dispersion coefficient are the analytical solution of the triple integral described by Fischer [1979], numerical integration [Fischer, 1979], geomorphological estimation [Deng et al., 2001], one step Huber method or nonlinear multiregression method [Seo and Cheong, 1998], dye studies [Yotsukura etal., 1983]. Some of the proposed predictors are based on dimensional analysis and regression techniques applied to laboratory and field data, including both straight and meandering rivers [Iwasa and Aya, 1991; Seo and Cheong, 1998; Kashefipour and Falconer, 2002]. Other relationships have been derived combining theoretical analysis and empirical closures [Fischer, 1967; Deng et al., 2001; Deng et al., 2002; Liu, 1977]. Among these latter formulations, only those developed by Fischer [1967] and Deng et al., [2002] explicitly tackle out, even if in an approximate form, the effects of stream meandering. The analytical expression for the longitudinal dispersion coefficient obtained by Deng et al. [2002], in particular, was based on an empirical relationship for transverse distribution of flow depth in stable straight channels, corrected to account for channel sinuosity. The relationship, which is in general valid for straight and sinuous channel, turned out to predict the longitudinal dispersion coefficient with a certain accuracy, i.e., 90% of calculated values ranged from 0.5 to 2 times the observed values, including indistinctly both straight and meandering streams.

Consequently, a number of empirical or semi-empirical relationships has been so far developed which do not require detailed dye tests. All these relationships can be

Table 1.1: Values attained by the constants of the formula (1.1), summarizing the various longitudinal dispersion predictors available in literature. (a) Fischer et al. [1979]; (b) Seo and Cheong, [1998]; (c) Liu, [1977]; (d) Kashefipour and Falconer, [2002]; (e) Iwasa and Aya, [1991]; (f) Deng et al., [2001].

	(a)	(b)	(c)	(d)	(e)	(f)
κ_0	0.044	9.1	0.72	10.612	5.66	0.4105
κ_1	1.0	-0.38	1.0	-1.0	0.5	0.67
κ_2	1.0	4.38	-0.5	1.0	-1.0	1.0

cast in the general form

$$\mathcal{D}^* = \kappa_0 \frac{\beta^{\kappa_1}}{\sqrt{c_f}^{\kappa_2}} B^* U_0^* \tag{1.1}$$

where β is the ratio of half channel with, B^*, to mean flow depth, D_0^*, c_f is the friction coefficient, U_0^* is the mean value of the cross sectionally average flow velocity within the reach of interest, and $k_i (i = 0, 1, 2)$ are suitable constants, specified in Table 1.1.

In the work a theoretical method for predicting the longitudinal dispersion coefficient is developed based on the flow depth and velocity distribution in natural streams. An adequate velocity profile is implemented for the cross sections of fluvial rivers, and this profile is incorporated into the expression providing the longitudinal dispersion coefficient.

In particular, it will be shown that, introducing a rational perturbative framework and exploiting the most recent knowledge on the structure of the flow field which actually establishes in alluvial movable bed rivers, it is possible to obtain a relatively simple analytical expression which yields a robust estimation of the dispersion coefficient in these streams. Moreover, the proposed approach has the advantage to explicitly distinguish the contributions of the different physical mechanisms to the spreading of the contaminant along the channel.

The purpose of this work is to explicitly address this balance, to provide a

physically-based, yet relatively simple analytical relationship which relates the longitudinal dispersion coefficient to the bulk properties of the flow and, owing to sediment dynamics shaping the bed, to sedimentological parameters. To this aim, we apply to the flow field which establishes in sinuous movable bed channels the perturbative procedure developed by Smith [Smith, 1983] to account for the fast variations of concentration induced across the section by irregularities in channel geometry and the presence of bends. This methodology, introducing a reference system moving downstream with the contaminant cloud and using a multiple scale perturbation technique, allows one to derive a dispersion equation relating entirely to shear flow dispersion the along channel changes in the cross-sectionally averaged concentration. Moreover, taking advantage of the weakly meandering character of many natural rivers, it is possible to clearly separate the contributions to longitudinal dispersion provided by the various physical mechanisms.

A close comparison between mathematical models and field observations is undoubtedly rather difficult to achieve, but at the same time it would mark a major step forward in the knowledge of longitudinal dispersion processes.

1.3   Approach

In chapter 2, the description of concentration dynamics for a passive pollutant has been considered, starting from the advection-diffusion equation of the depth averaged concentration [Yotsukura, 1977]. Then, dispersion coefficient is derived introducing a rational perturbative framework eventually providing the longitudinal dispersion coefficient for straight and meandering channels.

In chapter 3, the model is particilarized to the case of a the straight alluvial channel. The cross sectional shape of the channel is expressed in terms of the transverse distribution of flow depth which is used to find out the flow field. The structure of the flow field that establishes in a given section is determined by considering

separately a central region of, nearly uniform depth, and a bank region where it is assumed that the bed shear stress equals the threshold for incipient sediment motion. The solution is determined analytically by assuming that transverse variations of the bed topography are relatively slow [Tubino and Colombini, 1992]. The general analytical solution, obtained by matching together the bank and the central region solutions, is used to estimate in closed form the longitudinal dispersion coefficient.

In chapter 4, a comparisn has been done with Elder [1959], alluvial dispersion co-efficient obtained for a plane flow (i.e. very wide cross section). The predicted dispersion coefficients have then been compared with those resulting from the tracer experimentscarried out by Godfrey and Frederick [1970] which also provides the measurements of the velocities in a number of cross section of some alluvial rivers compared with [Godfrey and Fedrick, 1970]. Finally the dispersion predictions are compared with Deng et al., [2001].

In chapter 5 and 6, the second phase of the model is developed by considering an alluvial river characterized by a given but arbitrary distribution of the channel axis curvature. In this case the flow field solution proposed by Frascati and Lanzoni, [2013] is adopted to calculate the longitudinal dispersion coefficient of meandering river. Comparison has been made with test data of six mindering rivers

1.4 Literature Review

1.4.1 Stream

A stream is a body of water with a current, confined within a bed and stream banks [Langbain and Iseri, 1995]. Every stream in their natural state is a dynamic hydrological system that is continually altered by the changing character of the watershed. Natural streams convey water and sediment, filter and entrap sediment and pollutants in overbank areas, recharge and discharge groundwater. Modification

of a stream channel (through which a natural stream of water runs or used to run) causes channel adjustments such as bank erosion, channel deepening, or sediment deposition, for some distance both upstream and downstream [Perez et al., 1997].

1.4.2 Channel

Stream channels can be classified either on the basis of observable bed morphology or on the basis of their dynamics. On the basis of bed morphology five types of natural water stream channel can be defined: (1) alluviallive bed sand; (2) alluvial live bed gravel; (3) alluvial threshold gravel; (4) mixed bedrock-alluvial; and (5) bedrock [Howard, 2013; Howard et al., 1994; Howard, 1987; Howard, 1980].

Alluvial channels are typified by their transportable sediment on both the bed and the banks which consist of riverine deposits that determine channel geometry in response to changes in flow conditions and sediment load. Live alluvial channel bed conditions imply that the channel gradient is set primarily by sediment flux, whereas threshold conditions imply that the channel gradient is set primarily by the critical shear stress for the initiation of motion. Alluvial channels in a given drainage basin tend to share similarity in their hydraulic geometry, that is, the mean depth, top width and velocity relationships for typical cross sections [Whipple, 2002; Allen, 1970].

Bedrock channels are characterized by frequent exposures of bedrock in the bed and banks and a lack of a coherent blanket of sediment. Mixed bedrock-alluvial channels either have alternating bedrock and alluvial segments or are bedrock channels with a thin and patchy alluvial cover (at low flow). Hard-bed or rock-bed channels are relatively resistant to down cutting but may have alluvial banks that allow for rapid lateral adjustments. Sediment deposits may cover portions of a hard-bed or rock-bed channel giving it the appearance of an alluvial channel [Whipple, 2002; Allen, 1970].

1.4.3   Channel Pattern

Natural stream channels can be classified as straight, meandering or braided. The distinction between straight and meandering channels depends on the degree of sinuosity, that is, the ratio of channel length to valley length see equation (1.2) and figure (1.1) . Channels with sinuosity greater than 1.5 are generally considered to be meandering. Braided channels contain sediment bars that cause multiple channels to form during low-flow conditions [Shelby, 1990; Ferguson, 1977; Mueller, 1968; Bridge, 2009; Gupta, 2011]. Figure (1.1) reports a table classifying the different pattern of channels depending on sinuosity, as well as a sketch of the main planform features, straight, meander and braided channels. Finally figure (1.3) reports a skchematic diagram of meandering channel in an alluvial floodplain.

$$sinuosity = \frac{L_c}{L_v} \tag{1.2}$$
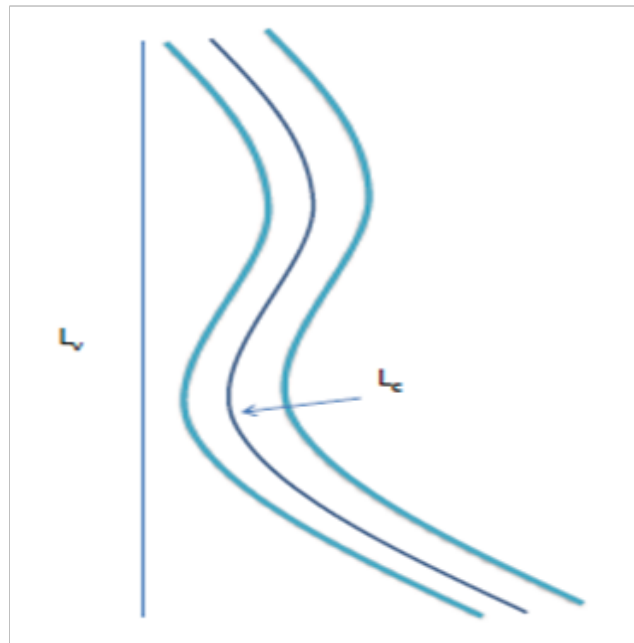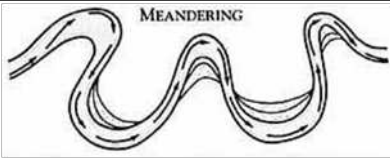
Figure 1.1: sinuosity=$\frac{L_c}{L_v}$

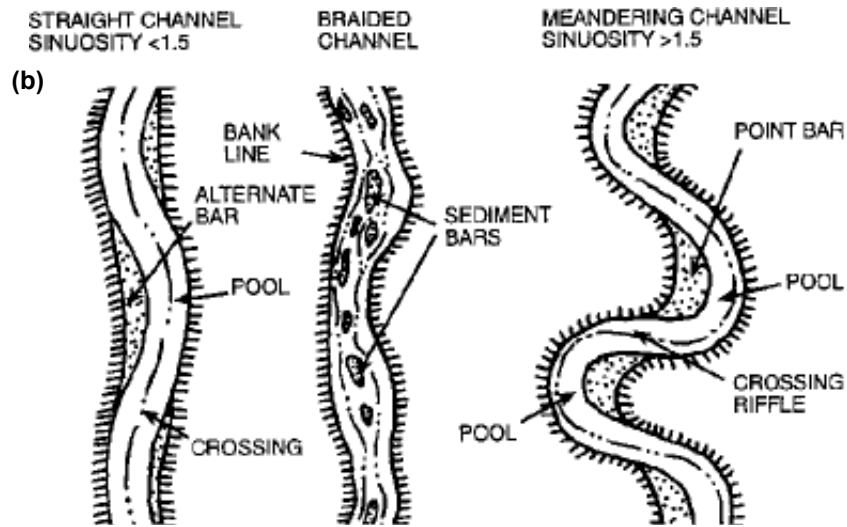| (a)		
Channel Pattern	View	Sinuosity
straight		1-1.5
Meander		> 1.5

Figure 1.2: (a)The above table reporting the classification of alluvial streams interms of sinuosity; (b) Plain view of the typical planform features of straight, meander and braided channel. (Source: http: // ohiodnr.com/ water/ pubs/ fs_st/ stfs03/ tabid/ 4159/ Default.aspx).

1.4.4   Straight Channels

Straight segments in alluvial streams are typical (Figure 1.4), but common to bedrock-controlled channels. Straight channels, mainly unstable, develop along the lines of faults and master joints, on steep slopes where rills closely follow the surface gradient, and in some delta outlets. A straight alluvial stream typically has a
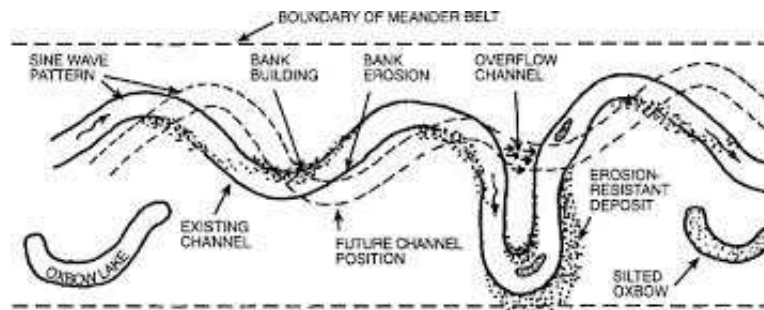
Figure 1.3: Meandering stream in an alluvial floodplain. (Source: http: // ohiodnr.com/ water/ pubs/ fs_st/ stfs03/ tabid/ 4159/ Default.aspx).

suspended-load channel, low gradient, sluggish flow, and very little load. Although the channel is straight there is a tendency for the flow to oscillate from side-to-side like all other channels. Flume experiments show that straight channels of uniform cross section rapidly develop pool-and-riffle sequences [Allen, 1970].

Figure 1.4: A Straight river channel. (Source: http: //www.geograph. org. uk/ photo/ 483359).

1.4.5 Meander Channels

Channel meandering is quantify by the degree of sinuosity (Figure 1.5). Meander forms of alluvial streams tend to exhibit sine wave patterns of predictable geometry, but non-uniformities in the alluvial deposits (consisting of erosion resistant material) along the streams and in the flood plains as well as cutoff events generally disrupt the regular pattern [Ferguson, 1977; Allen, 1970].

Figure 1.5: A meander river channel. Source: http://www.geo.uu.nl/ fg/ palaeo-geography/ results/ fluvialstyle.

Meandering streams upstream may have gentle sinuous bends to broadly looping channels, which strongly reflect channel load. The spacing of bends is controlled by flow resistance, which reaches a minimum when the radius of the bend is between two and three times the width of the bed. As bedload increases channels become less sinuous, bars develop, the width to depth ratio increases and eventually braiding occurs. The longitudinal profile of the bed of a meandering stream includes pools at (or slightly downstream upstream of) the extremities of bends and riffles at the inflections between bends. Increased tightness of bend, expressed by reduction in

radius and increase in total angle of deflection, is accompanied by increased depth of pool. A highly meandering stream typically has a cohesive, suspended-load channel and low flow velocity. All of the various positions that a meandering stream occupies over time defines a meander belt with outer boundaries at the extreme meander positions (Figure 1.3). The meandering pattern typical of many alluvial streams is an adjustment of the stream to its most stable form [Gore, 1985].

1.4.6   Channel flow

Channel flow or runoff, is the flow of water in streams, rivers, and other channels. It is a function of water discharge and velocity. Flow in natural channels normally occurs as turbulent, gradually-varied flow. Under conditions of gradually-varied flow, the streams velocity, cross-section, bed slope and roughness vary from section to section. Steady-uniform flow occurs when conditions at any given point in the channel remain the same over time and velocity of flow along any streamline (line of flow) remains constant in both magnitude and direction. Flow disturbances caused by channel obstructions, sinuosity, and channel roughness, create different forms of large-scale turbulence that are important because of their connection to channel erosion and sediment transport processes. Depth of flow has an equally complex and varied effect on the relationship between discharge of bed material and stream power and has, except at low shears, a large but simpler effect on the discharge of bed material as related to shear velocity with respect to the sediment particles. In most flume experiments, the range of depth is relatively small and the discharge of bedload frequently is on the order of magnitude smller then the discharge of suspended bed material.

1.4.7 Channel bed

A channel bed is the bottom of a stream, river or creek, the area between the banks of a channel that confines the normal water flow. As a general rule, the bed is that part of the channel, just at the "normal" water line and the banks are that part above the water line. The nature of any stream bed is always a function of the flow dynamics and the local geologic materials, influenced by that flow. The nature of the stream bed is strongly responsive to conditions of precipitation runoff [NC Division of Water Quality, 2010]. Gravel riffle bed is one of he natural channel bed example (Fgure 1.6).

Many rivers exhibit a sinuous planar pattern which determines, within each bend, a centrifugally induced secondary flow directed outwards close to the free surface and inward close to the bed. In fixed-bed conditions, the flow at the inner bend accelerates relative to the outer bend; proceeding downstream, the secondary flow transfers momentum towards outer bend and, hence, the thread of high velocity progressively moves from the inner to the outer bend. The erodible nature of river beds further complicates the flow field structure. Secondary helical currents enhance a transverse, inward directed, sediment transport which leads to the formation of a rhythmic sequence of bars and pools at inner and outer bends, respectively. The topographically induced component of the secondary flow promoted by this bed configuration further affects the non-uniform distribution of the velocity field across the channel section [Seminara, 2006] and, hence, the dispersion dynamics.

1.4.8 Channel depth-width

The physical changes to the channel bed and banks ultimately cause a modification to the bed morphology, i.e, depth and width of the channel. A natural stream channel generally shows a degree of width and depth variability, supporting deep, narrow
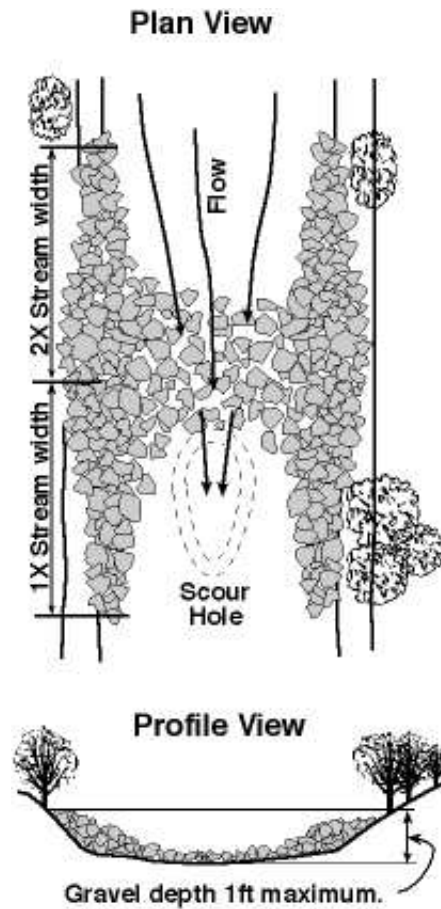
Figure 1.6: Example of gravel riffle bed. Source: http://www.dnr.state.oh.us/ water/ pubs/ fs-st/ stfs22/ tabid/ 4177/ Default.aspx

reaches and wider, shallower reaches depending on localized geomorphological controls. The width-depth variability of a channel is dependent upon factors such as the substrate type, flow regime and underlying geology [Finnegan et al., 2005].

1.4.9   Channel velocity

The velocity of a channel is the speed at which water flows along it. The velocity will change along the course of any channel, and is determined by factors such as the gradient (how steeply the river is losing height), the volume of water (flow discharge), the shape of the river channel and the amount of friction created by the

bed, rocks and plants [http: //www.ehow.com/ info _8223150 _factors- affecting-rivers- velocity.html]. The velocity of a river channel is influenced by three factors:

Shape of cross section The shape of the channel or its cross section affects the wetted perimeter. The wetted perimeter refers to the extent to which water is in contact with the channel sediments. The greater is the wetted perimeter, the greater is the friction between the water and the banks and the bed of the channel, and the slower is the flow of river.

Roughness of channel banks and bed A smooth stream bottom allows a higher velocity. Conversely, a channel that flows through a rough or an uneven bed with boulders on it as well as with rocks that protrude out from the bankexperiences a larger friction and, therefore, the velocity of the river is reduced.

Channel slope A channel flowing down a steep slope (or gradient) has higher velocity than one which flows down a gentler slope. In general, the higher is the gradient, the faster is the flow.

1.4.10 Dispersion in natural stream

Dispersion in natural stream is the ability of a stream to dilute soluble pollutants. Different types of pollution such as accidental spill of toxic chemicals, intermittent discharge from combined sewer overflows and temperature variations produced by thermal outflows may generate a cloud whose longitudinal spreading strongly affects the pollutant concentration dynamics. Estimating the dispersion of a stream is a vital issue for the efficient management of riverine environment. The flow depth within a flow of channel is correlated with the morphology of the channel and strongly influence the pollutant dynamics. In figure (1.7) shows an example of diluting of asoluable pollutant observed in a river.

Figure 1.7: Example of Dispersion of real channel (www.utsc.utoronto.ca).

1.4.11   Longitudinal dispersion

The longitudinal dispersion coefficient in a river generally depends on the channel geometry, the velocity distribution, the rate of transverse mixing and a dimensionless parameter that includes the mean velocity and length of an average bend [Fischer, 1969]. The formulation of relationships relating cross sectional area, lateralcoordinate, local flow depth, deviation of local depth averaged velocity from the cross sectional mean velocity, channel width and local transverse mixing coefficient in natural streams then requires the knowledge of the cross sectional geometry and of the flow field that establishes on it. A schematic diagram of longitudianl dispersion process with time is shown in figure (1.8).

A reliable estimation of longitudinal dispersion in natural streams is crucial for determining both acceptable levels of relation and estimating efficient inputs into natural streams. Early modeling was based of experimental laboratory and field
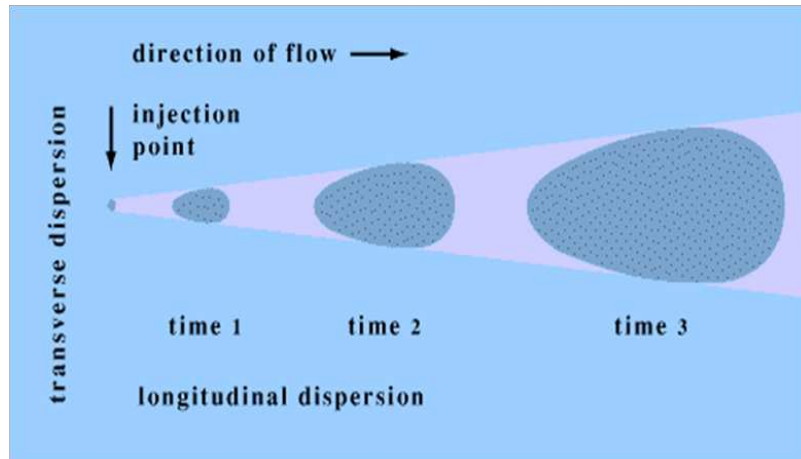
Figure 1.8: Typical behaviour of the pollutant cloud resulting from a point injection in a stream (http://proceedings.esri.com/ library /userconf /proc98 /proceed /to200 /pap193 /p193.htm).

test carried out with passive tracers (e.g. Rhodamine WT). A relevant improvement in understanding longitudinal dispersion has been ensured by the analysis of interactions between the pattern of bed deformation, transverse mixing coefficient and velocity flow [e.g., Fischer, 1979; Deng et al., 2001]. Nevertheless, the recent advances in modelling the flow field in alluvial rivers [e.g., Frascati and Lanzoni, 2013] pose the basis for a physical based estimation of the longitudinal dispersion coefficientand, hence, the derivation of more robust predictions.

Chapter 2

Longitudinal Dispersion in Alluvial River

2.1 Introduction

In the late 1960s early 1970s, many waterways in the US and in many other industrial countries were heavily polluted [Forsman, 2000; Bartlett, 1995]. For example, the Cuyahoga River in Ohio (USA) caught fire; the Lake Erie was so polluted that it was close to be declared dying, pollution due to human sewage, agricultural practices and industrial waste commonly caused the dramatic reduction of fish pollutants and significant damages of the riverine ecosystem. Public concern grew so overwhelming that in 1972 the United States Congress enacted the Federal Water Pollution Control Act. The law, commonly known as the Clean Water Act, set two national goals: elimination of the discharge of pollutants into the various waterbodies, and achievement of water quality to protect biodiversity, economical activities as fishing, and recreatinal activities [Zhang, 2011], A reliable assesment of the dynamics of the concentration of a given pollutant has thus a crucial role for a correct and rational management of water bodies. The estimation of the longitudinal dispersion

coefficient a fundamental step represents to quantify the rate of pollutant decay in rivers and natural streams. Fick [1855] on the other hand was thw first to tackle the problemof diffusion of a passive substance, by introducing the well known the Fick's law, covering molecular diffusion, Taylor [1953; 1954], introduced the concept of dispersion, by analyzing the spreading of a solute due to the joint effects of molecular turbulent diffusion and cross-sectional velocity gradient in circular pipes. The longitudinal disppersion coefficient resulting from Taylor's analysis in the case of turbulent flow conditions reads

$$K_s = 10.1ru^* \tag{2.1}$$

Where r is the pipe radius and u^* is the shear velocity $(= \tau_0/\rho)^{1/2}$, with τ_0 the shear stress at the wall and ρ the fluid density. Taylor's work resulted in the general advection-dispersion theory that, since then, has been widely applied to the analysis of transport phenomena in different fluids and with various boundary conditions. Among these analysis, transport in open channels is one of those of most interesting to environmental hydrologists. Elder [1959] extended Taylor's analysis to a plane channel flow (i.e., with infinite width, vanishing transverse velocity gradient) whereby the vertical velocity gradient is the major component of dispersion. He obtained

$$K_s = 5.93du^* \tag{2.2}$$

where d is the flow depth, u^* is the shear velocity. One of the most recognized contributors to the study of transport in open channel flow is Hugo B. Fischer. He was the first who applied Taylor's analysis to natural open channel flow. Fischer [1967] showed that Elder's equation significantly underestimates the dispersion coefficient, because it does not take into account the transverse variation of the velocity profile across the river. He thus used the lateral distribution of the depth averaged veloc-

ity instead of the vertical velocity profile considered by Elder [1959] to obtain the following relationship for the longitudinal dispersion coefficient:

$$K_s = -\frac{1}{A} \int_0^B h(y) u'(y) \int_0^y \frac{1}{\epsilon_y h(y)} \int_0^y h(y) u'(y) \, dy \, dy \, dy \tag{2.3}$$

where B is the channel width; $h(y)$ is the local water depth; A is the cross sectional area; y is the coordinate in lateral direction; ϵ_y is the local transverse mixing coefficient and $u'(y)$ is the deviation of local depth-average velocity from the cross sectional mean velocity. The fundamental difficulty in determining dispersion coefficient from equation (2.3) is the lack of knowledge of transverse profiles of both velocity and depth. Hence, Fischer (1975) developed a simpler equation by introducing a reasonable approximation of the triple integral, velocity deviation and transverse turbulent diffusion coefficient as follows:

$$K_s = 0.11 \frac{U^2 B^2}{H U^*} \tag{2.4}$$

McQuivey and Keefer [1974] developed the following simple equation to predict the dispersion coefficient, using the similarity based on combining the linear one-dimensional flow and the dispersion equation for the Froude number less than 0.5 as follows:

$$K_s = 0.058 \frac{HU}{s} \tag{2.5}$$

Liu [1977] obtained a dispersion coefficient equation using Fischer's equation accounting for the role of lateral velocity gradient, namely

$$K_s = \beta \frac{U^2 B^2}{H u^*} \tag{2.6}$$

the parameter β depending on the channel cross section shape and the velocity distribution across the stream, and can be computed as:

$$\beta = 0.18\left(\frac{u^*}{U}\right)^{1.5} \tag{2.7}$$

Iwasa and Aya [1991] derived an equation to predict the dispersion coefficient in natural streams using a regression of laboratory data and previous field data which yields:

$$\frac{K_s}{HU^*} = 2\left(\frac{B^2}{H}\right)^{1.5} \tag{2.8}$$

Seo and Cheong [1998], dimensional analysis and a regression analysis for the one step Huber method obtained the following equation:

$$\frac{K_s}{Hu^*} = 5.915\left(\frac{B}{d}\right)^{0.620}\left(\frac{U}{u^*}\right)^{1.428} \tag{2.9}$$

More recently, Deng et al.[2001] using an improved formula for the transverse mixing coefficient derived the following equation predict the longitudinal dispersion coefficient in natural rivers:

$$\frac{K_s}{du^*} = \frac{0.15}{8\epsilon_{t0}}\left(\frac{B}{d}\right)^{\frac{5}{3}}\left(\frac{U}{u^*}\right)^2 \tag{2.10}$$

in which ϵ_{t0} is the transverse mixing coefficient calculated as:

$$\epsilon_{t0} = 0.145 + \frac{1}{3520}\left(\frac{B}{d}\right)^{1.38}\left(\frac{U}{u^*}\right) \tag{2.11}$$

Kashefipour and Falconer (2002) developed an equation for predicting dispersion coefficient in rivers based on data collected in several US rivers. This equation can be written as:

$$K_s = 10.612\,d\,U\left(\frac{U}{u^*}\right) \tag{2.12}$$

combining equation (2.12) with that's proposed by Seo and Cheong [1998] they obtained as:

$$K_s = \left[7.428 + \left(\frac{B}{d}\right)^{0.620}\left(\frac{U}{u^*}\right)^{0.572}\right]HU\left(\frac{U}{u^*}\right) \qquad (2.13)$$

Most of the researches in this period of time were imprinted with the characteristics of the background. The discrepancies between the predicted and the observed results range from 1 to 3 orders of magnitude of the observed values. Such substantial discrepancies are attributed to the irregularity, spiral flow and the storage in dead zones in natural streams [Deng et al., 2002]. While the one-dimensional (1D) advection-dispersion (AD) model have been successfully used in the streams that are physically low slope, deeper than the roughest bed feature, and relatively uniform (possibly due to flow regulation), it is found not applicable to model many other situations. Fischer et al. [1979] concluded that, some streams may be so irregular that no reasonable analysis can be applied. For instance, a mountain stream that consists of a series of pools and riffles is not a suitable place to apply Taylor's analysis. Because Taylor's analysis was developed on idealized conditions (i.e., straight, uniform channels) and resulted in a Fickian-type diffusion equation that predicts a Gaussian solute concentration distribution. In the seminal work, Fischer [1967], demonstrated that a meandering stream has a twofold role on longitudinal dispersion. Firstly, the concentration of the thread of high velocity on the outside of river bends and transverse variations of bed topography associated to the rhythmic sequence of bars and pools result in an increased shear flow dispersion. On the other hand, secondary currents favor transverse mixing, enhancing a more uniform distribution of pollutant concentration across the section, and thus reducing the longitudinal dispersion. Simplest channel has longitudinal dispersion as there is velocity gradients in the flow, caused by friction velocity. When the channel is complex then its flow is complex which effects the dispersion. Also dispersion increase with increasing discharge as turbulence develops [Wallis and Manson,2004].

So an injected tracer or spilled contaminant moves downstream, it spreads and the peak concentration reduced. The variation of dispersion coefficients is more important in natural rivers with meandering configuration, which is one of the most typical geometric configurations. In meandering rivers, one must consider not only the undulating primary flow path along watercourses but also the repeating generation and dissipation of secondary currents. Following the alternating bends, the flow periodically induces the secondary currents that alter the magnitude of both transverse mixing and longitudinal dispersion [Fischer, 1969]. Therefore, when accurate results are required in the modeling of solute mixing in meandering rivers, the more detailed information of the spatially varied dispersion coefficient is needed to be incorporated into the model than the modeling in the field with any other geometric configurations. Research on the variable mixing coefficient in meandering streams has been performed based on the tracer test in the Chang [1971] conducted studies of transverse mixing in meandering channels and suggested a cyclic variation in the transverse mixing coefficient [Boxall and Guymer, 2003; Boxall et al., 2003; Marion and Zaramella, 2006] analyzed the characteristics of transverse dispersion coefficients in sinuous open channel flows on the basis of the laboratory experiments that allowed natural development of the channel bed. They maintained that the maximum values of the transverse dispersion coefficient are found in the regions of strong secondary circulation, directly downstream of the bend apex and minimum values are found in the straighter regions. They showed the inverse relationship between the variation of longitudinal and transverse coefficients in the longitudinal direction in their later research on the prediction of longitudinal dispersion coefficient in meandering channel [Boxall and Guymer 2007]. The mathematical model formulated in the following section tackles the problem of two-dimensional (i.e., depth averaged) pollutant mixing for the steady flow in an alluvial channel. The model generally,which accounts for the dynamic effects of secondary flows induced

by the planform meandering configuration of the river enhancing transverse mixing, and, hence, a more uniform distribution of the pollutant concentration across the section. The novel feature of the present model is the solution of the problem in terms of pertubations of a basic flow, consisting of the uniform flow in a straight prismatic channel.

2.2 Formulation of the Problem

2.2.1 Notation

We analyze the behavior of a passive, non-reactive contaminant which (e.g., due to an accidental spill) is suddenly released in an alluvial channel which, in general, have a meandering planform configuration. The channel has non erodible banks, a constant width $2B^*$, large enough for the flow to be modeled as two dimensional, and a quite small mean slope S, as typically occurs in alluvial rivers. A given constant discharge Q^* flows under uniform condition with average flow depth D_0^* and mean velocity U_0^*. This system is characterized by the depth averaged velocity (u^*, v^*) and the eddy viscosity ν_T^*. The erodible bed is assumed to be made up of a uniform cohesionless sediment with grain size d_{gr}^*, which is transport mainly as bedload. The gravity acceleration is g. Hereafter a star superscript denotes dimensional quantities.

2.2.2 Reference system

The problem can be conveniently studied introducing the curvilinear orthogonal coordinate system (s^*, n^*, z^*), where s^* is the longitudinal coordinate (directed downstream), n^* is the transverse curvilinear coordinate (with origin at the channel axis) and z^* is the axis normal to the bed (pointing upward). In alluvial channel the cross sectionally averaged concentration undergoes relatively small and rapidly changing gradient associated with the spatial variations of the flow field and a slower evolution

due to longitudinal dispersion. In order to deal with the fast concentration changes acting at the meander scale, it proves convenient to introduce a pseudo-lagrangian, volume following co-ordinate ξ^* , which travels downstream with the contaminat cloud [Shinohara et al., 1969; Smith 1983] and accounts for the fact that the cross sectionally averaged velocity U_0^* is not constant along the channel. This co-ordinate is defined as:
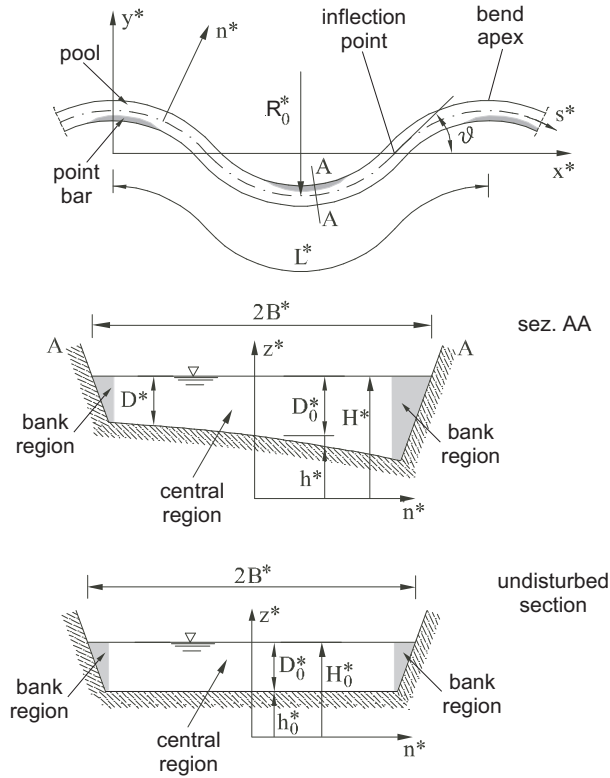
Figure 2.1: Sketch of Meandering channel

$$\xi^* = \frac{\mathcal{V}^*}{A_0^*} = \frac{1}{A_0^*} \int_0^{s^*} h_{s0} A^* ds^* \qquad (2.14)$$

where, $\mathcal{V}^*$ is the water volume from the origin of the coordinate system to the generic co-ordinate s^*, $A_0^*(= 2B^* D_0^*)$ is the average cross sectional area within the

investigated reach, while

$$A^* = \int_{-B^*}^{B^*} d^* dn^*, \quad h_{s0} = \frac{1}{A^*} \int_{-B^*}^{B^*} h_s d^* dn^* \tag{2.15}$$

with h_s the metric coefficient associated withthe longitudinal co-ordinates Generally, $\mathcal{V}^*$, h_{s0} and A^* can vary along s^* as a consequence of the variations of section geometry induced by bed topography and/or channel narrowing or widening. However, requiring that the volume $\mathcal{V}^*$ is a material one (and, hence, that ξ^* is a volume following coordinate) leads, in general, to the following derivation rules

$$\frac{\partial}{\partial s^*} = \frac{\mathcal{A}^*}{A_0^*} \frac{\partial}{\partial \xi^*}, \quad \frac{\partial}{\partial t^*} = \frac{\partial}{\partial t^*} - U_\xi^* \frac{\mathcal{A}^*}{A_0^*} \frac{\partial}{\partial \xi^*} \tag{2.16}$$

where, $\mathcal{A}^* = h_{s0} A^*$ is a modified cross sectional area and U_ξ^* is the velocity of the moving pseudo lagrangian co-ordinate ξ^*. Denoting by L_c^* the length of the pollutant cloud and L^* the length of the reach under investigation The later can be determined recalling that, for a stationary flow field as the one investigated here, the flow discharge is constant and therefore $U_\xi^* \mathcal{A}^* = U^* A_0^*$. Thus adopting the scaling $\xi = \frac{\xi^*}{L_c^*}, \quad \mathcal{A} = \frac{\mathcal{A}^*}{A_0^*}$ we obtain

$$\xi = \frac{\xi^*}{L_c^*} = \frac{\epsilon}{\gamma} \int_0^s \mathcal{A}(\hat{s}) d\hat{s} \tag{2.17}$$

Note that, for an observed pollutant cloud moving with velocity U_ξ^* the dillution of the pollutant concentration associated with longitudinal dispersion occurs at a length scale comparable with the length of the contaminant cloud, L_c^*.

2.2.3   Two dimensional Advection-Diffusion Equation

The two dimensional advection diffusion equation for the depth averaged concentration equation is [Yotsukura, 1997]

$$h_s d^* c_{,t^*} + d^* u^* c_{,s^*} + h_s d^* v^* c_{,n^*} = \left(\frac{d^*}{h_s} k_s^* c_{,s^*} \right)_{,s^*} + \left(h_s d^* k_n^* c_{,n}^* \right)_{,n^*} \tag{2.18}$$

Where c is the depth averaged concentration, t^* denotes time, d^* is the local flow depth, u^* and v^* are the depth averaged longitudinal and transverse component of the velocity k_s^* and k_n^* the longitudinal and transverse mixing coefficient, h_s is the metric coefficient arising from curvilinear character of the longitudinal coordinate, defined as,

$$h_s = 1 + \frac{n^*}{r^*} = 1 + \nu n \mathcal{C} \tag{2.19}$$

where $\nu = \frac{B^*}{R_0^*}$ is the curvature ratio, $\mathcal{C} = \frac{R_0^*}{r^*}$, is the dimensionless channel curvature, $r^*(s^*)$ is the local radius of the channel axis of curvature, assumed to be positive when the center of curvature lies along the negative n^* axis and R_0^* is twice the minimum value of r^* within the meandering reach. The governing equation of this system assumed the shallow water conditions. This assumption applies when the longitudinal and the lateral scales are much larger than the flow depth, and implies a hydrostatic distribution of the mean pressure. In the following, the assumption of slowly varying flow field conditions will be assumed. For a straight river this implies that the central part of the cross section is connected gradually to the banks; for a meandering river the bends are assumed to be mild. Moreover, steady conditions for the flow is assumed considering a typical hiearchy of scales whereby meander geometry varies on a much longer time span with respect to bed defomation, and to the scale of flow unsteadiness.

2.2.4 Scaling

In order to investigate the order of magnitude of the various terms contributing to equation (2.18) it is useful to make it dimensionless introducing the following scaling:

$$t = \frac{B^{*2}t}{k_{n0}^*}, \quad s = \frac{s^*}{L^*}, \quad n = \frac{n^*}{P_0^* + b^*}, \quad d = \frac{d^*}{D_0^*}$$
$$u = \frac{u^*}{U_0^*}, \quad v = \frac{V^*}{U_0^*}\frac{L^*}{B^*}, \quad k_n = \frac{k_n^*}{k_{n0}^*}, \quad k_s = \frac{k_s^*}{k_{n0}^*} \tag{2.20}$$

where, B^* the overall is half channel width, b^* is (the half width of the central part of the channel), L^* is the average intrinsic meander length within the investigated reach, $\frac{B^{*2}t}{k_{n0}^*}$ is the typical scale of transverse mixing and k_{n0}^* is the transverse mixing coefficient for a straight channel configuration. We then obtain,

$$h_s dc_{,t} + \gamma[duc_{,s} + \left(\frac{\delta\beta}{1 + \delta\beta_c}\right)h_s dvc_{,n}] =$$
$$\left(\frac{\delta\beta}{1 + \delta\beta_c}\right)^2 \left(h_s dk_n c_{,n}\right)_{,n} + \left(\gamma\,\epsilon\right)^2\left(\frac{d}{h_s}k_s c_{,s}\right)_{,s} \tag{2.21}$$

Three fundamental parameters arise from the above scaling namely $\delta = \frac{D_0^*}{P_0^*}$, $\gamma = \frac{B^{*2}U_0^*}{k_{n0}^*L^*}$ and,

$$\epsilon = \frac{k_{n0}^*}{B^*U_0^*} = k_{n0}\frac{\sqrt{c_f}}{\beta} \tag{2.22}$$

This latter parameter physically represents the inverse of a Peclet number in the transverse direction. It typically attains small values as it immediately results considering the equivalent form $\epsilon = k_{n0}\frac{\sqrt{c_f}}{\beta}$, where the dimensionless transverse mixing coefficient $k_{n0} = \frac{k_{n0}^*}{\sqrt{gD_0^*SD_0^*}}$ usually falls in the range $0.15 - 0.30$ [Rutherford, 1994] The parameter γ describes the relative importance of transverse mixing, which tends to homogenize the contaminant concentration, enhances, and nonuniform transport

at the bend-scale which, on the contrary, concentration gradients. Typically,

$$\gamma = \lambda/(2\epsilon\pi) \tag{2.23}$$

where the dimensionless meander wavenumber $\lambda = 2\pi\frac{B^*}{L^*}$ usually ranges between 0.1 to 0.3 [Leopold et al., 1964]. It then turns out that typically ϵ and γ can be taken as small parameters. We exploit this fact in the following section.

2.3 Expansion

The derivation of the longitudinal dispersion coefficient takes advantage of the small character of the parameter ϵ. Equation (2.17) indicates that the spatial variations of c associated with longitudinal dispersion at the scale of the contaminant cloud are described by the slow ($\frac{\epsilon}{\gamma} = \frac{L^*}{L_c^*} << 1$) variable ξ whereas the comparatively small and rapidly changing variations in concentration across the flow associated with stream meandering are accounted for through the fast variables s, n. Similarly, a fast and a slow temporal variable emerge as a consequence of the sharp separation between the time scales characterizing the various physical processes [Taylor, 1953; Fischer, 1967; Smith, 1983]. The fast time variable, $t_1 (= \frac{t^* U_0^*}{L_c^*})$ is related to non-uniform advection within the cloud, which typically acts much slowly than transverse mixing. It is in fact easy to show that $t_1 = \epsilon t$, provided that, $\frac{B^*}{L_c^*} = \epsilon^2$ i.e., the contaminant cloud has reached a length of order of kilometers. On the other hand slow time variable $t_2 = \frac{t^* D^*}{L_c^{*2}}$ is determined by the time scale at which longitudinal dispersion operates. In terms of ϵ it results that $t_2 = \epsilon^2 t$, provided that $\mathcal{D}^*$ is at maximum of order $\epsilon^{-1} B^* U_0^*$, a condition typically satisfied in natural channel, as also suggested by the semi-empirical relationship developed by [Fischer et al., 1979], according to which $\mathcal{D}^* = 0.044 k_{n0} \epsilon^{-1} B^* U_0^*$ (see Table 1.1 and Figure 1.1). The presence of different spatial and temporal scales can be handled employing a multiple scale technique

[Nayfeh, 1973]. To this purpose we assume that $c = c(s, n, \xi, t_1, t_2)$ and transform the governing equation making use of the derivation chain rules . We end up wit following advection-diffusion equation for c:

$$\mathcal{L}c = -\epsilon\left(h_s dc_{,t_1} + du\mathcal{A}c_{,\xi}\right) - \epsilon_2 h_s dc_{,t_2} + \left(\epsilon\gamma\right)^2 \left(\frac{d}{h_s}k_s c_{,s}\right)_{,s} + \epsilon^4 \mathcal{A}\left(\frac{d}{h_s}k_s \mathcal{A}c_{,\xi}\right)_{,\xi}$$
(2.24)

where the differential operator $\mathcal{L}$ reads:

$$\mathcal{L} = \gamma\left[du\frac{\partial}{\partial s} + \left(\frac{\delta\beta}{1 + \delta\beta_c}\right)h_s dv\frac{\partial}{\partial n}\right] - \left(\frac{\delta\beta}{1 + \delta\beta_c}\right)^2 \frac{\partial}{\partial n}\left(h_s dk_n\frac{\partial}{\partial n}\right)$$
(2.25)

We next introduce the following expansion for c

$$c = c_0 + \epsilon c_1 + \epsilon^2 c_2 + \dots$$
(2.26)

into equation (2.24) and considering exploiting the small parameter ϵ, substituting the problem arising at various order of approximations we obtain:

$$\mathcal{O}(\epsilon^0) \Rightarrow \mathcal{L}c_0 = 0,$$
(2.27)

$$\mathcal{O}(\epsilon) \Rightarrow \mathcal{L}c_1 = -h_s dc_{0,t_1} - du\mathcal{A}c_{0,\xi},$$
(2.28)

$$\mathcal{O}(\epsilon^2) \Rightarrow \mathcal{L}c_2 = -h_s dc_{0,t_2} - (h_s duc_{1,t_1} + du\mathcal{A}c_{1,\xi}),$$
(2.29)

These equations used to be coupled with the requirements that $\frac{\partial c_i}{\partial n} = 0 (i = 1, \dots)$ at the channel banks, where the normal component of the contaminant flux vanishes. The partial differential equation (2.27),(2.28),(2.29) provide a clear insight into the structure of the contaminant and concentration. It is easily seen from equation (2.27) that does not depend on s, n and hence, it is not affected by the fluctuations

induced by flow with the channel, i.e.it coincides with the cross sectional average C_0.
Equation (2.28) suggests for c_1 a solution of the form $c_1 = [g_1(s,n) + \alpha_1]\frac{\partial C_0}{\partial \xi}$, with
α_1 an arbitrary constant and g_1 a function describing the nonuniform distribution
across the section of the contaminant concentration, Similarly equation (2.29) can
be solved by setting $c_2 = [g_2(s,n) + \alpha_2]\frac{\partial^2 C_0}{\partial^2 \xi}$, with α_2 an arbitrary constant. The
depth averaged contaminant concentration then results;

$$c(s,n,\xi,t_1,t_2) = C_0(\xi,t_1,t_2) + \epsilon[g_1(s,n) + \alpha_1]\frac{\partial C_0}{\partial \xi} + \epsilon^2[g_2(s,n) + \alpha_2]\frac{\partial^2 C_0}{\partial \xi^2} + \mathcal{O}(\epsilon^3)$$
(2.30)

This relationship clearly discriminates the slower evolution due to longitudinal dispersion, embodied by the terms C_0, $\frac{\partial C_0}{\partial \xi}$, $\frac{\partial^2 C_0}{\partial^2 \xi}$, from the small and rapidly varying
changes associated with the spatial variations of the flow field, described by the
function g_1 and g_2. Integrating equation (2.30) across the section and along an alluvial channel, it is immediately recognized that with a suitable choice of the arbitrary
constants α_1 and α_2, the effects of c_1 and c_2, leading to a term proportional to $\frac{\partial C_0}{\partial \xi}$,
$\frac{\partial^2 C_0}{\partial^2 \xi}$, will not emerge until $\mathcal{O}(\epsilon^3)$ i.e., $(C = C_0 + \mathcal{O}(\epsilon^3))$. Such a result is met by setting $\alpha_i = - < G_i >$ $(i = 1, 2)$, where, cross section averaging and reads averaging
are defined by :

$$G_i = \frac{1}{\mathcal{A}} \int_{-1}^{1} h_s \, g_i \, f \, dn$$
(2.31)

$$< G_i > = \frac{1}{L} \int_{s+\frac{L}{2}}^{s-\frac{L}{2}} G_i ds$$
(2.32)

It is important to note that only averaging $g_i(s,n), (i = 1, 2)$ along the entire meander length leads to a value of α_i which does not depend on s, as required by the
$\mathcal{O}(\epsilon^0)$ and $\mathcal{O}(\epsilon^2)$ problems.

2.4 Longitudinal Dispersion Coefficient

We are now ready to derive the advection diffusion equation, governing the evolution of the cross sectionally averaged concentration C_0 and the related longitudinal dispersion coefficient. We sum together equations (2.28) and (2.29), averaged across the section, and require that the flux of contaminant does not vary on the fast scale s, a condition needed in order to eliminate secular term which would lead c_2 to grow systematically with s. We obtain the following equation

$$\frac{\partial C_0}{\partial t} + \epsilon \frac{\partial C_0}{\partial \xi} = \epsilon^2 K_s \frac{\partial^2 C_0}{\partial \xi^2} + \mathcal{O}(\epsilon^3) \tag{2.33}$$

Where the longitudinal dispersion coefficient defined as

$$K_s = \frac{1}{\mathcal{A}} \int_{-1}^{1} \left(h_s d \frac{\int_{-1}^{1} du \mathcal{A}}{\mathcal{A}} - d\tilde{u}\mathcal{A} \right) g_1 dn \tag{2.34}$$

and the function g_1 results from the solution of the $\mathcal{O}(\epsilon)$ equation

$$\mathcal{L}g_1 = h_s d - du\mathcal{A} \tag{2.35}$$

Supplimented with the requirement that $\frac{\partial g_1}{\partial n} = 0$ at the channel banks, where the normal component of the contaminant flux vanishes. Before to proceed further on some observations on equation (2.34) are worthwhile. In accordance with [Fischer, 1967], the contribution to longitudinal dispersion provided by vertical variations of the velocity profile (embodied by the term of (2.21) containing k_s) is of minor importance. Longitudinal dispersion is essentially governed by shear flow dispersion induced by the nonuniform distribution across the section of both the contaminant concentration accounted for through the function $g_1(s, n)$ and the flow field quantified by $(h_s - u\mathcal{A})d$. This later term, however, differs from the much simpler term

$1 - u$ using in the classical treatment persued by [Fischer 1967] as a consequence
at the fact that here the mean flow vwlocity can in general vary along the channel,
a circumstance specifically accounted for through the volume following coordinate
ξ. It is in particular important to observe that in the presence of river reaches
characterized by rapid longitudinal variations of the flow field the dispersion coeffi-
cient K can locally attain negative values, thus favoring spurious instabilities. As
pointed out by Smith [1983] such a problem can be prevented by introducing a bend
averaged longitudinal dispersion coefficient defined as:

$$\mathcal{K} =< \mathcal{A}K > \tag{2.36}$$

that is always positive. Finally, it can be demonstrated that the local and the
bend averaged coefficient K and $\mathcal{K}$, are related to the classically adopted local
coefficient K arising when considering the usual coordinate s, by the relationships
$K = \mathcal{A}^2 K$ and $\mathcal{K} =< \mathcal{A}^3 K >$. The perturbation technique developed so far allows
us to calculate the dimensionless longitudinal dispersion coeffiient, in natural streams
once the structure of the flow field, of bottom topography and of depth averaged
concentration distributions are specified. To this aim, we take advantage of the fact
that in nature the curvature ratio appearing in equation (2.19) is typically a small
parameter, ranging in the interval 0.1-0.2 [Leopold et al. 1964). We then assume
that flow and topography perturbations originating from deviations from a straight
channel configuration are small enough to inroduce the expansions:

$$[u(s,n), d(s,n), \mathcal{A}(s,n)] = [u_0(n), d_0(n), \mathcal{A}_0(n)]$$
$$+\nu[u_c(s,n), d_c(s,n), \mathcal{A}_1(s,n)] + \mathcal{O}(\nu^2) \tag{2.37}$$

The unperturbed $\mathcal{O}(\nu^0)$ straight channel configuration is in general characterized
by a cross section in which the transverse variations of both u_0 and d_0 are mainly

concentrated near the banks (see fig 3.3), where the depth (and, therefore the velocity) varies smoothly from the cocstant value characterizing the central part of the section zero. [Parker, 1978]. In many alluvial rivers, however the aspect ratio β is high enough (ranging approximately in the intervals 5-20, 20 and 60 in gravel and in sandy river, respectively) to neglect the effect of this side wall regions. By substituting (2.37) into the two dimensional continuity and momentum equations for the fluid and in the sediment balance equation, it is then possible to obtain, although at a linearized level of approximation, the spatial distribution of the flow field and of the bed tpopography in movable bed meandering channels [Blondaux and Seminara, 1985; Seminara and Tubino, 1992; Zolezzi and Seminara, 2001]. We will use this information later on to determine the effects of centrifugally and topographically induced secondary helical flow on contaminant spreading. Let us now move to quantify the nonuniform distribution in the natural stream of the depth averaged contaminant concentration. As for the flow field, we expand in terms of ν the relevant quantifies, namely the dimensionless transverse mixing coefficient k_n and the function g_1

$$[k_n(s,n), g_1(s,n)] = [k_{n0}(s,n), g_{10}(n)] + \nu[k_{n1}(s,n), g_{11}(s,n)] + \mathcal{O}(\nu^2) \qquad (2.38)$$

The structure of the longitudinal dispersion coefficientnt in meandering channels is easily determined by substituting (2.37) and (2.38) (2.34), and recalling (3). We obtain:

$$K = K_{s0} + \nu K_{s1} + \nu^2 K_{s2} + \mathcal{O}(\nu^3) \qquad (2.39)$$

The $\mathcal{O}(\nu)$ and $\mathcal{O}(\nu^2)$ terms are specifically related to the complex structure of flow field. Substituting (2.37) and (2.38) into (2.35), we obtain a sequence of problems

whose general form reads

$$\gamma[du\frac{\partial g_{1i}}{\partial s} + (\frac{\delta\beta}{1+\delta\beta_c})h_s dv\frac{\partial g_{1i}}{\partial n}] - (\frac{\delta\beta}{1+\delta\beta_c})^2\frac{\partial g_{1i}}{\partial n}(h_s dk_n\frac{\partial g_{1i}}{\partial n}) = f_{1i}(s,n) \quad (2.40)$$

subject to the constraint that $\frac{\partial g_{1i}}{\partial n} = 0$ at the walls. As it will be shown in the following it is sufficient to know only the functions, g_{10} and g_{11}, solution of the $\mathcal{O}(\epsilon\nu^0)$ and $\mathcal{O}(\epsilon\nu)$ problems respectively to get and estimate of K correct up to the order $\mathcal{O}(\nu^3)$. The function g_{10}, accounts for the non uniform distribution of the concentration across the section in the case of a straight channel. It is determined solving the problem,

$$(\frac{\delta\beta}{1+\delta\beta_c})^2\frac{\partial}{\partial n}\left(d_0 k_{n0}\frac{\partial g_{10}}{\partial n}\right) = -f_{10} \quad (2.41)$$

$$\frac{\partial g_{10}}{\partial n} = \frac{1}{d_0\,k_{no}}\int_{-1}^{n}-f_{10}\left(\frac{1+\delta\beta_c}{\delta\beta}\right)^2 dn^* \quad (2.42)$$

$$g_{10}(n) - g_{10}(-1) = \int_{-1}^{n}\frac{d\hat{n}}{d_0 k_{n0}}\int_{-1}^{\hat{n}}-f_{10}\left(\frac{1+\delta\beta_c}{\delta\beta}\right)^2 dn^* \quad (2.43)$$

with the boundary conditions:

$$\frac{\partial g_{10}}{\partial n} = 0, \quad n = \pm 1 \quad (2.44)$$

$$\int_{-1}^{1}g_{10}(n)\,dn = 0, \quad (2.45)$$

At the order $\mathcal{O}(\epsilon\nu^0)$ f_{10} reads:

$$f_{10} = \int_{-1}^{1}\left(\frac{\int_{-1}^{1}d_0 u_0 \mathcal{A}_0}{\mathcal{A}_0} - \mathcal{A}_0\tilde{u}\right)d_0\,dn \quad (2.46)$$

The solution g_{10} must account for the fact that, in the case of a sudden release of contaminat here considered, the concentration tends to be distributed uniformly

across the section, far downstream of the input section, i.e., $g_{10}(s \to \infty) = 0$. This condition equivalent to imposing that the $\mathcal{O}(\epsilon)$ contribution to the pollutant flux must vanish. The solution of (2.40) can be easily obtained.

$$g_{10}(n) = \int_{-1}^{n} \frac{1}{d_0 \, k_{n0}} \int_{-1}^{\hat{n}} \Big(\frac{\int_{-1}^{1} d_0 u_0 \mathcal{A}_0}{\mathcal{A}_0} - \mathcal{A}_0 \tilde{u} \Big) d_0 \Big(\frac{1 + \delta \beta_c}{\delta \beta} \Big) d\hat{n} \, dn \qquad (2.47)$$

Owing to the symmetry of the generalized channel shape, the numerical integration is conducted only for $n = 0$ to 1.
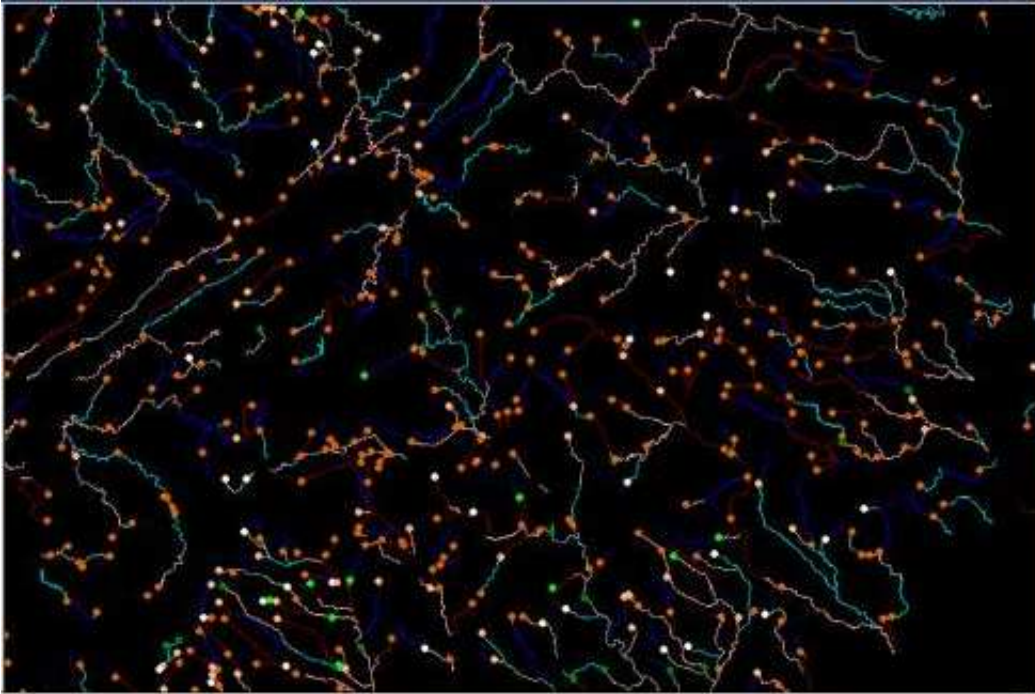
Figure 2.2: River water concentration layer with WWTP effluent concentration layer (Source: http://proceedings. esri. com/ library/ userconf/ proc02/ pap1259/ p1259.htm).

The river water concentration layer with WWTP effluent concentration layer is shown in figure (2.2).
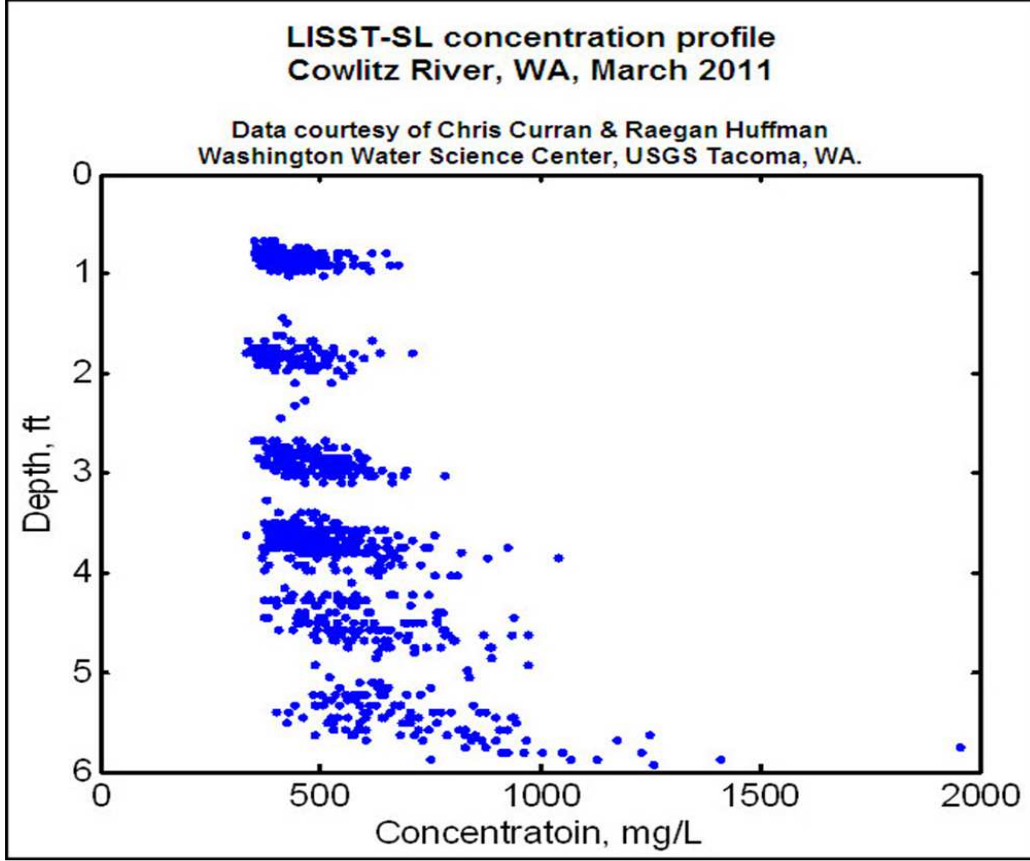
Figure 2.3: Concentration profile of Coelitz River (Source: http://www.sequoiasci. com/ article/ lisst- sl- data- from- cowlitz- river- march- 2011)

For a straight channel ($\gamma = 0$), we can write (2.34) and (2.35) as:

$$K_{s0} = \frac{1}{\in \mathcal{A}_0} \int_{-1}^{1} \left(\frac{\int_{-1}^{1} d_0 u_0 \mathcal{A}_0}{\mathcal{A}_0} - \mathcal{A}_0 \tilde{u} \right) d_0 \, g_{10} \, dn + g_{10}(-1) \qquad (2.48)$$

The longitudinal dispersion coefficient,then turns out yo be (2.48):

$$K_{s0} = \left(\frac{\delta \beta}{1 + \delta \beta_c} \right)^2 \frac{1}{\mathcal{A}_0} \int_{-1}^{1} \left(\frac{\int_{-1}^{1} d_0 u_0 \mathcal{A}_0}{\mathcal{A}_0} - \mathcal{A}_0 \tilde{u} \right) d_0 \int_{-1}^{n} \frac{1}{d_0 \, k_{n0}} \int_{-1}^{n} \left(\frac{\int_{-1}^{1} d_0 u_0 \mathcal{A}_0}{\mathcal{A}_0} - \mathcal{A}_0 \tilde{u} \right)$$

$$d_0 \, dn \, dn \, dn$$

$$(2.49)$$

and returning to dimensional quantities:

$$K_{s0}^* = K_{s0} B^* U_0^*$$ (2.50)

It is immediately recognised that the leading order contribution (2.49) corresponds to the classical solution obtained by Fischer [1967] and accounts for dispersion effects which arise in a straight uniform flow as a consequence of the nonuniform distribution of the contaminant and of the cross sectional gradients, concentrated mainly near the banks (see figure 3.3). However, natural river involve many sources of nonuniformities, e.g., the secondary helical flow driven by channel bending. These uniformities are accounted for at the order $\mathcal{O}(\epsilon\nu)$, we obtain,

$$\frac{\partial}{\partial n}(d_0 k_{n0} \frac{\partial g_{11}}{\partial n}) - \gamma(d_0 u_0)\frac{\partial g_{11}}{\partial s} = -\Big(\frac{1 + \delta\beta_c}{\delta\beta}\Big)^2 f_{11}$$ (2.51)

$$f_{11} = \Big[(d_c + ncd_0) - (d_0 u_0 A_1 + d_0 u_c A_0 + d_c u_0 A_0\Big] - \\ \Big[\gamma(d_c + u_c)\frac{\partial g_{10}}{\partial s} + v_c \frac{\partial g_{10}}{\partial n} - \frac{\partial}{\partial n}(nc + d_c + k_{n1})\Big]$$ (2.52)

The structure of f_{11} indicates the existence of two distinct additive contributions to g_{11}. The first is related to the structure of the flow field which establishes in movable bed meandering channels. The second, decaying exponentially with s, depends also on the transverse distribution of the contaminant at the injection section, embodied by g_{10}, and on the deviation k_{n1} of the transverse mixing coeffcient from its straight flow value. It is then suffcient to move a few mixing lengths, γL^*, downstream of the source, where g_{10} is no more a function of s and tends to vanish,

$$\frac{\partial g_{10}}{\partial n} = \frac{1}{d_0 \, k_{no}} - f_{10}\Big(\frac{1 + \delta\beta_c}{\delta\beta}\Big)^2 dn^*$$ (2.53)

to ensure that the specific effect of flow meandering on g_{11} dominates. Separating the variables (i.e., writing the forcing term as $f_{11} = p(s)q(n)$), and introducing a suitable Green function [Morse and Feshbach, 1953]. We eventually obtain:

$$
g_{11}(s;n) = \sum_{m=1}^{\infty} \cos[\mu_m(n+1)] \int_{0}^{s-\infty} p(s-\chi)e^{\frac{-\mu_m^2 \chi}{\gamma}\left(\frac{\delta\beta}{1+\delta\beta_c}\right)^2} d\chi
$$
$$
\int_{-1}^{1} q(n_0) \cos[\mu_m(n_0+1)]dn_0
$$
(2.54)

and hence,

$$
K_{s1} = \frac{1}{2}\int_{-1}^{1}(1 - u_0 \mathcal{A}_0)(d_0 g_{11} + d_1 g_{10}) \, dn
$$
$$
+\frac{1}{2}\int_{-1}^{1}(n\mathcal{C} - u_c\mathcal{A}_0 - u_0\mathcal{A}_1)d_0 g_{10} \, dn
$$
(2.55)

Chapter 3

Flow Field in a Straight Equilibrium Channel

3.1 Introduction

The velocity of a stream, is responsible for determining the size of particles a stream can transport, as well as the way in which it carries the particles, or load (Larson and Birkland, 1994). Velocity is dependent on several factors which such as:

- width and confinement

- roughness of bed, bank and bottom of channel,

- discharge

- amount of sediment

In general, the higher the gradient, the faster the flow. Streams mountainous areas are thus characterized by higher and much more irregular velocities (Figure 3.1). Wide, shallow rivers have usuallu a smaller gradient and hence, lower velocities. Therefore, the wide character of the sectionimplies a more regular distribution of

Figure 3.1: Example of a rock bed river (Source http://www.krisweb.com/ hydrol/ channel.htm).

Figure 3.2: Example of sand bed river (Source http://www.doi.gov/ restoration/ news/ UCR-Draft-Injury-Assessment-Plan.cfm).

the flow across the section (Figure 3.2). Several procedure have so far been proposed

to estimate the longitudinal dispersion coefficient from velocity measurements at a

number of cross sections [Fischer, 1967; Liu, 1977; Iwasa and Aia, 1991; Kashefipour and Falconer , 2002]. In many cases, however, the proposed predictor provides only a rough estimate of longitudinal dispersion and the discrepancy between predicted and observed coefficient is quite high. The transverse distribution of local flow depth strictly depends on the section shape of a natural river. Owing to its importance, the cross-sectional shape of stable channels has long been the subject of numerous investigations [ASCE, 1998]. The channel shapes proposed by different investigators can be classified into three types: cosine shaped, exponential shaped and parabolic shaped. However, these channel shapes are usually applicable to irregular canals or to the bank regions of straight rivers. To predict the cross-sectional shape of natural alluvial rivers, the channels are usually schematized with a central flat-bed region and two curvature bank regions [Vigilar and Diplas 1997]. The width of the flat-bed region is determined numerically. It means that no available channel shape equation can be directly used to describe the cross-sectional channel shape of natural rivers. To investigate the river channel shape and the flow field establishing within it, it is assumed that the river channel is straight, its cross sectionis symmetrical about its axis and constant along the river. The cross-sectional channel shape of an alluvial river is governed by its hydraulic geometry, namely the interrelationship among water discharge, channel width, flow depth, velocity, and so forth. The first attempt to obtain the longitudinal dispersion coefficient taking into account the flow field variation due to the transverse velocity distribution within a cross section of a straight channel was made by Sooky [Sooky, 1969]. He proposed a transverse velocity distribution made by a combination of the logarithmic velocity profile and the linear function for the triangular channel cross section. In order to fit the velocity data measured in the Sacramento River and the Old River in the U.S., Bogol [1997] suggested an empirical equation based on a fourth degree polynomial, It has been shown that, in some Sacramento Delta channels, values of longitudinal dispersion

were at least one order of magnitude greater than those derived from the measured velocity profiles [Bogol 1997]. Seo and Gadalrab [1999] proposed a combined form of a fourth-degree polynomial and an exponential function.They applied this equation to the velocity data collected in the Han River and the Naktong River, in South Korea [Seo and Gadalrab, 1999]. The prediction thus derived gives values on average greater than there provided by Seo and Cheong's [Seo and Cheong, 1998] equations. Deng et al. [2001] used a power-law distribution of the transverse velocity to determine the longitudinal dispersion coefficient in Fischer's triple integral expression [Deng et al.2001]. This mathematical model gives closer predictions in 60.3% of cases of observed data. The statistical model declared by Seo and Cheong [1998] gives closer predictions in 50% of cases of observed data. In the present thesis an transverse velocity profile is derived for irregular cross sections of natural streams. following the perturbation approach of Tubino and Colombini [1992]; this velocity distribution then is incorporated into the expression for estimating the longitudinal dispersion coefficient.

3.2   Reference System
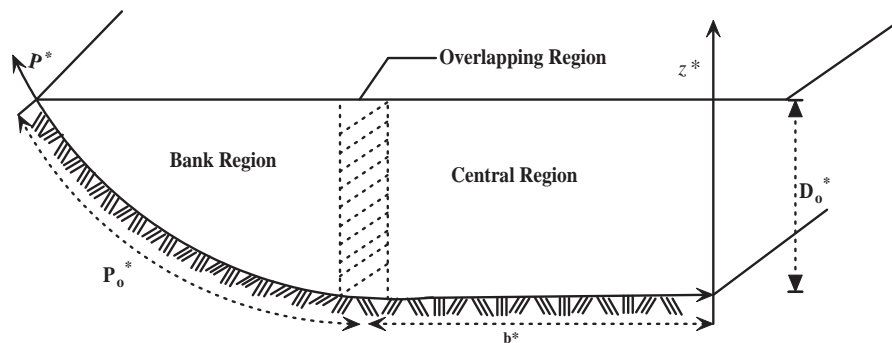
Figure 3.3: Sketch of the investigated half channel cross-section, divided into a center and a bank region, and relevant notations.

We consider the flow field of an incompressible fluid in a straight channel and assume that the bed is slowly variable in the transverse direction. This assumption allows for the adoption of a model of turbulence in which the turbulent viscosity ν_T^* is a function of the local flow condition. We want to determine the flow field and the bed shear stress distribution in a generic section of the channel, assumed to be in equilibrium. To this aim, the channel cross section (see Figure 3.3) is subdivided into
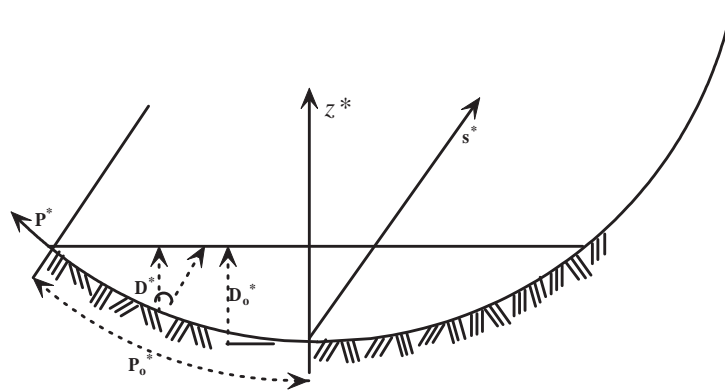
Figure 3.4: Sketch of the channel cross-section considered to determine the flow field in the bank region and relevant notations.

two distinct regions: i) a bank region and ii) a central region, In order to solve the flow field in the bank region, we consider the equilibrium section that is obtained by assuming that everywhere the bed shear stress equals the critical threshold for the sediment movement. We use the curvilinear coordinate system (s^*, p^*, z^*) shown in Figure (3.4), where s^* is the longitudinal coordinate, p^* is the transverse curvilinear coordinate (with origin at the channel axis) and z^* is the axis normal to the bed. Because of the transverse axis curvature, lateral distances measured along different transverse coordinate surfaces are in general not equal when moving from one normal co-ordinate surface to another, we need to introduce the metric coefficient

$$h_p = 1 - \frac{z^*}{R^*} \tag{3.1}$$

where R^* is the local axis of curvature of the cross-section bed profile. It can be easily demonstrated that, denoting by D^* the local flow depth, the local curvature radius reads:

$$R^* = -\frac{1}{\cos \beta} \frac{\partial^2 D^*}{\partial p^*}$$
(3.2)

with β the angle that the vertical forms with the normal to the cross sectionbed, resulting from the relation

$$\cos \beta = \sqrt{\left(1 - \frac{\partial^2 D^*}{\partial p^*}\right)}$$
(3.3)

3.3 Longitudinal Momentum Conservation Equation

Observing that in the investigated problem the horizontal scale of the relevant hydrodynamic processes largely exceeds the flow depth, we can assume that the pressure is distributed hydrostatically along the vertical and replace the pressure and the gravitational term with the gradient of the water surface elevation. Under the as-

Figure 3.5: Sketch of the investigated cross-section and notations.

sumption of uniform flow conditions, the longitudinal momentum equation, averaged over turbulence, then reads:

$$\frac{\partial U^*}{\partial t^*} + U^*\frac{\partial U^*}{\partial s^*} + \frac{V^*}{h_p}\frac{\partial U^*}{\partial p^*} + W^*\frac{\partial U^*}{\partial z^*} + \frac{V^*W^*}{h_p}\frac{\partial h_p}{\partial z^*} = -\rho g\frac{\partial H^*}{\partial s^*} + \frac{1}{h_p}\left[\frac{\partial(h_pT^*_{ss})}{\partial s^*} + \frac{\partial T^*_{ps}}{\partial p^*} + \frac{\partial(h_pT^*_{zs})}{\partial z^*}\right]$$

(3.4)

with U^*, V^*, W^* the components of the velocity along the three coordinate axes, H^* the elevation of water surface with respect to a given, p the pressure, ρ the water density, g the gravitational constant, h the elevation with respect to a given datum, and on T^*_{ss}, T^*_{ps}, T^*_{zs} the s^* component of the stress tensor of normal s^*, p^* and z^*.

We then take advantage of the uniform character of the turbulent flow in the longitudinal direction, simplifying equation (3.4) as

$$\frac{\partial T^*_{ps}}{\partial p^*} + \frac{\partial h_p T^*_{zs}}{\partial z^*} = \rho g h_p\frac{\partial H}{\partial s^*}$$

(3.5)

In order to specify the distributions along the normal to the bed of both the eddy viscosity ν_T^* and of the longitudinal velocity u^*, we write:

$$\nu_T^*(z^*) = u_* D_z^* \mathcal{N}(z^*),$$

(3.6)

with $\mathcal{N}(z^*)$ a function giving the required distributions, u_* $(= (\tau^*/\rho)^{0.5})$ the friction velocity, D_z^* the distance of the water surface from the bed and D^* the local flow depth. Moreover assuming the classical eddy viscosity closure to the stress tensor we can write:

$$\left(T^*_{ss}, T^*_{ps}, T^*_{zs}\right) = \rho\,\nu_T\left(\frac{\partial u}{\partial s^*}, \frac{1}{h_p}\frac{\partial u}{\partial p^*}, \frac{\partial u}{\partial z^*}\right)$$

(3.7)

We are interested to estimate the shear stresses τ^* acting at the channel bed, re-

sponsible of its morphological evolution. The instantaneous value of τ at each node of a given transect (see Figure 3.6) is calculated by considering the longitudinal momentum conservation equation (3.4). We next integrate the equation (3.5) along z^*, from the bed (at $z^* = 0$) to the free surface (at $z^* = D_z^*$),, requiring that the longitudinal shear stresses vanishes at the free surface, and takes the value τ^* at the bed:

$$\left[T_{z^*s^*} - \frac{1}{h_p} \frac{\partial D_z^*}{\partial p} T_{p^*s^*} \right]_{z^*=D_z^*} = 0, \qquad [T_{z^*s^*}]_{z^*=0} = \tau \qquad (3.8)$$

where $S = -\partial H^*/\partial s^*$ is the longitudinal slope of the water surface.

Figure 3.6: Bed shear stress of the investigated cross-section and notations.

3.4 Scaling and Expansion

In order to investigate the order of magnitude of the various terms contributing to equation (3.4) it is useful to make it dimensionless introducing the following scaling:

$$D_{z^*} = D_0^* \frac{D}{\sqrt{1 - \delta^2(\frac{\partial D}{\partial \eta^b})^2}}, \quad z = \frac{z^*}{D_z^*}, \quad \eta^b = \frac{p^*}{P_0^*}, \quad D = \frac{D^*}{D_0^*},$$

$$U = \frac{U^*}{\sqrt{gSD_0^*}}, \quad \nu_T = \frac{\nu_T^*}{D_0^* \sqrt{gSD_0^*}} \tag{3.9}$$

$$F_1 = \frac{1}{D} \frac{\partial D}{\partial \eta^b} \left[1 + \frac{\delta^2 D}{1 - \delta^2(\frac{\partial D}{\partial \eta^b})^2} \frac{\partial^2 D}{\partial(\eta^b)^2} \right], \quad F_2 = \frac{\sqrt{1 - \delta^2(\frac{\partial D}{\partial \eta^b})^2}}{D},$$

$$h_{\eta^b} = \frac{z\,D}{1 - \delta^2(\frac{\partial D}{\partial \eta^b})^2} \frac{\partial^2 D}{\partial(\eta^b)^2} \tag{3.10}$$

where D_0^* is the mean flow depth in the central region (see Figure 3.3) and P_0^* is the wetted perimeter of the bank under uniform flow conditions (hereafter a star apex will denote dimensional quantities). We assume that the bed variations of the cross section profile are slow enough such that the dimensionless parameter $\delta = \frac{D_0^*}{P_0^*}$ is small. Taking advantage of this fact, we expand the dimensionless form of equation (3.4) in terms of δ, obtaining:

$$F_2^2 \frac{\partial}{\partial z} \left[(1 + \delta^2 h_{\eta^b}) \nu_T \frac{\partial U}{\partial z} \right] + \delta^2 \left(\frac{\partial}{\partial \eta^b} - zF_1 \frac{\partial}{\partial z} \right) \left[\frac{\nu_T}{1 + \delta^2 h_{\eta^b}} \left(\frac{\partial}{\partial \eta^b} - zF_1 \frac{\partial}{\partial z} \right) U \right] +$$

$$1 + \delta^2 h_{\eta^b} = 0 \tag{3.11}$$

The dimensionless turbulent viscosity then can be expressed as:

$$\nu_T = \frac{u_f\,D}{\sqrt{1 - \delta^2(\frac{\partial D}{\partial \eta^b})^2}} \mathcal{N}(z) \tag{3.12}$$

where $u_f = u_f(\eta^b)$ is the dimensionless friction velocity along the section wetted perimeter, scaled as $u_f = u^*/(gSD_0^*)^{1/2}$ and, hence, expressed as

$$u_f = \mathcal{N}\frac{\partial U}{\partial z}\Big|_{z=0} \tag{3.13}$$

In the following we will assume either $\mathcal{N}(z) = 1/13$ [Engelund, 1964] a parabolical distribution corrected for the presence of the wake function [Dean, 1974], namely:

$$\mathcal{N}(z) = \frac{\kappa\, z(1-z)}{1 + 2Az^2 + 3Bz^3} \tag{3.14}$$

with $\kappa\ (= 0.41)$, the von Karman constant, $A = 1.84$ and $B = -1.56$.

Taking advantage of the slow variability of the boundary (i.e., $\delta^2 \ll 1$), we introduce the following expansions for the bank region:

$$(U^b, u_f^b) = (U_0^b, u_{f_0}^b) + \delta^2(U_1^b, u_{f_1}^b) + O(\delta^4) \tag{3.15}$$

and the central region:

$$[U^c, u_f^c] = [U_0^c, 1] + \delta^2[U_1^c, u_{f_1}^c] + O(\delta^4) \tag{3.16}$$

However,in order to ensure that the solution at the river banks matches the solution obtained for the central part of the cross section, we must modify the expansion in the bank region as follows:

$$(U^b, u_f^b) = (U_0^b, u_{f0}^b) + \delta^2(U_1^b + U_1^H, u_{f_1}^b + u_{f_1}^H) + O(\delta^4) \tag{3.17}$$

where U_1^H and u_{f1}^H are provided by the homogeneous solution of the boundary value problem. We next introduce the following expansion for the entire channel cross

section:

$$(\hat{u}, u_f) = (\hat{u}_0, u_{f0}) + \delta^2(\hat{u}_1, u_{f0}) + O(\delta^4) \tag{3.18}$$

We can solve the governing equation for bank region, central region, for patching of solution and for overall entire cross section of the channel for various order of the above equatios written for $\mathcal{O}(\delta^0)$ and $\mathcal{O}(\delta^2)$.

3.5   Flow field in the Bank Region

In the following equation (3.11) is solved to find the flow field for bank region. The boundary condition to be associated with the equation requires that the flow velocity at the bed is given by the classical logarithmic profile, i.e:

$$U|_{z=0} = u_f \left[2 + 2.5\, ln \left(\frac{D}{d_{gr}\sqrt{1 - \delta^2(\frac{\partial D}{\partial \eta^b})^2)}} \right) \right] \tag{3.19}$$

with d_{gr} $(= d_{gr}^*/D_0^*)$ the dimensionless grain roughness. Moreover we prescribe that the stress at the water surface vanishes while at the bed takes the value τ_0, namely:

$$\left[\nu_T(\frac{1}{D}\frac{\partial U}{\partial z} - \frac{\delta^2}{1 + \delta^2 h_{p_1}}\frac{\partial D}{\partial \eta^b}) \right]_{z=1} = 0, \qquad \left[F_2\nu_T\frac{\partial U}{\partial z} \right]_{z=0} = u_f^2 \tag{3.20}$$

Substituting expansions (3.15) into equation (3.11) with the conditions (3.19) and (3.20), at the various order of approximation we find:

- $O(\delta^0)$

$$u_{f_0}^b(\eta^b) = \sqrt{D} \tag{3.21}$$

$$U_0^b(z, \eta^b) = \left(-\frac{z^2}{2N} + \frac{z}{N} + 2 + \frac{5}{2}ln\frac{D}{d_{gr}} \right) \sqrt{D} \tag{3.22}$$

- $O(\delta^2)$

$$u_{f_1}^b(\eta^b) = \frac{\sqrt{D}}{13}\left[\left(5 + \frac{5}{8}ln\frac{D}{d_{gr}}\right)D\frac{\partial^2 D}{\partial\eta^{b2}} + \left(\frac{59}{8} + \frac{5}{4}ln\frac{D}{d_{gr}}\right)\left(\frac{\partial D}{\partial\eta^b}\right)^2\right]\tag{3.23}$$

$$U_1^b(z,\eta^b) = \sqrt{D}\left[\left\{\left(\frac{45}{8}\ln(\frac{D}{d_{gr}}) + \frac{7}{2} + \frac{25}{16}\ln(\frac{D}{d_{gr}})^2\right)N + \right.\right.$$
$$\left(-\frac{7}{8} - \frac{5}{16}\ln(\frac{D}{d_{gr}})\right)z^2 + \left(\frac{7}{4} + \frac{5}{8}\ln(\frac{D}{d_{gr}})\right)z +$$
$$\frac{5}{8}\ln(\frac{D}{d_{gr}}) + \frac{1}{2} + \frac{1}{N}\left(\frac{1}{4}z - \frac{1}{16}z^4 + \frac{1}{4}z^3 - \frac{3}{8}z^2\right)\right\}$$
$$D\frac{\partial^2 D}{\partial\eta^{b2}} + Bigg\{\left(\frac{205}{16}\ln(\frac{D}{d_{gr}}) + \frac{33}{4} + \frac{25}{8}\ln(\frac{D}{d_{gr}})^2\right)N -$$
$$\frac{5}{16}z^2 + \left(\frac{33}{8} + \frac{5}{4}\ln(\frac{D}{d_{gr}})\right)z + 2 + \frac{15}{16}\ln(\frac{D}{d_{gr}}) +$$
$$\left.\frac{1}{N}\left(-\frac{1}{16}z^2 - \frac{1}{16}z^4 + \frac{1}{12}z^3 - \frac{3}{8}z\right)\right\}\left(\frac{\partial D}{\partial\eta^b}\right)^2\right]\tag{3.24}$$

In particular, the longitudinal velocity at the bed (i.e. at $z = 0$,) reads:

$$U_{10}^b(z = 0,\eta^b) = \sqrt{D}\left[\left\{\frac{1}{13}\left(\frac{7}{2} + \frac{35}{4}\ln(\frac{D}{d_{gr}})\right) + \frac{5}{8}\ln(\frac{D}{d_{gr}}) + \frac{1}{2}\right\}D\frac{\partial^2 D}{\partial(\eta^b)^2} + \right.$$
$$\left.\left\{\frac{1}{13}\left(\frac{33}{4} + \frac{305}{16}\ln(\frac{D}{d_{gr}})\right) + \frac{15}{16}\ln(\frac{D}{d_{gr}}) + 2\right\}\left(\frac{\partial D}{\partial\eta^b}\right)^2\right]\tag{3.25}$$

Clearly, in order to determine the values attained by the friction velocity and the longitudinal velocity described by equations (3.21), (3.23) and (3.22), (3.24), we must specify the bed roughness d_{gr} (e.g., $3d_{90}$ or $2d_{50}$, with d_{50} and d_{90} provided by the grain size distribution of bed sediment) and, more importantly, the distribution of the flow depth $D(\eta^b)$ across the section. This latter distribution is obtained by assuming that the friction velocity at the bed is equal to the threshold value for sediment incipient motion and at the leading order of approximation takes the form

of parabola [Glover and Florey, 1951], namely:

$$D(\eta^b) = 1 - (\eta^b)^2 \tag{3.26}$$
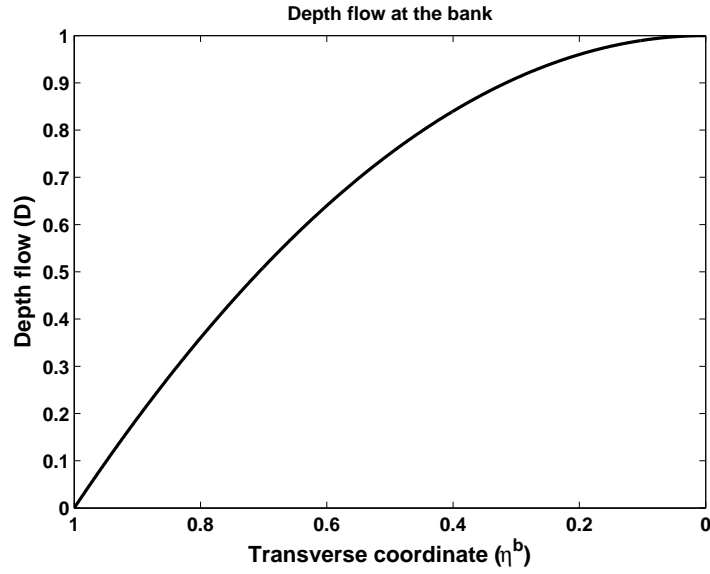
Figure 3.7: Depth of the flow at bank region as a fuction of the transverse coordinate η^b.
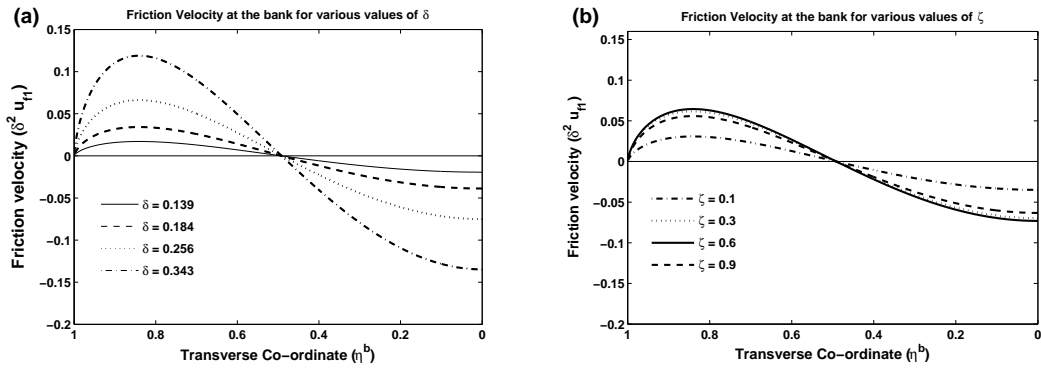
Figure 3.8: The second order correction to the friction velocity is plotted as a function of the transverse co-ordinate η^b at the bed of the bank region: (a) u_{f1}^b for constant value of $\mathcal{N} = \frac{1}{13}$ and various values of δ, (b) u_{f1}^b for $\delta = 0.256$ and $\mathcal{N}(z) = \frac{kz(1-z)}{1+2Az^2+3Bz^3}$ (here, $k = 0.41$).
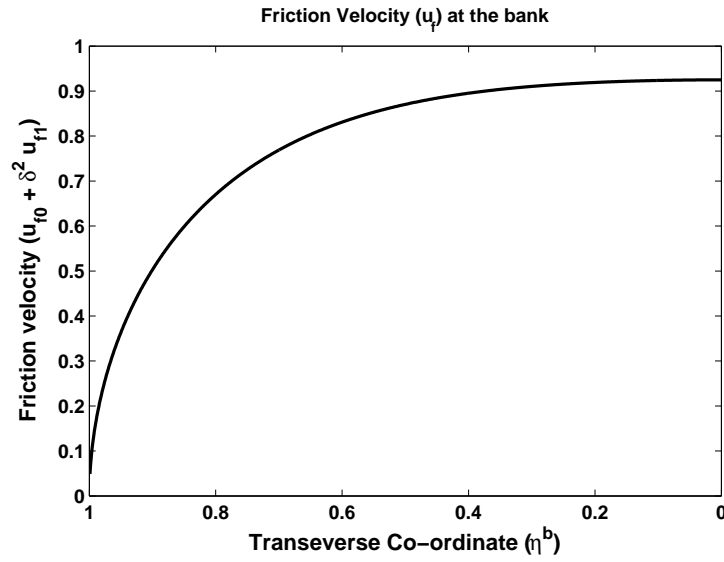
Figure 3.9: The friction velocity u_f^b $(= u_{f0}^b + \delta^2 u_{f1}^b)$ is plotted versus the transverse curvilinear coordinate η^b of the bank region for, $d_{gr} = 0.02$, and a parabolic profile $\mathcal{N} = \frac{1}{13}$.
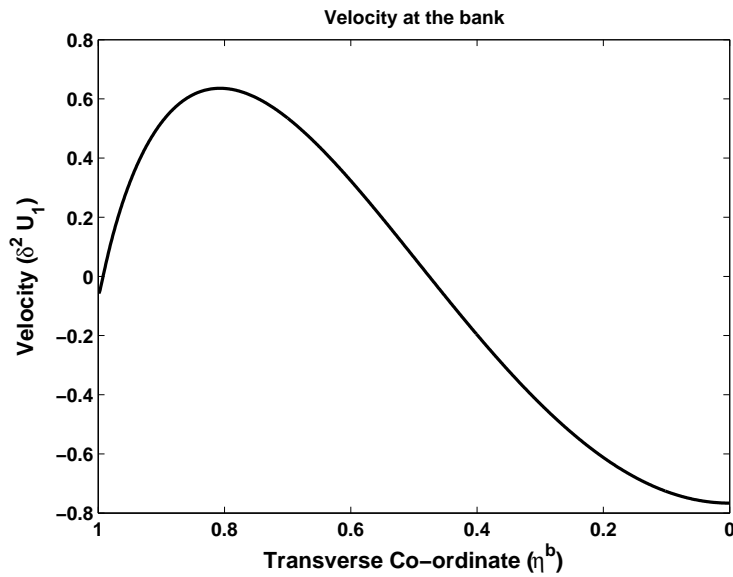
Figure 3.10: The second order velocity $\delta^2 U_1^b$ is plotted as a function of the transverse coordinate η^b at the bed of the bank region ($z = 0$), $\mathcal{N} = \frac{1}{13}$, $\delta = 0.256$ and $d_{gr} = 0.02$.
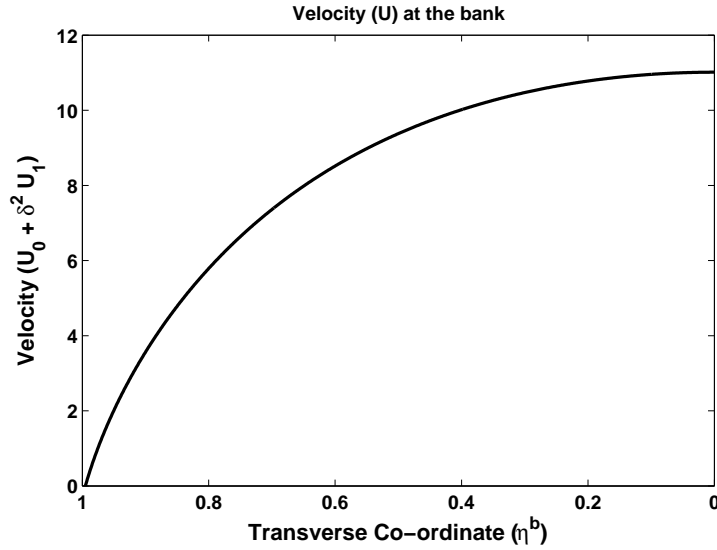
Figure 3.11: The velocity $U^b = U_0^b + \delta^2 U_1^b$ is plotted as a function of the curvilinear coordinate p in the bank region for $(z = 0)$, $\mathcal{N} = \frac{1}{13}$, $\delta = 0.256$ and $d_{gr} = 0.02$.

Figure (3.8) reports the transverse distribution of the $\mathcal{O}(\delta^2)$ correction to the dimensionless friction velocity $\delta^2 u_{f1}^b$ for various values of the relevant parameters while figure (3.9) presents the transverse distribution of the overall dimensionless friction velocity u_f^b. Both Figures (3.10) and (3.11) refer to the case of a parabolic bank profile. Figure (3.8) (b), on the other hand, reports velocity for $\zeta = 0.1$, 0.3, 0.6 and 0.9 at bank for $D(\eta^b)$.

3.5.1 Flow field in the central region

In the central region (see Figure 3.3), where $\partial D / \partial \eta^c = 0$, the differential problem given by equation (3.11), complemented by the boundary conditions (3.19) and (3.20), can be rewritten in terms of the transverse coordinate η^c $(= p^*/D_0^*)$, and takes the form:

$$\frac{\partial}{\partial z}(\nu_T^c \frac{\partial U^c}{\partial z}) + \frac{\partial}{\partial \eta^c}(\nu_T^c \frac{\partial U^c}{\partial \eta^c}) = -1 \qquad (3.27)$$

under the conditions:

$$\left.\frac{\partial U^c}{\partial z}\right|_{z=1} = 0, \qquad U^c|_{z=0} = u_f^c[2 - 2.5ln(d_{gr})], \tag{3.28}$$

$$\nu_T^c \left.\frac{\partial U^c}{\partial z}\right|_{z=0} = (u_f^c)^2, \qquad \frac{\partial U^c}{\partial \eta^c}|_{\eta^c=0} = 0, \qquad U^c|_{\eta^c=\beta} = U^b|_{\eta^b=0}. \tag{3.29}$$

Stipulating that $\tau = 0$ at the water surface, $\tau = \tau_b$ at the bed , $\beta_c = b^*/D_0^*$ and that the velocities has to match in the overlapping region located between the bank region and central region.
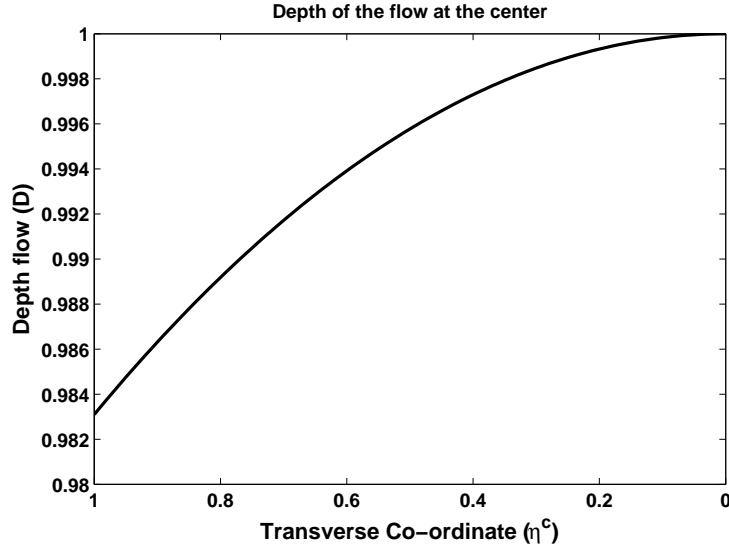
Figure 3.12: Depth of the flow in central region, the relation between the transverse coordinate η^b and η^c of the bank and central region is $\eta^b = \eta^c\delta$.

The $O(\delta^0)$ solution can be obtained by a simple integration, and reads:

$$U_0^c(z) = \frac{z}{N} - \frac{z^2}{2N} + (2 - 2.5\ln(d_{gr})), \qquad u_{f0}^c = 1 \tag{3.30}$$

The $O(\delta^2)$ solution can be obtained by separating the variables and assuming a solution of the form:

$$U_1^c(z, \eta^c) = \sum_k A_k^c \frac{\cosh(\lambda_k \eta^c)}{e^{\lambda_k \beta}} F_k(z) \tag{3.31}$$

where

$$F_k(z) = \cot \lambda_k \cos(\lambda_k z) - \cot \lambda_k + \sin(\lambda_k z) + R\lambda_k, \qquad R = \frac{1}{13}[2 - 2.5ln(d_{gr})] \tag{3.32}$$

where the coefficients A_k^c are obtained by solving the linear systems

$$A_k^c C_{km} = b_m \quad (m = 0, 1, 2, ...) \tag{3.33}$$

with $C_{\lambda m}$ and b_m derived from equations (3.31) and (3.15), and reading:

$$C_{km} = -\frac{2\lambda_k^2 \cot(\lambda_k)}{M\pi[\lambda_k^2 - (M\pi)^2]}, \qquad b_m = \frac{23 - \frac{5}{4}\ln(d_{gr}) - \frac{39}{(M\pi)^2}}{(M\pi)^3} \left.\frac{\partial^2 D}{\partial(\eta^b)^2}\right|_{\eta^b=0}, \tag{3.34}$$
$$M = \frac{2m+1}{2}.$$

Values of A_k^c are:

$$A_{k1}^c = -10.8494, \quad A_{k2}^c = -0.3352, \quad A_{k3}^c = -0.0166, \quad A_{k4}^c = -0.0023,$$

$$A_{k5}^c = -0.0005, \quad A_{k6}^c = -0.0002, \quad A_{k7}^c = -0.0001, \quad A_{kj}^c = 0 \quad j \geq 8 \tag{3.35}$$

At the channel bed $(z = 0)$ it then results:

$$U_1^c(0, \eta^c) = \sum_k A_k^c R\lambda_k \frac{\cosh(\lambda_k \eta^c)}{e^{\lambda_k \beta_c}} \tag{3.36}$$

The friction velocity at the bed then yields:

$$u_{f1}^c = N(0)\left.\frac{\partial U_1^c}{\partial z}\right|_{z=0} = \sum_k A_k^c \frac{\lambda_k}{13} \frac{\cosh(\lambda_k \eta^c)}{e^{\lambda_k \beta_c}} \tag{3.37}$$

where the eigenvalues λ_k are the positive roots of the equation:

$$\lambda_k \cot(\lambda_k) = R\,\lambda_k^2 - 1 \tag{3.38}$$

namely: $\lambda_1 = 1.25$, $\lambda_2 = 3.48$, $\lambda_3 = 6.46$, $\lambda_4 = 9.54$, $\lambda_5 = 12.65$, $\lambda_6 = 15.78$, $\lambda_7 = 18.91$, $\lambda_8 = 22.04$, $\lambda_9 = 25.17$, $\lambda_{10} = 28.31$, $\lambda_{11} = 31.45$, $\lambda_{12} = 34.59$, $\lambda_{13} = 37.73$, $\lambda_{14} = 40.86$, $\lambda_{15} = 44.0\ldots$.
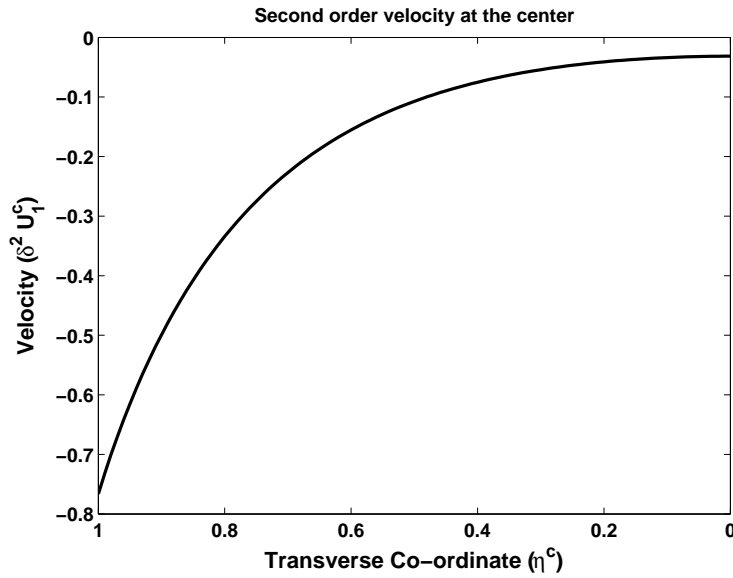
Figure 3.13: The second order contribution to the velocity $(= \delta^2 U_1^c)$, is plotted as a function of the transverse coordinate η^c in the central part of the cross section for $\delta = 0.30328$, $d_{gr} = 0.02$ and $\beta_c = 3$.

Figure (3.12) represents the depth of flow for the central coordinte system such that $D = 1$ at the cross section $\eta^c = 0$. Figure (3.13) shows second order velocity in central region, $\delta^2 U_1^c$, while the Figure (3.14) shows the transverse distributions of the overall velocity U^c.

The solution (3.31) quantifies the effect of bank region on the flow field in the central region. In the absence of these effects the velocity profile (and hence the depth averaged velocity, as well as the friction velocity) would not vary in the trans-
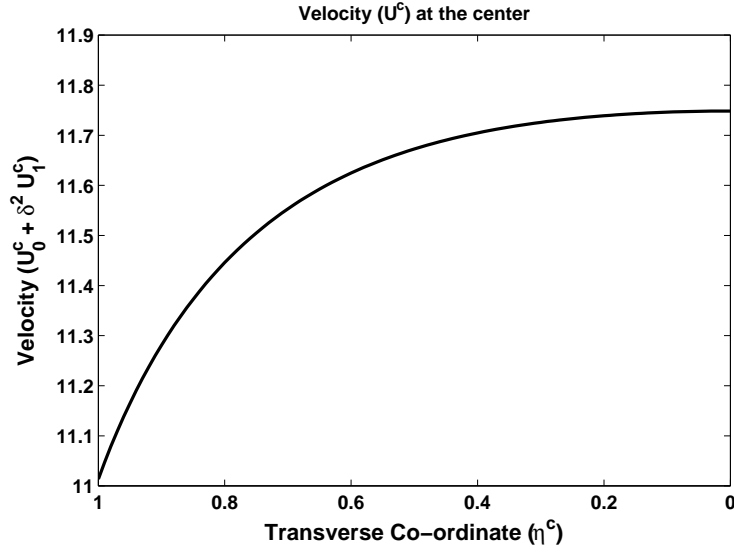
Figure 3.14: The velocity $U^c = U_0^c + \delta^2 U_1^c$, is plotted as a function of the transverse coordinate η^c in the central part for $\delta = 0.30328$, $d_{gr} = 0.02$ and $\beta_c = 3$.
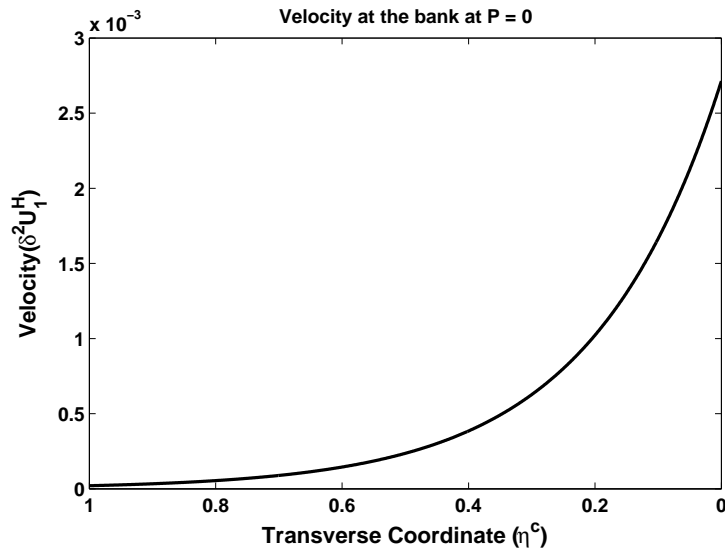
Figure 3.15: The second order contribution to the velocity $\delta^2 U_1^H$ is plotted as a function of the transverse coordinate η^c of the central region for $\delta = 0.256$, $d_{gr} = 0.02$ and $\beta_c = 4$.

verse direction. This effect is proportional to δ^2 and increases with decreasing β_c

and, conversely, it decreases with increasing β_c. Indeed,

$$\lim_{\beta_c \to 0} \frac{\cosh(\lambda_k p)}{e^{\lambda_k \beta_c}} = 1, \qquad \lim_{\beta_c \to \infty} \frac{\cosh(\lambda_k \eta^c)}{e^{\lambda_k \beta_c}} = \frac{1}{2} \qquad (3.39)$$

3.5.2   Patching of the solutions
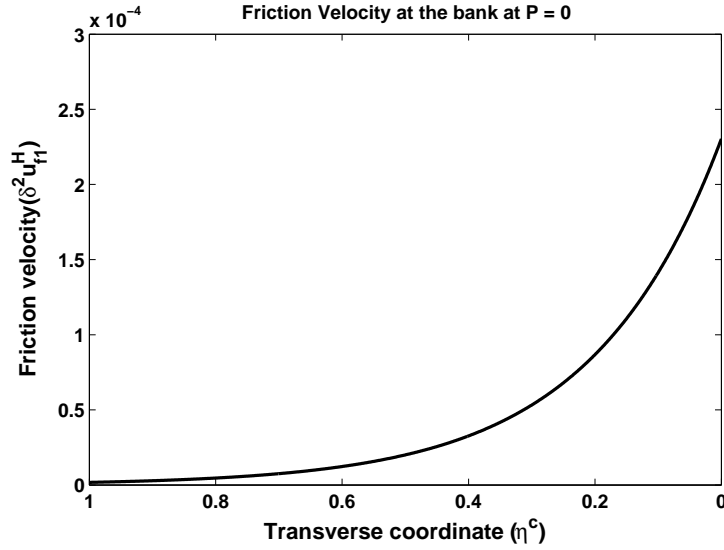
Figure 3.16: The friction velocity $\mathcal{O}(\delta^2)$ is plotted as a function of the transverse coordinate η^c for $\delta = 0.256$, $d_{gr} = 0.02$ and $\beta_c = 4$.

The homogeneous solution of equation (3.27) is used to match together the bank and central region solutions under the assumption that the overlapping is concentrated in a layer of thickness $O(\delta)$ near the section $\eta^b = 0$ (i.e., $p = \beta_c$). In this layer we can assume that:

$$D = 1 + \mathcal{O}(\delta^2), \qquad \frac{\partial D}{\partial \eta^c} = \mathcal{O}(\delta^2), \qquad \frac{\partial^2 D}{\partial (\eta^c)^2} = \mathcal{O}(\delta^2) \qquad (3.40)$$

Moreover, recalling the boundary conditions (3.20), in the limit of $\eta^b \to 0$ (i.e, $\eta^c \to \beta_c$), we require that:

$$\lim_{\eta^c \to \beta_c} U_1^H \longrightarrow 0, \qquad \left.\frac{\partial U_1^H}{\partial \eta^c}\right|_{\eta^b=0} = \left.\frac{\partial U_1^c}{\partial \eta^c}\right|_{\eta^c=\beta_c} \tag{3.41}$$

The solution that meets these conditions is:

$$U_1^H(z, \eta^c) = \sum_k -A_k^c \frac{\sinh(\lambda_k \beta_c)}{e^{\lambda_k \beta_c}} e^{-\lambda_k(\eta^c + \beta_c)} F_k(z) \tag{3.42}$$

Figure (3.16) shows second order corrected bank region friction velocity $\delta^2 u_{f1}^H$ at central region. It then turns out that, at the bed $(z = 0)$,

$$U_1^H(0, \eta^c) = -\sum_k A_k^c R \lambda_k \frac{\sinh(\lambda_k \beta_c)}{e^{\lambda_k \beta_c}} e^{-\lambda_k(\eta^c + \beta_c)} \tag{3.43}$$

$$u_{f1}^H = N \left.\frac{\partial U_1^c}{\partial z}\right|_{z=0} = \frac{1}{13} \left.\frac{\partial U_1^c}{\partial z}\right|_{z=0} \tag{3.44}$$

and, hence,

$$u_{f1}^H = -\sum_k A_k^c \frac{\lambda_k}{13} \frac{\sinh(\lambda_k \beta_c)}{e^{\lambda_k \beta_c}} e^{-\lambda_k(\eta^c + \beta_c)} \tag{3.45}$$

3.5.3 Overall solution

In order to solve the flow field, we consider the equilibrium stable channel section that, under uniform flow conditions, is obtained by assuming that everywhere the bed shear stress equals the critical threshold for sediment movement. We assume the curvilinear coordinate system (s^*, n^*, z^*) shown in Figure (3.17), where s^* is the longitudinal coordinate, n^* is the transverse curvilinear coordinate (with origin at the channel axis) and z^* is the axis normal to the bed. The cross section in subdivide in i) a central region, of width $2b^*$ and depth D_0^* and ii) two bank regions, of width

$(B^* - b^*)/2$, varying flow depth d^* and a overall wetted perimeter P_0^* (see Figure (3.17)).
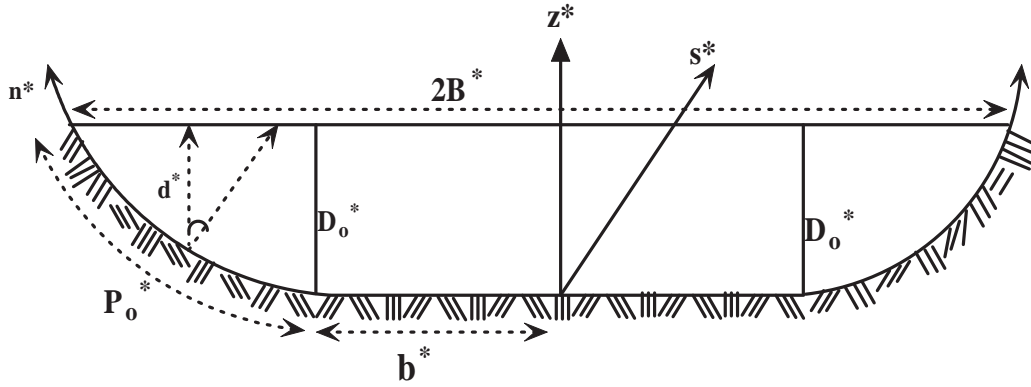
Figure 3.17: Sketch of the entire channel cross-section considered to determine the flow field and related notations.
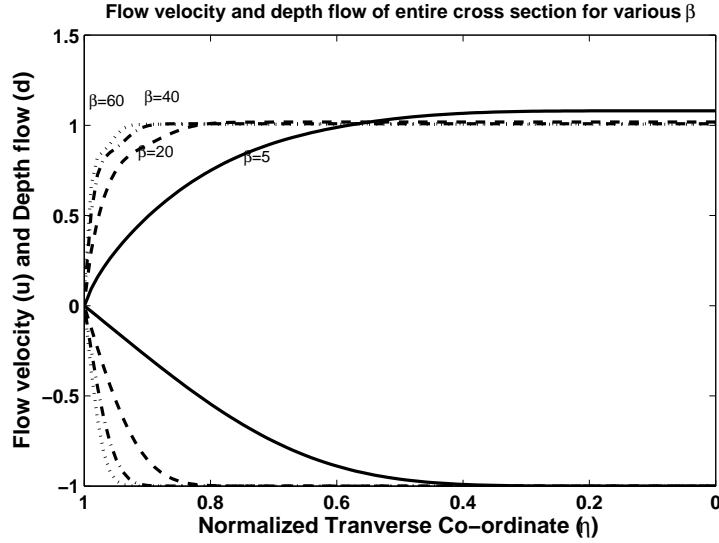
Figure 3.19: Depth of flow and corresponding velocity of entire cross section is plotted as a function of the normalized co-ordinate η, $D = erf\left(\beta(1 - \sqrt{(\eta)})\right)$.

Under the assumption of uniform flow conditions, the longitudinal momentum

Depth flow of the entire cross section for various β
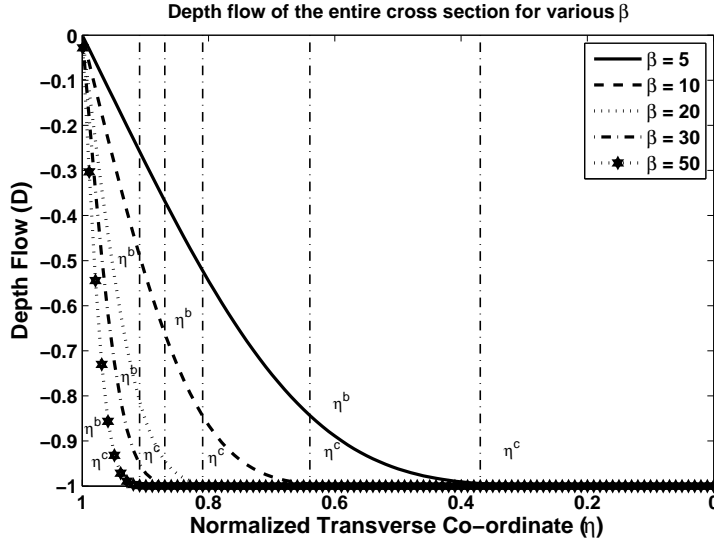
Figure 3.18: Depth of flow of entire cross section is plotted as a function of the normalized co-ordinate η for a bank region profile for the type, $D = erf\Big(\beta(1 - \sqrt{(\eta))}\Big)$.

Friction Velocity ($\delta^2 u_{f1}$) of entire cross section for β_c = 4 and δ = 0.256
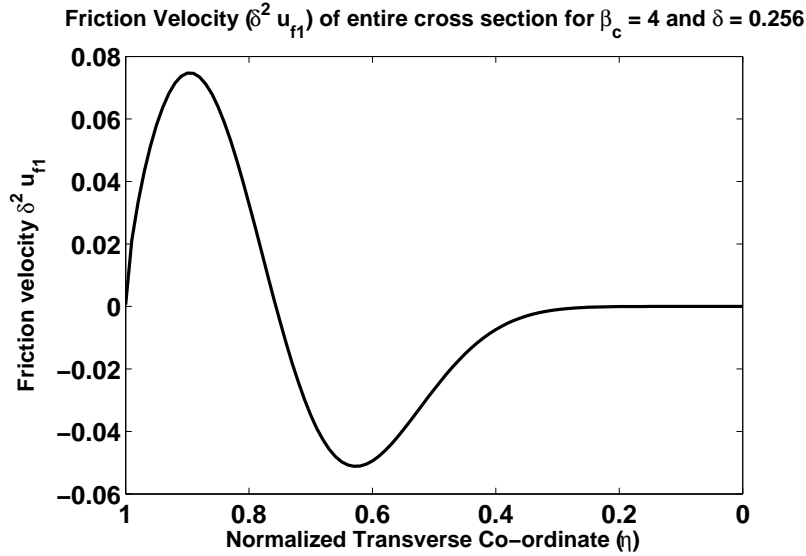
Figure 3.20: The corrected friction velocity u_f $(= \delta^2 u_{f1})$ of entire cross section as a function of the transverse coordinate η for $\delta = 0.256$, $k_s = 0.02$ and $\beta = 4$.

equation, averaged over turbulence, reads:

$$\frac{\partial}{\partial z^*}\Big(h_\eta \nu_T^* \frac{\partial u^*}{\partial z^*}\Big) + \frac{\partial}{\partial n^*}\Big(\frac{\nu_T^*}{h_\eta}\frac{\partial u^*}{\partial z^*}\Big) + gSh_\eta = 0 \tag{3.46}$$
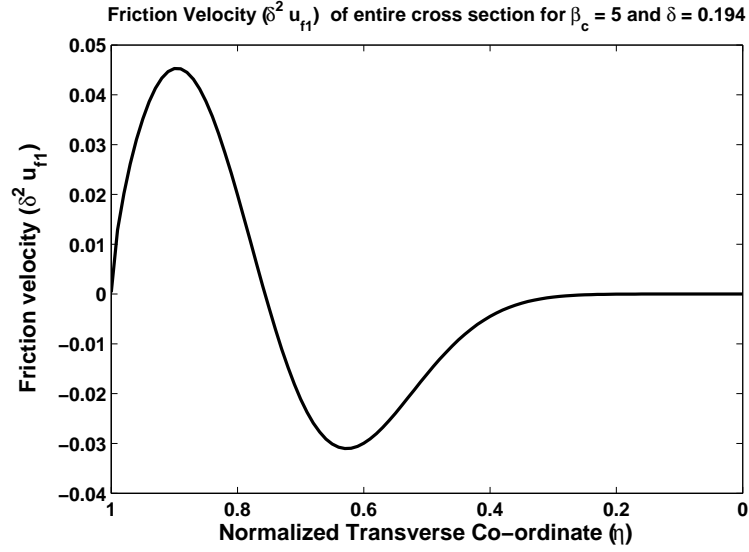
Figure 3.21: Friction velocity $\delta^2 u_{f1}$ is plotted as a function of the normalized co-ordinate (η) across the entire equilibrium section for $\delta = 0.194$, $k_s = 0.02$ and $\beta = 5$.
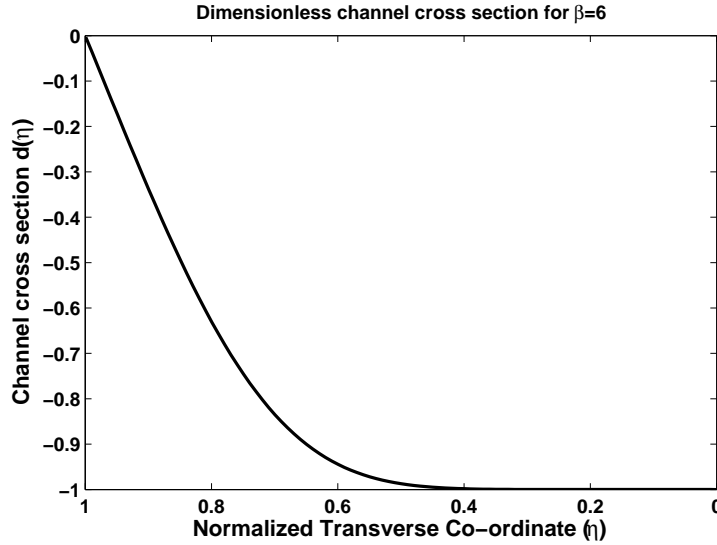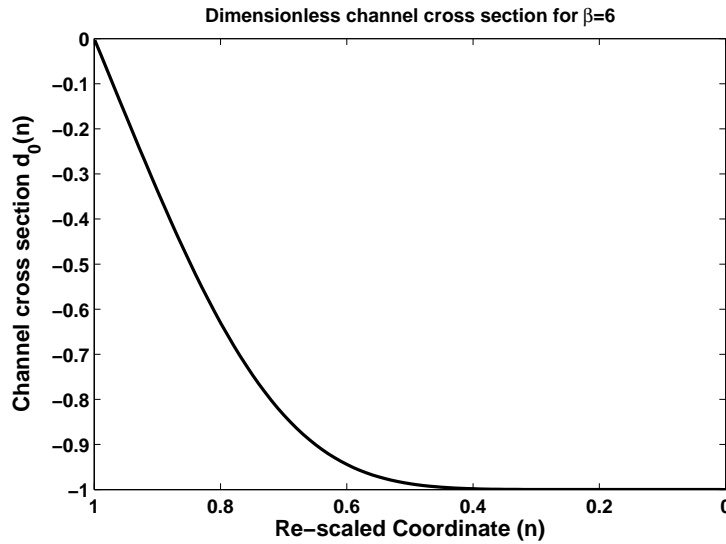

Figure 3.22: Channel cross section (of the friction velocity given below) is plotted as a function of the normalized co-ordinate $D = erf\left(\beta(1 - \sqrt{(\eta)})\right)$ for $\beta = 6$.

where g is the gravitational constant, S is channel bed slope, $u^*(z^*, n^*)$ is the turbulence averaged longitudinal velocity component, ν_T^* is the turbulent viscosity and
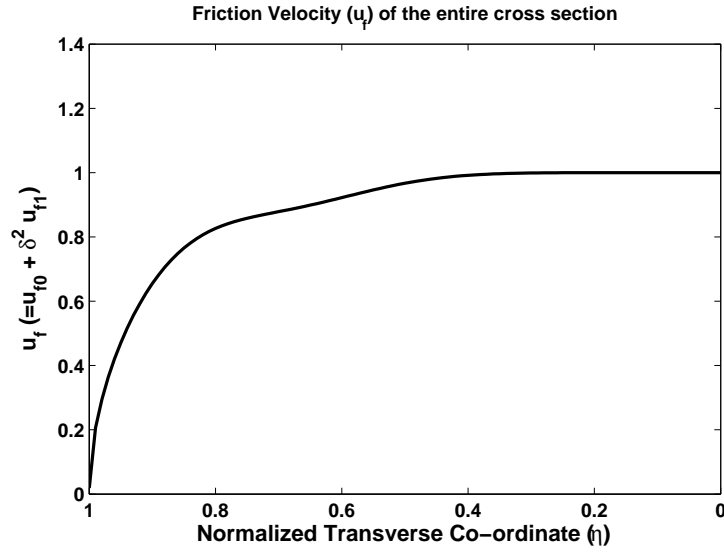
Figure 3.23: The corrected friction velocity u_f $(= u_{f0} + \delta^2 u_{f1})$ of entire cross section as a function of the transverse coordinate η for $\delta = 0.256$, $d_{gr} = 0.02$ and for $\beta = 6$.
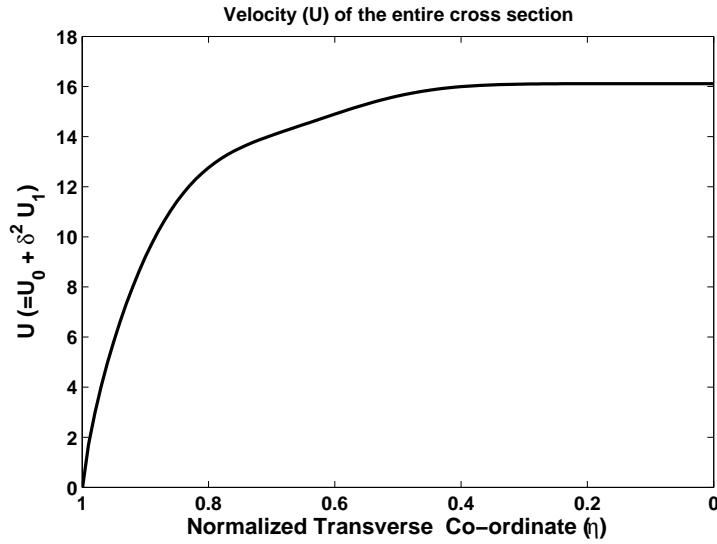
Figure 3.24: The corrected velocity $(= U_0 + \delta^2 U_1)$ of entire cross section as a function of the transverse coordinate η for $\delta = 0.256$, $d_{gr} = 0.02$.

h_η is the transverse metric coefficiente defined as:

$$h_\eta = 1 + z^* \frac{\partial^2 d^*/\partial n^{*2}}{\sqrt{1 - (\partial d^*/\partial \eta^*)^2}} \tag{3.47}$$

In order to express the solution with respect to a unique reference system, we introduce the normalized coordinate η defined as:

$$\eta = \frac{n^*}{P_0^* + b^*} \tag{3.48}$$

Expressing the governing equation (3.46) in terms of dimensionless co-ordinate n, and assuming that the transverse variations of the transverse profile are slow (i.e., the dimensionless parameter $\delta = D_0^*/P_0^*$ is small), $\beta_c = \frac{b^*}{D_0^*}$ then yields,

$$F_2^2 \frac{\partial}{\partial z}\left[\left(1 + (\frac{\delta}{1+\delta\beta_c})^2 h_{\eta_1}\right)\nu_T \frac{\partial \hat{u}}{\partial z}\right] + (\frac{\delta}{1+\delta\beta_c})^2\left(\frac{\partial}{\partial \eta} - zF_1\frac{\partial}{\partial z}\right)$$

$$\left[\frac{\nu_T}{1+(\frac{\delta}{1+\delta\beta_c})^2 h_{\eta_1}}\left(\frac{\partial}{\partial \eta} - zF_1\frac{\partial}{\partial z}\right)\hat{u}\right] + 1 + \left(\frac{\delta}{1+\delta\beta_c}\right)^2 h_{\eta_1} = 0 \tag{3.49}$$

where,

$$z = \frac{z^*}{\hat{D}^*}, \quad d = \frac{d^*}{D_0^*}, \quad \hat{D}^* = \frac{d^*}{\cos\alpha} = D_0^*\frac{d}{\sqrt{1-(\frac{\delta}{1+\delta\beta_c})^2(\frac{\partial d}{\partial \eta})^2}}, \quad \hat{u} = \frac{u^*}{\sqrt{gSD_0^*}},$$

$$\nu_T = \frac{\nu_T^*}{D_0^*\sqrt{gSD_0^*}}$$

$$\tag{3.50}$$

$$F_1 = \frac{1}{d}\frac{\partial d}{\partial \eta}\left[1 + \frac{(\frac{\delta}{1+\delta\beta_c})^2 d}{1-(\frac{\delta}{1+\delta\beta_c})^2(\frac{\partial d}{\partial n})^2}\frac{\partial^2 d}{\partial \eta^2}\right], \quad F_2 = \frac{\sqrt{1-(\frac{\delta}{1+\delta\beta_c})^2(\frac{\partial d}{\partial \eta})^2}}{d}$$

$$h_{\eta 1} = \frac{z\,d}{1-(\frac{\delta}{1+\delta\beta_c})^2(\frac{\partial d}{\partial \eta})^2}\frac{\partial^2 d}{\partial \eta^2} \tag{3.51}$$

Moreover, the dimensionless turbulent viscosity can be expressed as:

$$\nu_T = \frac{u_f\,d}{\sqrt{1-(\frac{\delta}{1+\delta\beta_c})^2(\frac{\partial d}{\partial \eta})^2}}\mathcal{N}(z) \tag{3.52}$$

where $u_f = u_f(\eta)$ is the dimensionless friction velocity along cross section bed, scaled as $u_f = u_f^*/(gSD_0^*)^{1/2}$, and $\mathcal{N}(z)$ is the vertical distribution of the turbulent viscosity.

The boundary condition to be associated with equation (3.49) requires that the flow velocity at the bed follows a classical logarithmic profile, i.e:

$$\hat{u}|_{z=0} = u_f \left[2 + 2.5 ln \left(\frac{d}{d_{gr}\sqrt{1 - (\frac{\delta}{1+\delta\beta_c})^2(\frac{\partial d}{\partial\eta})^2)}} \right) \right] \tag{3.53}$$

with d_{gr} $(= d_{gr}^*/D_0^*)$ the dimensionless grain roughness. d_{gr} is from 0.001 to 0.05.

Moreover we prescribe that the stresses at the water surface and at the bed are equal to $\tau = 0$ and $\tau = \tau_b$, respectively, and hence :

$$\left[\nu_T \left(\frac{1}{d}\frac{\partial\hat{u}}{\partial z} - \frac{(\frac{\delta}{1+\delta\beta_c})^2}{1 + (\frac{\delta}{1+\delta\beta_c})^2 h_{\eta_1}} \frac{\partial d}{\partial\eta} \right) \right]_{z=1} = 0, \qquad \left[F_2\nu_T\frac{\partial\hat{u}}{\partial z} \right]_{z=0} = u_f^2 \tag{3.54}$$

Moreover, we assume that the dimensionless friction velocity can be expressed as:

$$u_f = \mathcal{N}\frac{\partial\hat{u}}{\partial z}\Big|_{z=0} \tag{3.55}$$

At the various order of approximation we find:

- $O(\delta^0)$

$$\hat{u}_0(z, \eta) = \left(-\frac{z^2}{2N} + \frac{z}{N} + 2 + \frac{5}{2}ln\frac{d}{d_{gr}} \right) \sqrt{d} \tag{3.56}$$

- $O(\delta^2)$

$$
\begin{aligned}
\hat{u}_1(z,\eta) \;=\; \frac{\sqrt{d}}{1+\delta\beta_c}\Bigg\{ &\left[\left(\frac{45}{8}\ln(\frac{d}{d_{gr}})+\frac{7}{2}+\frac{25}{16}\ln(\frac{d}{d_{gr}})^2\right)N + \right.\\
&\left(-\frac{7}{8}-\frac{5}{16}\ln(\frac{d}{d_{gr}})\right)z^2 + \left(\frac{7}{4}+\frac{5}{8}\ln(\frac{d}{d_{gr}})\right)z + \\
&\left.\frac{5}{8}\ln(\frac{d}{d_{gr}})+\frac{1}{2}+\frac{1}{N}\left(\frac{1}{4}z-\frac{1}{16}z^4+\frac{1}{4}z^3-\frac{3}{8}z^2\right)\right]d\frac{\partial^2 d}{\partial\eta^2} + \\
&\left[\left(\frac{205}{16}\ln(\frac{d}{d_{gr}})+\frac{33}{4}+\frac{25}{8}\ln(\frac{d}{d_{gr}})^2\right)N - \frac{5}{16}z^2 + \right.\\
&\left(\frac{33}{8}+\frac{5}{4}\ln(\frac{d}{d_{gr}})\right)z + \frac{7}{4}+\frac{5}{8}\ln(\frac{d}{d_{gr}}) + \\
&\left.\frac{1}{N}\left(-\frac{1}{8}z^2+\frac{1}{16}z^4+\frac{1}{4}z\right)\right]\left(\frac{\partial d}{\partial\eta}\right)^2\Bigg\}
\end{aligned}
\tag{3.57}
$$

where $d = d(\eta)$ describes the cross section profile (Figure 3.18). And Figure (3.19) represents the depth of flow and corresponding velocity for various β

$$
d(\eta) = erf\left(\beta(1-\sqrt{\eta})\right)
\tag{3.58}
$$

where η describes the cross section profile at the bank region. Following equation (3.58), we assume that this region is described by a function of the form and $\beta = \frac{B^*}{D_0^*}$ is the channels aspect ratio.

Finally, we calculate the depth averaged longitudinal velocity, $\bar{u}(\eta)\ (= \bar{u}_0 + \delta^2\bar{u}_1)$, by along the vertical, obtaining:

$$
\begin{aligned}
\bar{u}_0(\eta) &= \frac{\sqrt{d}}{3N} + \left[2 + \frac{5}{2}ln(\frac{d}{d_{gr}})\right]\sqrt{d} \\
&= \left(\frac{19}{3} + 2.5ln\frac{d}{d_{gr}}\right)\sqrt{d}
\end{aligned}
\tag{3.59}
$$

$$\bar{u}_1(\eta) = \frac{\sqrt{d}}{1 + \delta\beta_c} \left(\left(\frac{781}{390}d + \frac{229}{256}dln(\frac{d}{d_{gr}}) \right) d\frac{\partial^2 d}{\partial n^2} \right.$$

$$\left. + \left(\frac{5357}{780} + \frac{315}{104}ln(\frac{d}{d_{gr}}) \right) \left(\frac{\partial d}{\partial n} \right)^2 \right) \tag{3.60}$$

We now recall that the cross section area A and the cross sectionally averaged velocity are given by:

$$A^* = 2\left(\int\limits_0^{P_0^*} d^* \, dn^* + \int\limits_{P_0^*}^{b^*} d^* \, dn^* \right) \qquad U_0^* = \frac{1}{A^*}\left(\int\limits_0^{P_0^*} d^*\bar{u}^* \, dn^* + \int\limits_{P_0^*}^{b^*} d^*\bar{u}^* \, dn^* \right)$$

$$\tag{3.61}$$

and, in dimensionless form:

$$A(\eta) = \frac{A^*}{D_0^*(P_0^* + b^*)} = 2\int_0^1 d \, d\eta \qquad U_0(\eta) = \frac{U_0^*}{\sqrt{gD_0^*S}} = \frac{1}{A}\int_0^1 d\,\bar{u} \, d\eta$$

$$\tag{3.62}$$

We finally rescale the depth averaged velocity as:

$$\hat{u}(n) = \frac{\bar{u}}{U_0} = A\frac{\bar{u}_0 + \delta^2\bar{u}_1}{2\int_0^1 d\,\bar{u} \, d\eta} \tag{3.63}$$

so that the depth averaged velocity can be written in the form:

$$\hat{u} = u_0(n) = 1 + \tilde{u}(n) \tag{3.64}$$

As a consequence, the term $\tilde{u}$ which quantifies the departure from the cross sectionally average controlling longitudinal dispersion process, is given by:

$$\tilde{u}(n) = u_0(n) - 1 = A\frac{\bar{u}_0 + \delta^2\bar{u}_1}{2\int_0^1 d\,\bar{u} \, d\eta} - 1 \tag{3.65}$$

and flow depth is

$$d_0(n) = erf\left(\beta(1 - \sqrt{(n)})\right) \tag{3.66}$$

Figure (3.18) shows theoritical depth of flow for the entire channel cross section

Figure 3.25: Channel cross section (of the rescaled velocity given below) is plotted as a function of the normalized co-ordinate n, $d_0 = erf\left(\beta(1 - \sqrt{(n)})\right)$ for $\beta = 6$.

for varios width and figure (3.19) represents both channel cross section for both bank and central part and corresponding velocity. The calculated friction velocity $(\delta^2 u_{f1})$ is justified with Tubino and Colombini [1992] (see figure (3.20) and (3.21)). In figure (3.22), channel cross section is drawn for the corrected friction velocity given in figure (3.23) u_f and corrected velocity u figure (3.24). And figure (3.25), (3.26) are for rescaled channel cross section and rescaled velocity.

Rescaled velocity of entire cross section
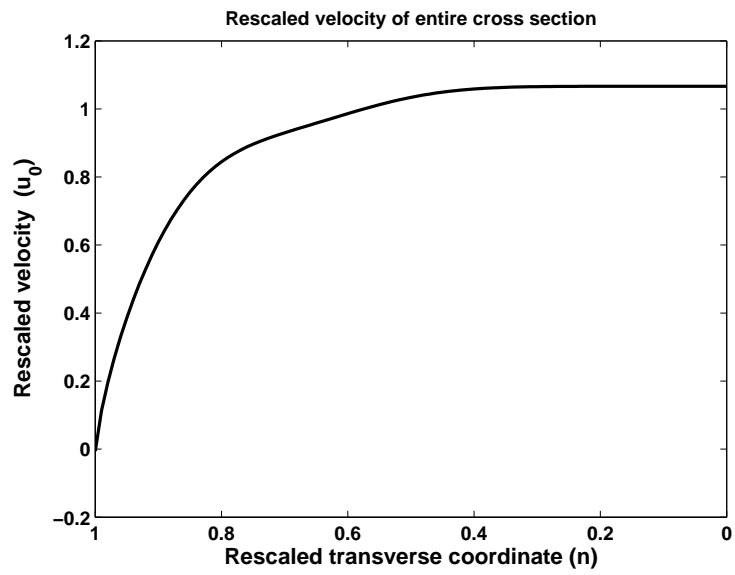
Figure 3.26: Re-scaled velocity of entire cross section

Chapter 4

Longitudinal Dispersion in Straight Equilibrium Channel

In this chapter we compare the theoretical dispersion coefficient estimated on the basis of the flow field considered in 3 with the data collected by Godfrey and Frederick [1970] in a few rivers. Substituting eqution (3.64) and (3.58) into (2.49) and assuming that the cross sectional bed profile is described by the relation 83.66) we obtained the dispesion coefficient for various β (See Figure 4.1).

4.1 Determination of transverse mixing coefficient

In order to estimate the longitudinal dispersion coefficient through equation (2.49) it is convenient to express the transverse mixing coefficient k_n as a sum of the two terms, reflecting two different kinds of mixing process:

$$k_n = E_n + \epsilon_n \tag{4.1}$$
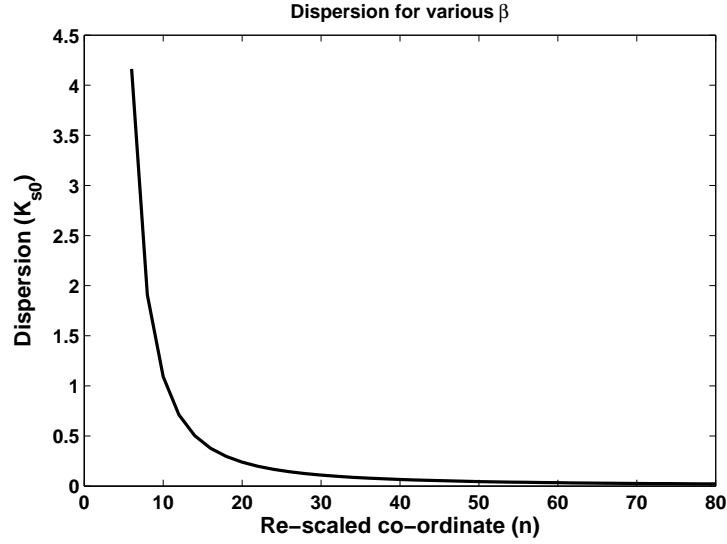
Figure 4.1: The Longitudinal dispersion coefficient in a straight river for various values of the width to depth ratio β.

where E_n accounts for the transverse turbulent diffusion coefficient and ϵ_n is related to the transverse dispersion.

The transverse turbulent diffusion coefficient E_n usually falls in the range $0.15-0.30$ [Rurherford, 1994], with the average value 0.145 determined on the basis of 138 sets of experimental data collected from different investigators,

On the other hand, for large rivers the transverse dispersion coefficient can be estimated through the relation [Smeithlov, 1990]:

$$\epsilon_n = \frac{1}{3520}\left(\frac{U_0^*}{\sqrt{gD_0^*S}}\right)\left(\frac{2B^*}{D_0^*}\right)^{1.38} \tag{4.2}$$

As a first approximation, we can estimate the transverse mixing coefficient through the relation

$$k_n = 0.145 + \frac{1}{3520}\left(\frac{U_0^*}{\sqrt{gD_0^*S}}\right)\left(\frac{2B^*}{D_0^*}\right)^{1.38} \tag{4.3}$$

4.2 Comparison with the theory of Elder [1959]

From Figure (4.1)($i.e., the K_{s0} - \beta$ graph), it can be observed that the dispersion coefficient is higher for smaller aspect ratios (i.e., the ratio of width to depth) for large enough values of β, the dispersion coefficient approaches the constant value prescribed by Elder [1959]. For example, if we consider $\beta = 46$ we obtain

$$K_{s0} = 0.05201 \tag{4.4}$$

and returning to similar dimensionless quatities, $\frac{K_{s0}^*}{D_0^* u_*} = 5.20$, which is quite close to the value 5.86 corresponding to an infinitely wide channel.

4.3 Comparison with the experiments of Godfrey and Frederick (1970)

Godfrey and Frederick [1970] carried out a series of tracer experiments to estimate the dispersion coefficient in six reaches of four rivers. To this aim they measured the concentration and the velocity across a number of cross sections (6) of the following rivers.

1. Clinch River (above gage), near Clinchport, Va.,

2. Clinch River (below gage), near Speers Ferry, Va.,

3. Copper Creek (above gage), near Gate City, Va.,

4. Copper Creek (below gage), near Gate City, Va.,

5. Powell River, near Sneedville, Tenn.,

6. Coachella Canal, near Holtville, Calif..

The cross sections (six for each channel reach) interested by the flow field measurements are shown in Figures (4.2) - (4.4).
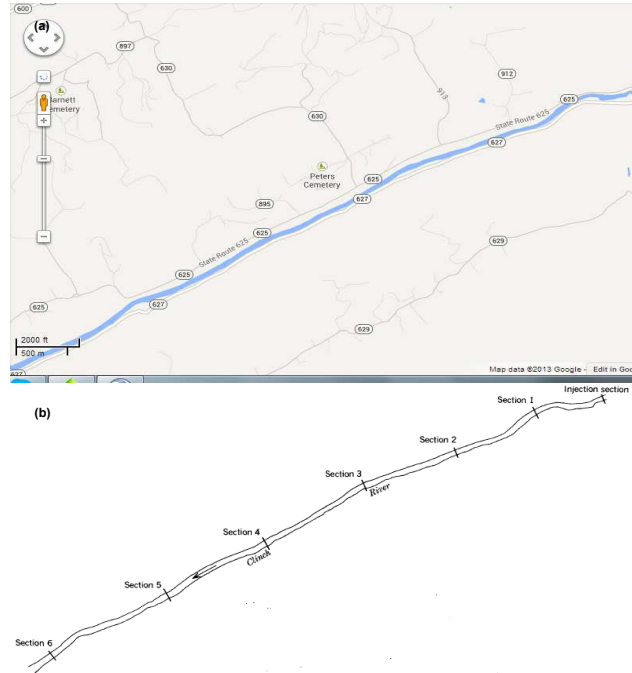
Figure 4.2: Experimental cross section considered in the case of the Clinch River for tests 2, 7 and 10 carried out by Godfrey and Frederick [1970] a) Google map image; b) Planform river configuration

Godfrey and Frederick [1970] examined the influence of channel geometry and flow characteristics on dispersion. They calculated the longitudinal dispersion coefficient dividing the variance of concentraion by double of time and calculated the concentration from the basic equations for turbulent dispersion under steady uniform flow that satisfies the initial condition of concentration material. To determine the longitudinal dispersion coefficient they also measured the discharge, mean velocity, shear velocity, slope, flow depth, width, cross sectional area of each surveyed cross section . In particular, for each vertical, the velocities are measured at relative elevations with respect to the flow depth $\frac{z_1^*}{d_n^*} = 0.1, 0.2, 0.4, 0.6, 0.8$ and 0.9
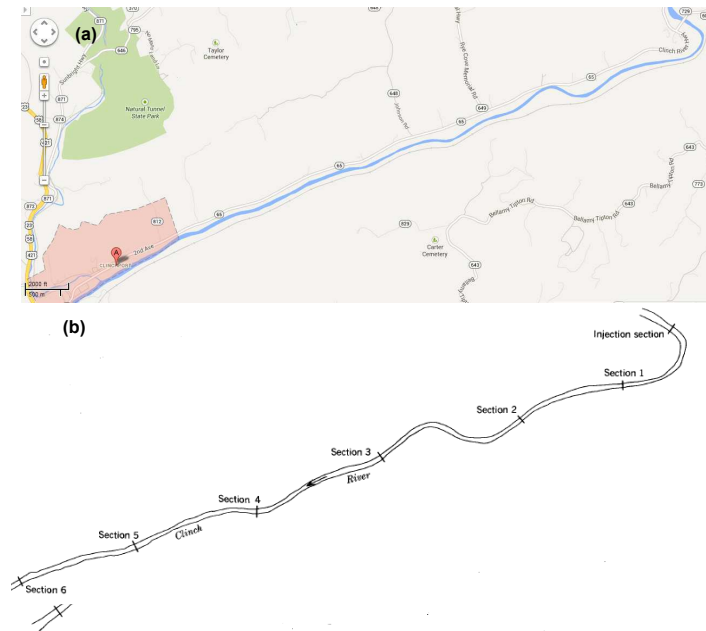
Figure 4.3: Experimental cross section considered in the case of the Clinch River for test 5 carried out by Godfrey and Frederick [1970] a) Google map image; b) Planform river configuration
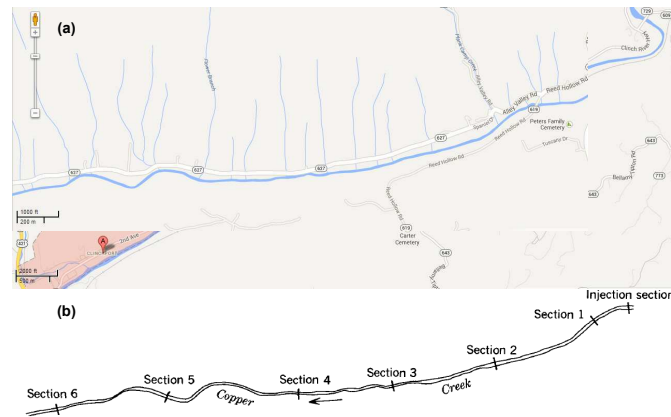
Figure 4.4: Experimental cross section considered in the case of the Copper River for test 6 carried out by Godfrey and Frederick [1970] a) Google map image; b) Planform river configuration

The cross-section distributions of the dimensional and dimensionless depth averaged velocities resulting from the analysis presented in 3 are here compared with
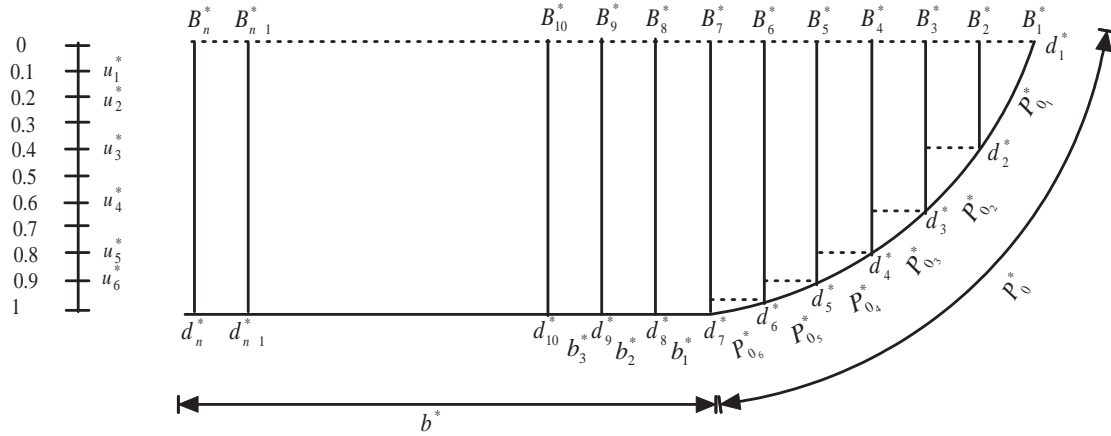
Figure 4.5: Sketch of the equilibrium cross-section considered to determine the dimensional Depth average velocity, wetted perimeter, central part and related notations.
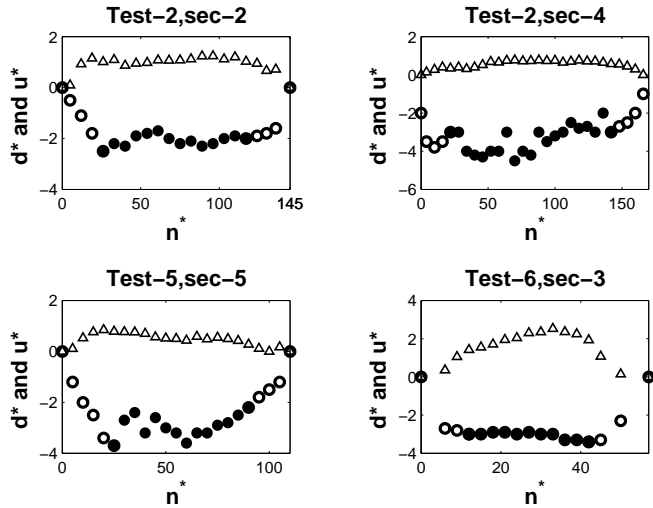
Figure 4.6: Dimensional flow depth (d^*) and depth averaged velocity (u^*) measured across sections surveyed by Godfrey and Frederick (1970) in various tests (The solid black circles denote the central region while the white circles are located in the bank regions).

those measured by Godfrey and Frederick [1970]. The cross sectional area A^*, the depth-averaged velocity, $\bar{u}^*$, and the cross sectional averaged velocity, U_0^*, are determined by integrating along the vertical across the section, using the trapezoidal
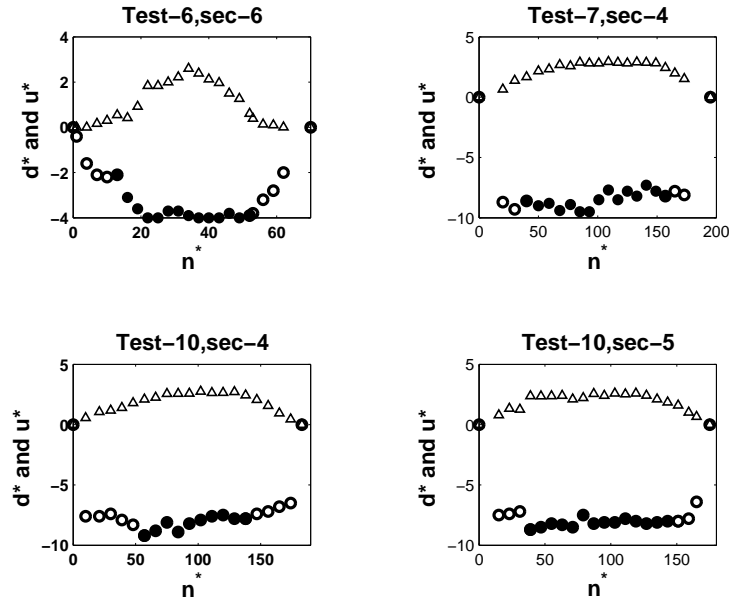
Figure 4.7: Dimensional flow depth (d^*) and depth averaged velocity (u^*) measured across sections surveyed by Godfrey and Frederick (1970) in various tests (The solid black circles denote the central region while the white circles are located in the bank regions).

rule. The wetted perimeter P_0^* is evaluated as follows:

$$P_0^* = P_{10}^* + P_{20}^* + \ldots + P_{n0}^* \tag{4.5}$$

where, (4.5) P_{i0}^* are the straight segments approximating the transverse bed profile. The predicted and observedtransverse distributions of depth averaged velocities are shown in figures (4.6) and (4.7). In the figures the bank and central regions are distinguished with white and black circles, respectively. Similarly, Figures (4.8) and (4.9) shows the dimensionless transverse velocity profiles. To investigate the accuracy of the predicted longitudinal dispersion coefficients. Their values are reported in Table (4.1) and in Figure (4.10) together with measured values and the estimations provided by some empirical and theoretical relations. Note that only the data concerning straight channel reaches are considered.
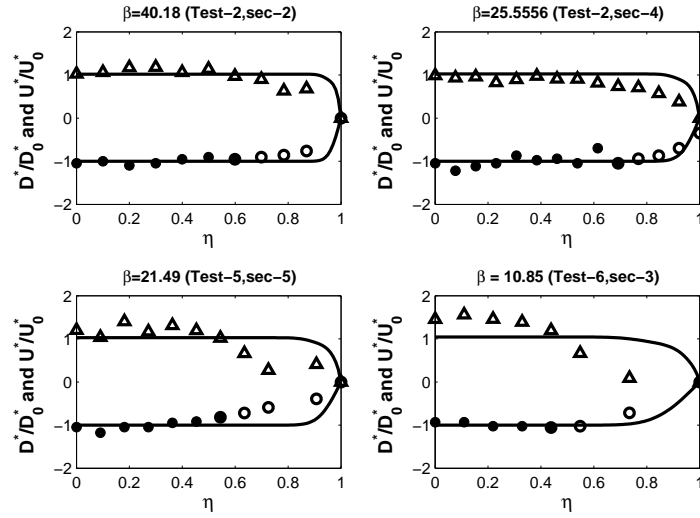
Figure 4.8: Comparison with dimensionless depth flow (d) and depth average velocity (u) of entire cross section from Godfrey and Frederick (1970) in various tests (The solid black circles denote the central region while the white circles are located in the bank regions).

Table 4.1: Comparison of observed longitudinal Dispersion Coefficient of Godfrey and Frederick [1970] and with others.

		Dispersion co-efficient K_{s0}					
Stream	Measured	Present model	Fischer [1975]	Liu [1977]	Iwasa and Aya [1991]	Seo and Cheong [1998]	Koussis and Ridriguez -Mirasol [1998]
Test-2, sec-2	0.96	0.81	1.30	5.04	13.12	2.00	10.74
Test-2, sec-4	1.60	1.0	2.16	8.40	21.83	3.35	17.88
Test-5, sec-5	3.19	2.10	9.25	11.15	37.57	6.86	16.07
Test-6, sec-3	4.20	1.80	2.44	1.88	18.9	6.90	5.70
Test-6, sec-6	4.33	1.95	32.5	3.89	9.58	7.12	5.89
Test-7, sec-4	1.70	1.32	3.58	2.70	17.07	7.45	3.28
Test-10, sec-4	1.91	1.53	3.27	2.90	17.8	7.70	3.70
Test-10, sec-5	1.97	1.19	3.30	3.00	18.30	7.90	3.8
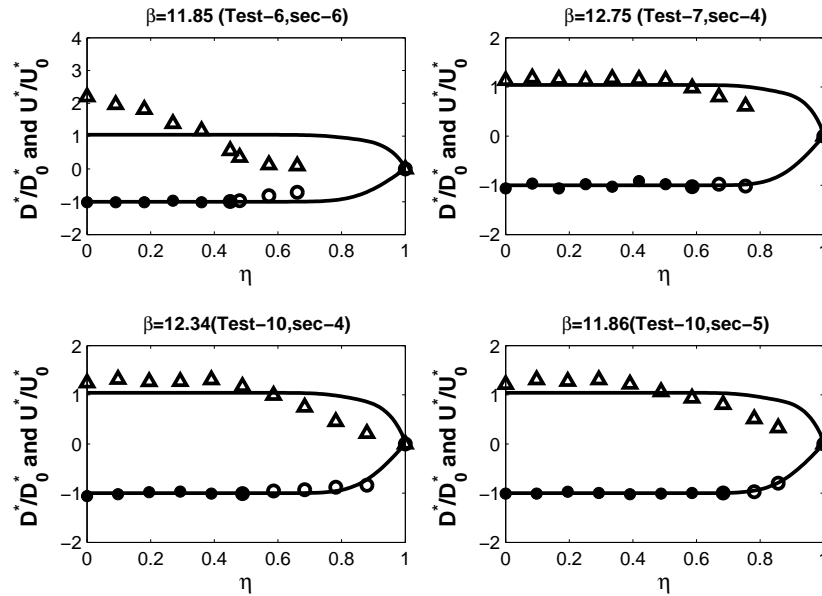
Figure 4.9: Comparison with dimensionless depth flow (d) and depth average velocity (u) of entire cross section from Godfrey and Frederick (1970) in various tests (The solid black circles denote the central region while the white circles are located in the bank regions
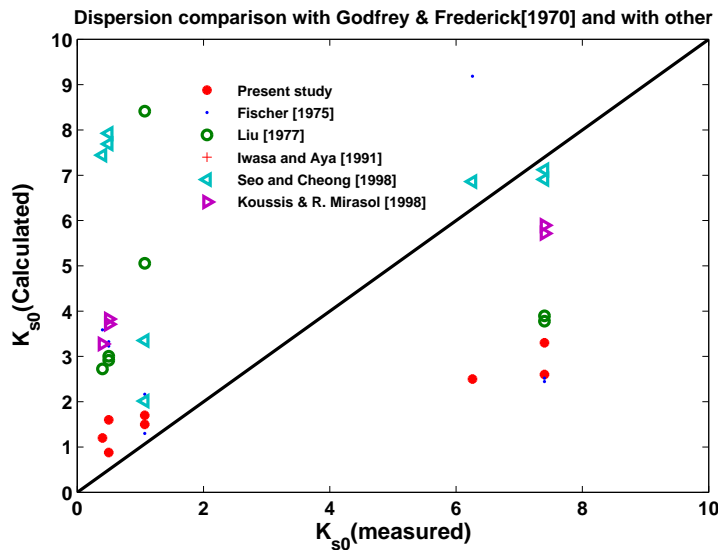
Figure 4.10: Comparison of calculated dispersion coefficients with those observed by of Godfrey and Frederick [1970] and with other.

It clearly appears that that the present theoretical presentationsare in reasonable in good agreementwith the measured data and in any case, ensure a better accuracythen the other predictors available in literature (see figure 4.10).

4.4   Comparison of dispersion with the theoretical predictions of Deng [2001]

The prediction given the present modelare here compared with the longitudinal dispersion coefficient (53) measured in the reaches of 29 rivers in the United States. These data are taken from Deng (2001) who usedthe dataset to validate his theoretical predictor. The relation developed by Deng [2001] gives the dispersion coefficient on the basis of empirical description of transverse velocity, distribution of the transverse mixing coefficient. The data reported in Table (4.2) indicate that the percentage of predictions falling within the range of $0.5 < D_{predicted}/D_{measured} < 2$ are 51/53 in the present methodology is employed and 47/53 when the relationship proposed by Deng[2001] is used. Moreover, as predictions given by the present theory are closer to the observed values than Deng′s. This means that 81% of the estimates obtainedwith the present modelare close to the observed dispersion coefficients. Figure (4.11) presents the corresponding comparison to a $\pm 30\%$ error usually adopted measured data of Deng [2001] to quantify the maximum acceptable error. Present model shows a better agreement with respect to observed data. The discrepancy ratios shown in Figure (4.12) confirm that the present model provides an overall better agreement with the measure dispersion coefficient than the approach developed by Deng [2001].
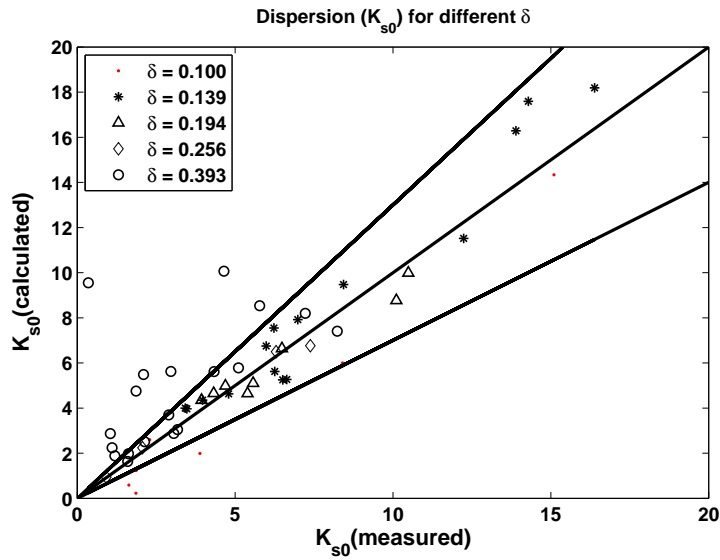
Figure 4.11: Comparison of calculated dispersion coefficients with the observed in the field, datum from the database of provided by Deng [2001]
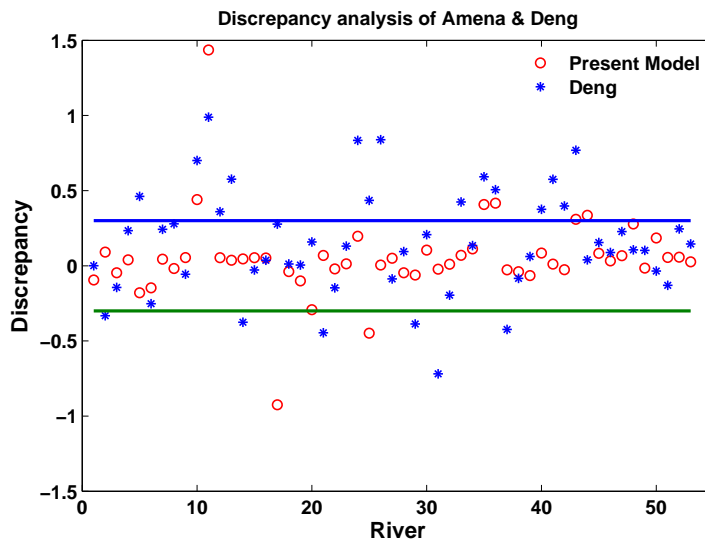
Figure 4.12: Discrepancy ratios d_r of each dispersion coefficient equation for the considered rivers. Horizontal lines identify the range ± 0.3.

Table 4.2: Comparison of Dispersion Coefficient of measured, present study and Deng [2001].

No	River	Dispersion	co-efficient K_{s0}	
		Measured	Calculated	Deng[2001]
1	Antietam creek, MD.	6.51	5.24	6.52
2		14.28	17.59	6.65
3		8.23	7.40	5.90
4		3.97	4.35	6.8
5	Monocacy River, MD.	1.86	1.23	5.38
6	Conococheague creek, MD.	8.4	5.99	4.7
7		3.93	4.35	6.87
8	Chattahoochee River, GA.	3.17	3.04	6.02
9		6.98	7.92	6.13
10	Difficult Run, Va.	1.04	2.87	5.22
11	Bear Creek, Colo.	0.35	9.55	3.41
12	Little Pincy Creek, MD.	2.29	2.59	5.24
13	Bayou Anacoco, LA.	2.06	2.24	7.77
14	Bayou Bartholomew, LA.	16.38	18.19	6.89
15	Tickfau River, LA.	5.1	5.77	4.78
16	Tangipahoa River, LA.	5.98	6.74	6.51
17	Red River, LA.	1.85	0.22	3.5
18	Red River, LA	5.57	5.1	5.73
19	Red River, LA	6.63	5.26	6.70
20	Sabine River, LA.	3.88	1.98	5.59
21	Sabine River, TEX.	13.89	16.28	4.98
22	Sabine River, TEX.	10.48	9.98	7.48
23	Sabine River, TEX.	6.3	6.49	8.52
24	Mississippi River, La.	1.19	1.87	8.12
25	Mississippi River, Mo.	1.63	0.58	4.44
26	Mississippi River, Mo.	0.92	0.93	6.35
27	Wind River, Wyo.	8.43	9.47	6.89
28	Wind River, Wyo.	6.25	5.62	7.77
29	Copprer Creek, Va.	10.1	8.77	4.14
30	Clinch River, Va.	2.9	3.69	4.67
31	Copper Creek, Va.	15.09	14.33	2.88
32	Powell River, Tenn.	6.48	6.64	4.13
33	Clinch River, Va.	2.13	2.5	5.66
34	Copper River, Va.	4.33	5.61	5.9
35	Clinch River, Va.	1.86	4.75	7.27
36	Clinch River, Va.	2.1	5.48	6.73
37	Missouri River, Iowa.	12.24	11.51	4.62
38	Bayou Anacoco, La.	7.38	6.74	6.08
39	Bayou Anacoco, La.	5.39	4.64	6.21
40	Nooksack River, Wash.	1.62	1.97	3.85
41	Wind River, Wyo.	1.59	1.63	5.98
42	Wind River, Wyo.	3.05	2.87	7.63
43	John Day River, Oreg.	1.10	2.24	6.46
44	John Day River, Oreg.	4.64	10.06	5.08
45	Minnesota River	6.23	7.54	8.9
46	Minnesota River	4.32	4.65	5.29
47	Amite River	3.42	3.99	5.77
48	Susquehanna River	2.96	5.61	3.78
49	Bayou Anacoco	4.79	4.62	6.06
50	Muddy River	5.77	8.53	5.32
51	Muddy River	7.22	8.2	5.35
52	Comite River	3.47	3.96	6.1
53	Missouri River	4.69	4.98	6.55
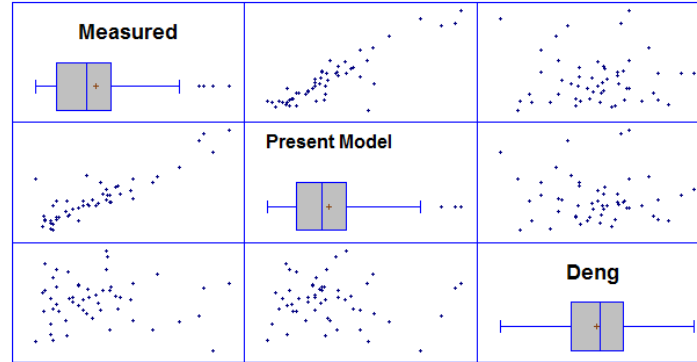
Figure 4.13: Scatter-matrix plot representation, comparing the present model data with measured dispersion coefficient and the prediction given by Deng [2001]

In order to better quantify the degree of accuracy of the predictions, a comparison analysis has also been carried out. Scatter-matrix plots shown in Figure (4.13) represent the multivariate relationship among a almost similar behaviour in the box-whisker plots characterized the measured dispersion coefficients and the estimates obtained with the present model. In particular an almost linear relationship seem to exist between these two sets of data (see box a and c). On the other hand, estimates obtained by Deng [2001] model have a shrinked variation (box —)but different from the actual measurements as well as present model. Table (4.3) summeries the statistics for each of the selected sets of data (i.e., measured values, estimates obtained with the present model, estimaates provided by Deng [2001]). It includes measures of central tendency (average), measures of variability (standard deviation, coefficient of variation, minimum, maximum, range), and measures of shape (standadized skewnwss and kurtosis). Of particular interest are the latter measures, which can be used to determine whether the sample comes from a normal distribution. Values of these statistics outside the range of -2 to +2 indicate significant departures from normality, which would tend to invalidate many of the statistical procedures normally applied to this data.

Table 4.3: Summery Statistics

	Measured	present model	Deng [2001]
Count	53	53	53
Average	5.32868	5.93679	5.87302
Standard deviation	3.84048	4.07989	1.31969
Coeff. of variation	72.0719%	68.7222%	22.4704%
Minimum	0.35	0.22	2.88
Maximum	16.38	18.19	8.9
Range	16.03	17.97	6.02
Stnd. skewness	3.55902	3.89008	-0.120823
Stnd. kurtosis	1.62868	2.74084	-0.209883

Chapter 5

Flow Field in Equilibrium Channels with Arbitrary Curvatures

5.1   Introduction

The development of the mathematical model that predict the longitudinal dispersion coefficient of alluvial rivers is based on a physical model simulating the outer bank erosion and the inner bank reconstruction considering distributions of channel axis curvature and cross section width.

The two dimensional flows plays a vital role in hydraulic geometry of alluvial channels i.e, defining flow patterns in meandering channel, determining the particle migration rate and the rate of alluvial channel deformation. A flow with secondary currents, has a structure with skewed shear profiles having different velocity profiles in two orthogonal directions.

Curvature, and sediment are acting planimetric effect considered for flow field (see Figure 5.1). Both of these predict the development of alternate bar topography
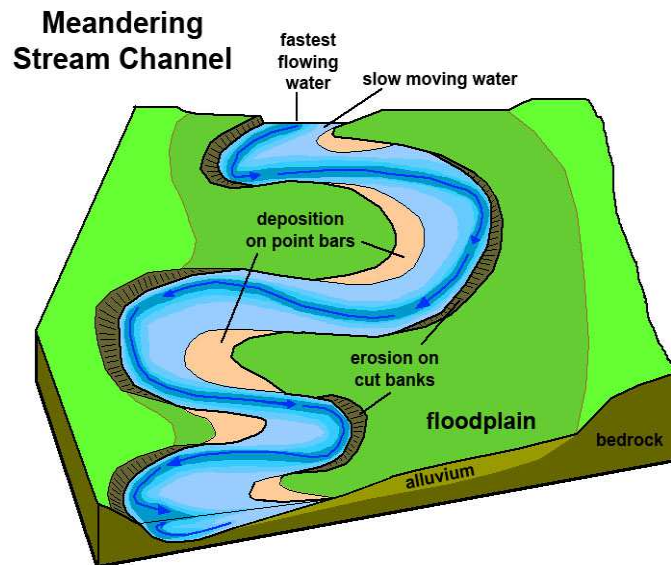
Figure 5.1: Flow field of a meandering channel (Source: http: //www.geologycafe. com/ class/ chapter9. html)
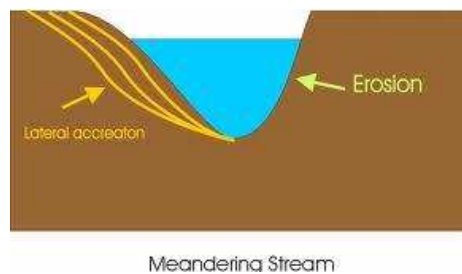
Figure 5.2: Depth of flow of a meandering river (Source: http: //www4.uwm.edu/ course/ geosci697/ rivers -deltas/ rivers-deltas.html.)

identified as the most typical antisymmetrical patterns in meander bends. In the classical linear meander solution [Ikeda et al., 1981; Blondeaux and Seminara, 1985; Zolezzi and Seminara, 2001] the bank erosion and the opposite bank accretion (see Figure 5.2) are assumed to work on the long term scale. Secondary flow (see Figure 5.4) contribute to river bed deformation through the construction of transverse near-bed shear stresses and the redistribution of longitudinal momentum. Several experimental and theoretical contributionsons flow field structure and bed topog-

raphy are available in literature (see Figure 5.3) [Rojovskij, 1957: Johanesson, and Parker, 1989b; Seminara and Solari 1998; Blanckaert and de Vriend, 2004a; Kalkwijk and de Vriend, 1980; Seminara and Tubino, 1980; Zolezzi and Seminara, 2001; Repetto et al. 2002]. Linear models of the steady flow in meandering channels have crucial role in disclosing the meandering dynamics [Seminara, 2006], and in exploring the long term (order of centuries) evolution [Howard, 1992; Sun et al., 1996; Frascati and Lanzoni, 2009]. Odgaard and Bergs [1988] used a power law to model velocity distribution in a curved channel, whereas Odgaard [1981] extended Falcon's [1979] analysis based on the power law to propose an improved model for steady-state transverse bed profile. As a next step for investigate longitudinal
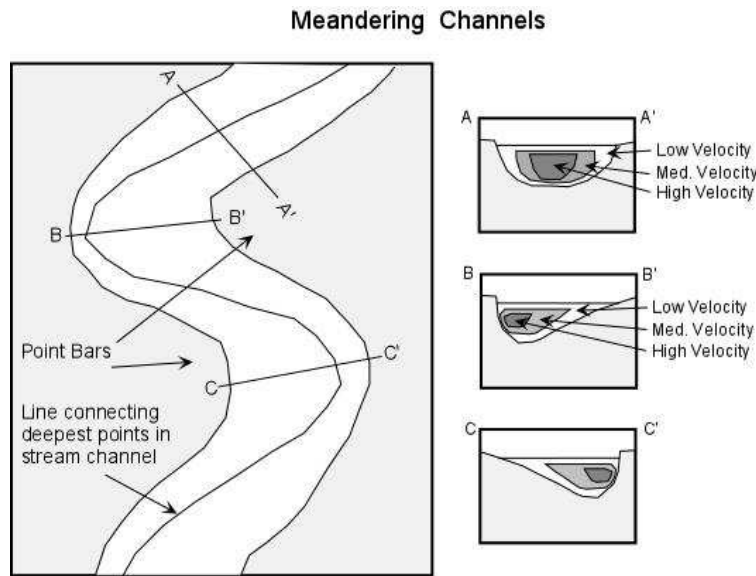
Figure 5.3: Flow field of a meandering river (Source: http: // snippetseamstress.blogspot.it/ 2009/ 01/ middle -course -of- river -formation -of.html).

dispersion coefficient in meandering river, in the present section flow field and depth of flow are considered for meandering river. The spatial variation of dispersion coefficients is more important in natural rivers with meandering configuration, which often occur in nature. In meandering rivers not both the primary flow path along watercourses and the repeating generation and dissipation of secondary currents
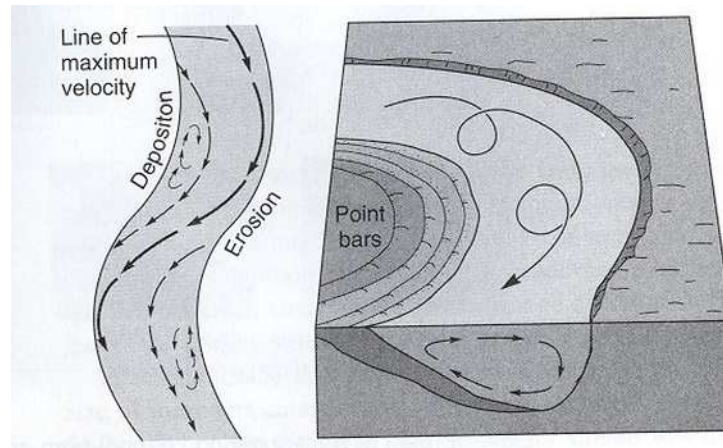
Figure 5.4: Helical flow in meandering river (Source: http:// thebritishgeographer.weebly.com/ river -landforms.html)

control the dispersion. The alternating bends, induces secondary currents that alter the magnitude of both transverse mixing and longitudinal dispersion [Fischer, 1969]. Therefore, when accurate results are required in the modeling of solute mixing in meandering rivers, a more detailed information on the spatially varied dispersion coefficient has possibly to be incorporated into the model. In open channels, once vertical mixing is completed in the initial period of solute transport, the vertical shear velocity profile increases the longitudinal spreading in the streamline direction [Taylor, 1953]. However, the secondary current around pronounced curvatures in many open channels introduces a large magnitude of transverse circulation combined with the principal longitudinal flow. Hence, the solute dispersion by the secondary current cannot be described by only the dispersion in the longitudinal direction; there is a dispersion effect in the transverse direction that is much more effective than the transverse turbulent diffusion. To introduce the spatial variation of mixing characteristics in modeling of solute transport, several efforts have been put forward that solved the depth-averaged advection dispersion equation using spatially varying mixing coefficients. The variation in the magnitude of the dispersion process in natural rivers has been reported through the determination of

dispersion coefficients by a dye tracer test; Day [1977] and Marivoet and Van Crae-
nenbroeck [1986] perceived a wide variation of longitudinal and transverse dispersion
coefficients in natural streams. Piasecki and Katopodes [1999] determined spatially
distributed dispersion coefficients in a channel of variable depth and a natural river
by adopting the adjoint sensitivity equation. Jamali et al. [2005] derived an approx-
imate analytical solution to the one-dimensional 1D advective dispersion equation
for rivers with variable dispersion coefficients. But their derivation is only limited
to the slow variation of the longitudinal dispersion coefficient accompanied by the
typical increase of hydraulic geometry in downstream of natural rivers. Barros et
al. [2006] obtained numerical-analytical solutions for 2D mathematical models with
spatially variable mixing coefficients that predict the dispersion of dissolved pollu-
tants in rivers, streams, and channels. Deng [2002] has established a method which
predict the dispersion coefficient using a channel shape equation.

In this chapter the flow field and depth of flow proposed by Frascati and Lanzoni
[Frascati and Lanzoni, 2013] is used to predict the spatial distribution of longitudinal
dispersion coefficient and the corresponding reach averaged value. The morphody-
namic model that predicts, at a linear level, the spatial distribution of the flow field
and depth of flow of an alluvial river characterized by a prescribed (generally irreg-
ular) distribution of channel axis curvature in a constant channel width. The two
dimensional depth averaged flow field is then used to estimate the correction k_{s1} to
the longitudinal dispersion coefficient for a straight channel analyzed in section 2.4
of the present thesis. And obtained the longitudinal dispersion coefficient for allu-
vial river using equation (2.55) figure (5.1) displays the flow variation of meandering
river with erosion a nd deposition.

5.2   Formulation of the problems

5.2.1   Notations

Let us consider the steady flow occurring in a meandering cohesionless channel characterized by a spatilly varying distribution of both channel axis curvature $\mathcal{C}^*(s^*)$ and channel width local $B^*(s^*)$. Moreover, $D^*(s^*)$ is the local flow depth, R_0^* is the minimum along reach, B_0^* is the maximum along reach B^* and D_u^* is uniform flow depth, θ_c is the angle that the local tangent to the channel axis form with a given (but arbitrary) reference axis x^*, d_{gn}^* is the mean bed grain size, h^* is the free surface elevation, computed with respect to the local horizontal plane containing n^* and x^*, ν_T^* is the turbulent eddy viscosity, $q^* = (q_s^*, q_n^*)$ is the sediment flux per unit width, g is the acceleration due to gravity, ρ and ρ_s are water and sediment density, respectively. Hereafter, a superscript asterisk will indicate a dimensional variables. Dimensionless parameters relevant to the problem we are going to investigate, the channel aspect ratio, $\beta_u = \frac{B_{avg}^*}{D_u^*}$ the dimensionless grain size, $d_s = \frac{d_s^*}{D_u^*}$ the Shields parameter, $\tau_{*u} = \frac{\tau^*}{(\rho_s - \rho)gd_s^*}$ and the Reynolds particle number, $R_{ep} = \frac{\sqrt{(\frac{\rho_s}{\rho-1})gd_s^3}}{\nu}$.

5.2.2   Coordinate system

Flow and bed topography are referred to as an ortogonal intrinsic reference system (s^*, n^*, z^*), where s^* is the longitudinal axis coordinate n^* is transverse axis coordinate and z^* is the vertical co-ordinate, pointing upward figure (5.5).

5.2.3   Scaling

In order to account for the curvilinear nature of the axis s^* following the channel axis, we must account for the fact that horizontal distances measured along different longitudinal coordinate surfaces are in general are not equai when moving from one
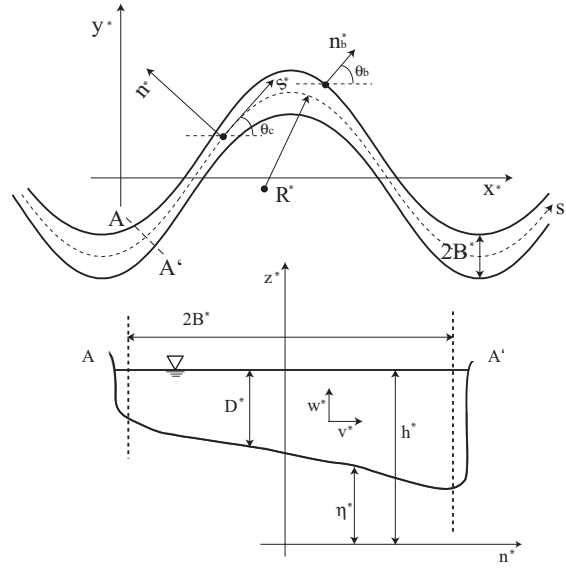
Figure 5.5: Sketh of meandering channel and notations.

transverse coordinate surface to the other. The metric coefficient account for the fact is,

$$h_s = 1 + \frac{n^*}{R^*(s^*)} \tag{5.1}$$

Considering channels with nonuniform width and curvature axis, it is convenient to define the following dimensionless variables

$$
\begin{aligned}
&s = s^*/B_{avg}^*, \quad n = n^*/B^* \\
&D = D^*/D_u^*, \quad B = B^*/B_{avg}^* \\
&u = u^*/U_u^*, \quad v = v^*/U_u^* \\
&U = U^*/U_u^*, \quad V = V^*/U_u^* \\
&\xi = \frac{z-(F_u^2 h - D)}{D} \quad \nu = \frac{B_{avg}^*}{R_0^*} \\
&\mathcal{C}(s) = \frac{R_0^*}{R^*(s^*)}
\end{aligned}
\tag{5.2}
$$

Furthermore, the longitudinal metric coefficient of the co-ordinate system, $N = \frac{1}{h_s}$, and the differential operator $\mathcal{L}_b$ are arising as a consequence of width variation

defined as follows

$$N = \frac{1}{1 + \nu n B \mathcal{C}} \qquad \mathcal{L}_b = \frac{\partial}{\partial s} - \frac{n}{B} B_s \frac{\partial}{\partial n} \tag{5.3}$$

Indeed, since the transverse co-ordinate n is normalized with the half channel width that, the following derivation chain rule has

$$\frac{\partial}{\partial s} \rightarrow \frac{\partial}{\partial s} + n \frac{B, s}{B} \frac{\partial}{\partial n}, \frac{\partial}{\partial n} \rightarrow \frac{1}{B} \frac{\partial}{\partial n} \tag{5.4}$$

5.2.4   Dimensionless equations

The model is represented by the steady-Reynolds equations for longitudinal and transversal momentum, along with the continuity equations for the fluid and solid phases.The dimensionless form of these equations reads as follows:

$$Nu\mathcal{L}_b u + \mathcal{B}^{-1} v u_{,n} + w u_{,z} + N\nu\mathcal{C} uv = -N(\mathcal{L}_b h - \beta \mathcal{C}_{fu}(\nu_T u_{,z} z)) \tag{5.5}$$

$$Nu\mathcal{L}_b v + \mathcal{B}^{-1} v v_{,n} + w v_{,z} - N\nu\mathcal{C} u^2 = -B^{-1} h, n + \beta \mathcal{C}_{fu}(\nu_T v_{,z} z)) \tag{5.6}$$

$$N\mathcal{L}_b u + (\mathcal{B}^{-1} \frac{\partial}{\partial n} + N\nu\mathcal{C})v + w_{,z} = 0 \tag{5.7}$$

$$N\mathcal{L}_b q_s + (\mathcal{B}^{-1} \frac{\partial}{\partial n} + N\nu\mathcal{C})q_n = 0 \tag{5.8}$$

where a comma indicate the partial derivative. In these equations $\mathcal{C}$ is the dimensionless channel axis curvature and ν is the curvature ratio, such that,

$$\nu = \frac{B^*_{avg}}{R^*_0}, \qquad \mathcal{C}(s) = \frac{R^*_0}{R^*(s^*)}, \qquad \frac{\partial \theta_c}{\partial s} = -\nu\mathcal{C}(s) \tag{5.9}$$

with θ_c is the angle that the local tangent to the channel axis forms with the direction of an arbitrary selected cartesian axis of reference, x^* and R^*_0 of the channel axis (e.g., its minimum value in the meandering reach). The operator $\mathcal{L}_b$ arises as a

consequence of the stretching of the co-ordinate n normalized with the local width $B^*(s^*)$ such that it varies in the interval ± 1. The above equations are associated with following boundary and integral conditions;

$$u = v = w = 0 \, (z = z_0)$$

$$u_{,z} = v_{,z} = w - N\mathcal{L}_b(F_u^2 hu) - B^{-1}F_u^2 h_{,n} \, v = 0 \, (z = F_0^2 h)$$

$$\int_{z_0}^{F_0^2 h} \vec{u}.\vec{n}_b \, dz = \vec{q}.\vec{n}_b = 0 \, (n = \pm 1) \tag{5.10}$$

Where $\vec{n}_b$ is the unit vector locally normal to the banks. These conditions impose no-slip condition at the bed $z = z_0$, no stress at the free surface, the requirement that the latter must be a material surface and the requirement that the, channel walls are impermeable both to the flow and channel sediment flux.

To close the problem three integral conditione are required, ensuring that flow discharge, sediment supply and averaged reached slope are not affected by perturbations of either the flow field or the bed configuration. The following velocity structured is then assumed to account for curvature driven and topographic drivensecondary flow [Kalkwijk and De vriend, 1980: Smith and Mclean, 1984; Johanesson and Parker, 1989; Zolezzi and Seminara, 2001]

$$u = U(s,n)\mathcal{F}(\xi)$$
$$v = \nu \, \tilde{v}(s,n,\xi) + V(s,n)\mathcal{F}(\xi) \tag{5.11}$$

Here U and V denote the depth averaged values of u, v, $\tilde{v}$ denotes the local distributionof the transverse secondary flow and $\mathcal{F}$ is a dimensionless function describing the vertical structure of the uniform flow (Figure 5.6). Furthemore, ξ is a normalized vertical coordinate defined as follows:

$$\xi = \frac{z - (F_u^2 h - D)}{D} \tag{5.12}$$
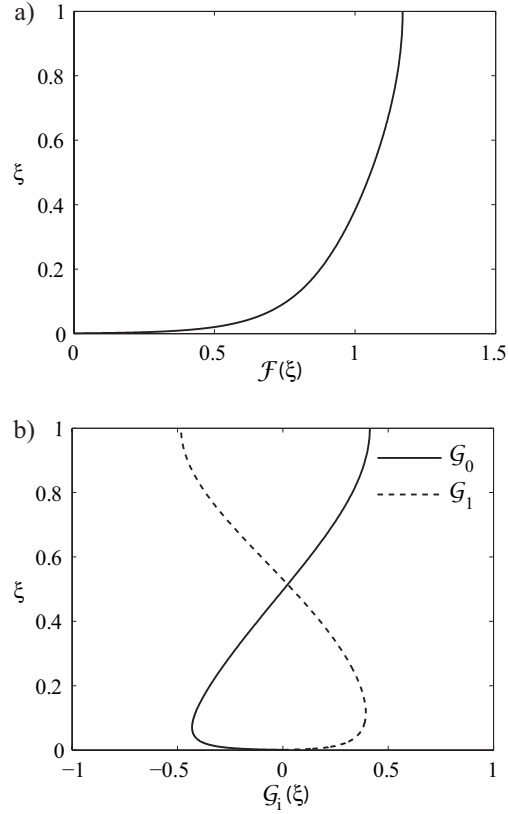
Figure 5.6: a) Vertical distribution of $\mathcal{F}$ and   b) Vertical distribution of $\mathcal{G}_0$ and $\mathcal{G}_1$

From equation (5.11) it follows that

$$\int_{\xi_0}^{1} \mathcal{F}(\xi)\ d\xi = 0$$

$$\int_{\xi_0}^{1} \tilde{v}(s,n,\xi)\ d\xi = 0 \tag{5.13}$$

If we assume that the curvature ratio is small, we can expand the solutionin terms of ν, at the leading order of approximation $\mathcal{O}(\nu)^0$, the function $\mathcal{F}(\xi)$ is found to follow the classical logarithmic distribution in a straight channel, corrected by the wake function. Moreover, from the first of the integral conditions (5.13) it results

that $\xi_0 = exp(-k/C_{fu} - 0.777)$. At the order of $\mathcal{O}(\nu)$ we obtain,

$$\tilde{v}(s, n, \xi) = \frac{DU\mathcal{C}}{\beta_u \sqrt{C_{fu}}} \mathcal{G}_0(\xi) + \frac{D^2(U\mathcal{C})_{,s}}{\beta_u^2 C_{fu}} \mathcal{G}_1(\xi) \qquad (5.14)$$

where the functions $\mathcal{G}_0(\xi)$, and $\mathcal{G}_1(\xi)$, obtained through the solutions of two second-order boundary value problems, describe the vertical structure of secondary flow (Figure 5.6). Substituting (5.11) and (5.14) into the governing equations (5.5)-(5.5), and neglecting the ν^2 terms yields the depth averaged shallow water equations. If as a first approximation, we neglect the effects width variations, we obtain

$$(UU_{,s} + VU_{,n}) + H_{,s} + \beta_u \frac{\tau_s}{D} = \nu f_{10} \qquad (5.15)$$

$$(UV_{,s} + VV_{,n}) + H_{,n} + \beta_u \frac{\tau_n}{D} = \nu g_{10} \qquad (5.16)$$

$$(DU)_{,s} + (DV)_{,n} = \nu m_{10} \qquad (5.17)$$

$$q_{s,s} + q_{n,n} = \nu n_{10} \qquad (5.18)$$

The quantities f_{10}, g_{10}, m_{10} and n_{10} which appear on the right hand side of equations (5.18) are the first order effects due to the presence of an arbitrary (although weak) curvature. The boundary conditions to be coupled with equations

$$V = 0, \quad -q_n = 0 \; (n = \pm 1) \qquad (5.19)$$

Moreover considering flow decomposition (5.11) and the solution for $\mathcal{G}_0(\xi)$ and $\mathcal{G}_1(\xi)$, we find

$$(\tau_s, \tau_n) = C_f \sqrt{(U^2 + V^2)}(U, \tilde{V}) \qquad (5.20)$$

where

$$\tilde{V} = V + v\left(\frac{DUC}{\beta_u\sqrt{(C_{fu})}}k_2 + \frac{D(DUC)_{,s}}{\beta_u^2 C_{fu}}k_3\right) \tag{5.21}$$

where the coefficients k_2 and k_3 read

$$k_2 = \left[\frac{\mathcal{G}_{l,\mathcal{F}}}{\mathcal{F}_{,\xi}}\right]_{\xi_0} \tag{5.22}$$

$$k_3 = \left[\frac{\mathcal{G}_{\infty,\mathcal{F}}}{\mathcal{F}_{,\xi}}\right]_{\xi_0} \tag{5.23}$$

Moreover, the longitudinal and transverse components of the sediment flux vector can be expressed as [Frascati and Lanzoni, 2013]

$$(q_s, q_n) = \Phi(\tau_*; D; R_p)\left(1, \frac{\tau_n}{\tau} - \frac{B^{-1}}{\beta_u}\frac{r}{\tau_*}\eta_{,n}\right) \tag{5.24}$$

Finally, the above formulated problemis is subject to the following integral constraints, namely,

$$\int_{-1}^{1} UDB\,dn = 2, \quad \int_{-1}^{1}\Phi B\,dn = 2\Phi_u \tag{5.25}$$

$$\int_{-1}^{1}\int_{-1}^{1}(F_u^2 H - D)B\,dn\,ds = const \tag{5.26}$$

5.2.5   Expansion

Taking advantage of the typically wide character of river bends, we expand the solution in powers of the small perameter ν

$$(U, V, D, H) = (1, 0, 1, H_0) + \nu(u_c, v_c, d_c, h_c) + \cdots \tag{5.27}$$

Similarly, the friction, the bed shear stress,the intensity of bedload can be written as

$$C_f = C_{fu} \left(1 + \nu \, C_{f1} \right)$$

$$\tau_* = \tau_{*u} \left(1 + \nu \, \tau_{*1} \right) \tag{5.28}$$

$$\Phi = \Phi_u \left(1 + \nu \, \Phi_1 \right)$$

5.3 Solution

The flow field induced by a spatially varying distribution of the channel curvature is described by $\mathcal{O}(\nu)$ non-homogeneous linear differential problem

$$\mathcal{L} \begin{pmatrix} u_c \\ v_c \\ d_c \\ h_c \end{pmatrix} = \begin{pmatrix} nb_1 \mathcal{C} \\ b_2 \mathcal{C} + b_3 \mathcal{C}' + b_4 \mathcal{C}'' \\ 0 \\ 0 \end{pmatrix} \tag{5.29}$$

Subjected to the non-homogeneous boundary conditions

$$v_c = 0, \quad \left(F_u^2 h_c - d_c \right)_{,n} = b_5 \mathcal{C} + b_6 \mathcal{C}' \quad (n = \pm 1) \tag{5.30}$$

with $\mathcal{C}'$ and $\mathcal{C}'$ the first and second derivatives of the curvature. The general solution for the flow field and depth obtained by solving above problem:

$$u_c = \sum_{j=1}^{4} c_{cmj} e^{\lambda_{cmj}} + A_{cm} \sum_{j=1}^{4} \left[g_{cj0} \int_0^s \mathcal{C}(\zeta) e^{\lambda_{cmj}(s-\zeta) \, d\zeta} + g_{cj0} \mathcal{C} \right] \tag{5.31}$$

$$d_c = \sum_{j=1}^{4} \delta_{mj} c_{cmj} e^{\lambda_{cmj}} + A_{cm} \sum_{j=1}^{4} \left[\delta_{mj} g_{cj0} \int_0^s \mathcal{C}(\zeta) e^{\lambda_{cmj}(s-\zeta) \, d\zeta} + \delta_{mj}^c g_{cj0} \mathcal{C} \right]$$

where $g_{cjk}(j = 1, \cdots, 4; k = 0, 1)$ are constant co-efficients depending on β_u, d_s, $\tau*_u, \lambda_{cmj}, (m = 1, \cdots, \infty)$, are characterstic exponent for the mth lateral fourier mode and c_{cmj} are integration constants to be specified on the basis of the boundary conditions at the channel ends. The curvature distribution function $\mathcal{C}(s)$ depends on the investigated meandering pattern formed by $\mathcal{C}(s)$, which can be determined by the analysis of satellite or aerial images of the river of interest. The two dimensional spatial distribution of the linearized flow field and depth of flow can be used to estimate the longitudinal dispersion coefficient, as well as the spatial distribution of the tracer concentration.

Chapter 6

Longitudinal Dispersion in Meandering Channels with Arbitrary Curvature

6.1 Available Data

Let us now move to examine the reliability of the theoretical framework developed so far by considering the dispersion data obtained from tracer tests carried out in meandering/ sinuous reaches of six natural streams, namely the Green-Duwamish River [Fischer, 1968a,b], the Missouri River [Yotsukura et al., 1970], the Powell River and the Copper Creek river [Godfrey and Frederick, 1970], the Lesser Slave River [Beltaos and Day, 1978], and the Miljacka River [Dobran, 1983]. Figure (6.1) shows the planform configurations of the investigated reaches, extracted from topographic maps, the location of the section in which the tracer has been injected and the extension of the equilibrium zone, where the theory can be applied. The geometrical and hydraulic parameters of each stream, averaged along the equilibrium reach,are reported in Table (6.1). Both the curvature ratio and the wavenumber, determined
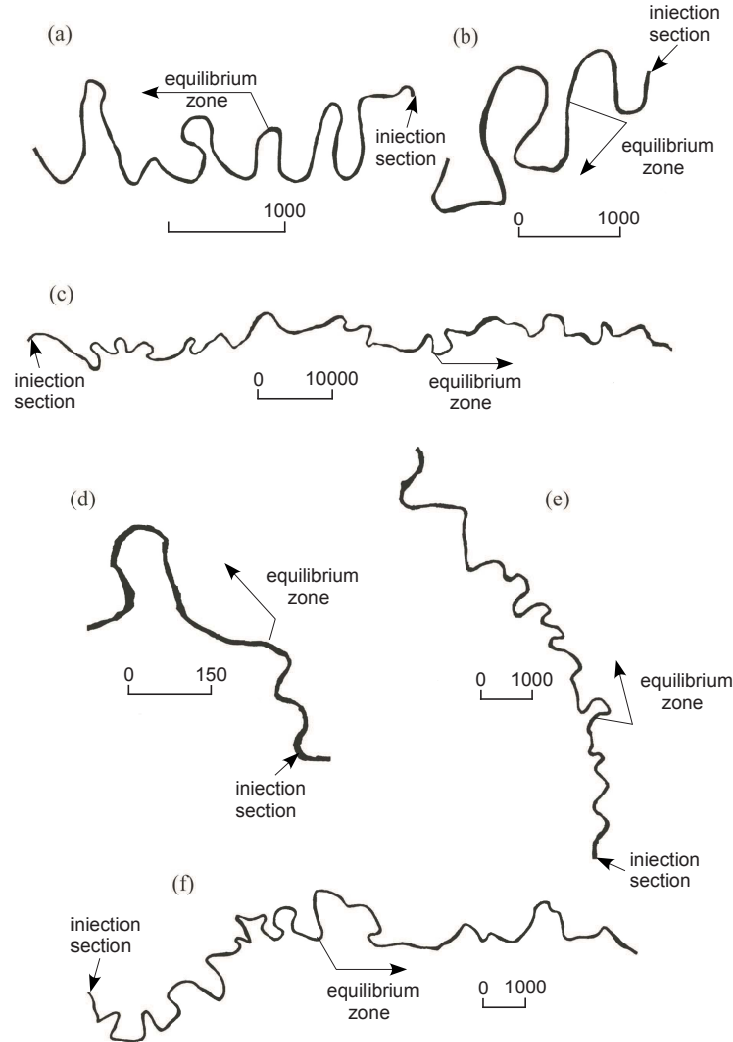
Figure 6.1: Planimetric patterns of some meandering rivers in which the longitudinal dispersion coeffcient has been determined experimentally through field tracer tests. a) Copper Creek (Virginia, USA); b) Powell River (Tennessee, USA); c) Missouri River, between Decatur (Iowa, USA) and Omaha (Nebraska, USA); d) Miljacka River (Sarajevo, Bosnia and Herzegovina); e) Green-Duwamish River, between Renton Junction and Foster Gould Course (Washington USA); f) Lesser Slave River (Alberta, Canada). Scales are expressed in meters.

through the automatic extraction procedure described by Marani et al. [2002], attain quite low values, thus ensuring the applicability of the theoretical analysis. The sinuosity s_r, defined as the ratio of intrinsic to cartesian meander length, indicates

that the Copper Creek, the Green-Duwamish (Figure 6.2), and the Powell River (Figure 6.3), having a sinuosity greater than 1.5, can be regarded as meandering, while the Lesser Slave River, the Missouri River (Figure 6.4) and the Miljacka River (Figure 6.5), exhibiting a sinuosity smaller than 1.5., can be ascribed to the category of sinuous streams [Leopold et al., 1995]. The mean grain size estimates reported in Table 6.1 have been determined on the basis of information available from literature [Beltaos and Day, 1978; Yotsukura et al., 1970; Shen et al., 1978], from the USGS National Water Information System [http://waterdata.usgs.gov/nwis] or from direct inspection (Dobran 2007, personal communication). The relevant
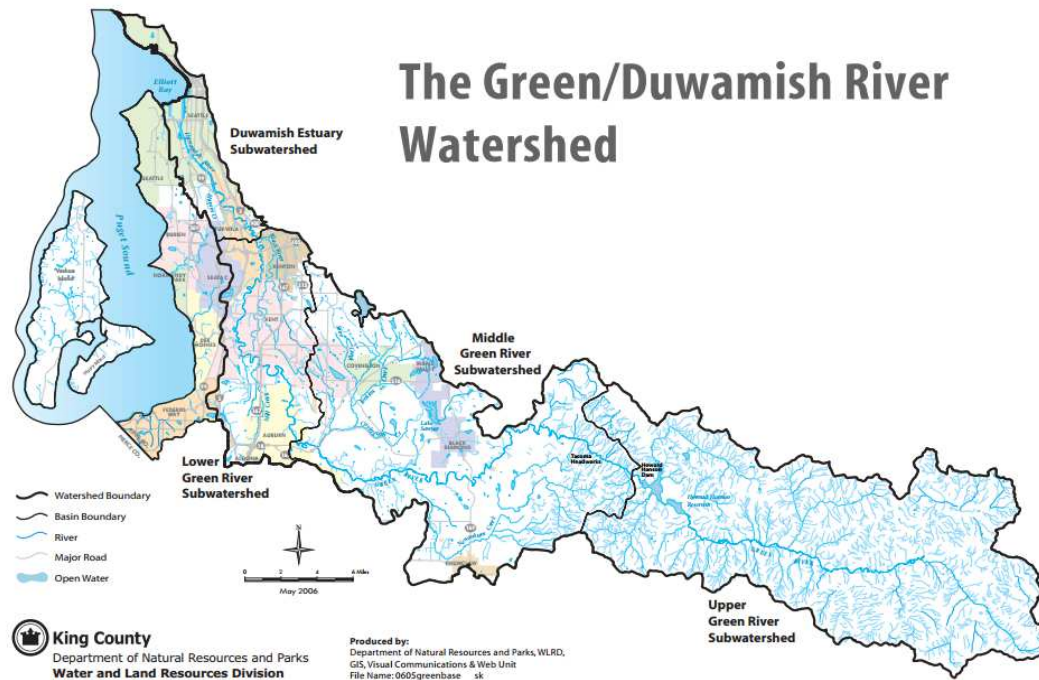
Figure 6.2: Green river (Source:http://your.kingcounty.gov/ dnrp/ library/ archive-documents/ wlr/ watersheds/ green/ pdf/ green- river- watershed- map.pdf).

dimensionless parameters β, d_s, τ_* and λ, transverse mixing coefficient k_{n1} also reported in Table 6.1, determine completely the characteristics of the linearized flow field. The transverse mixing coefficient are obtained from Deng [2002]. Here we only recall that the choice of bed configurations used in the computation of the
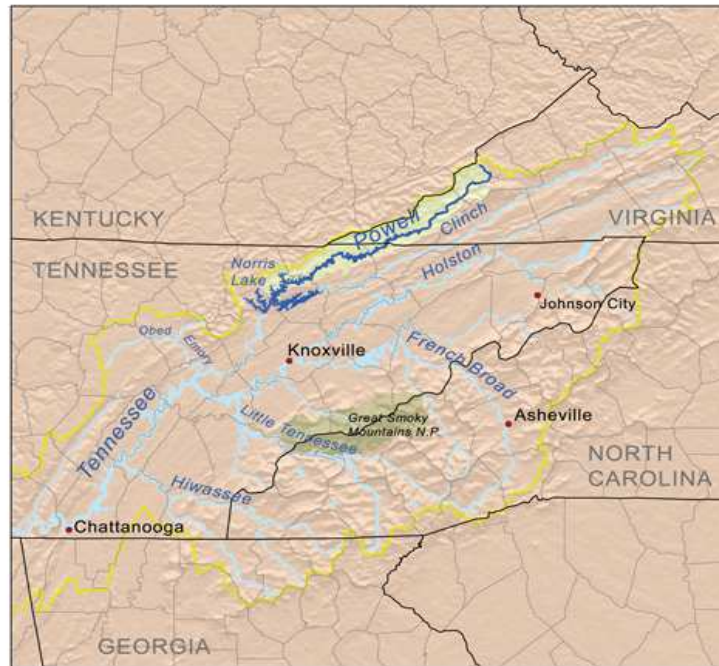
Figure 6.3: Powell river (Source: http: //en.wikipedia.org/ wiki/ File: Powelltnrivermap. png).

Figure 6.4: Missouri river (Source:Bhttp://earthobservatory. nasa. gov/ NaturalHazards/ view. php ?id= 51261).

Figure 6.5: Miljacka river (Source: http://bosepo. ba/ wp- content/ uploads/ 2012/ 11/ BOSNIA_PROJECT_2.pdf).

friction coefficient has been made according to the classification procedure proposed by van Rjin [1984]. In the particular case of the Miljacka River, a gravel bedded stream in which the tracer test was carried out for a flow discharge lower than that corresponding to incipient motion of sediment, the related bottom configuration was determined by assuming a value of the Shields stress slightly larger than its critical value (say $\tau_* = 0.1$). This assumption is in accordance with the observation that gravel bed rivers are shaped by a bankfull stress that is close to the critical value [Parker, 2004]. Copper creek and Powell rivers are gravel bedded rivers while Green-Duwamish [http://green.kingcounty.gov/ WLR/ Waterres/ StreamsData/ WaterShedInfo.aspx? Locator=0311] is a sand bed river. The Missouri river depending on the reach can have both a sand and a gravel bed river [http://www.epa.gov/ region07/ factsheets/ 2010/ lower/ missouri/ river/ sand/ gravel/ dredging.htm]. Similarly, The Lesser Slave river exhibits either sand or gravel bed river [http://www.10714.com/ pdf/ rgwa/ lesserslave.pdf].

Table 6.1: Reach averaged geometric and hydraulic parameters of the considered meandering streams. Sources of data are: 1. Fischer [1968a]; 2. Fischer [1968b]; 3. Yotsukura et al. [1970]; 4. Godfrey and Frederick [1970]; 5. Fukuoka and Sayre [1973]; 6. Dobran [1982]. Definitions are as follows: B_0^*, half channel width; D_0^*, cross sectionally averaged channel depth; U_0^* : cross sectionally averaged channel velocity; $u_* = \sqrt{gD_0^*S}$: cross sectionally averaged friction velocity; R_0^*: twice of average radius of curvature within the reach of interest; L^*, average intrinsic meander length; d_s^*, average grain size; β, aspect ratio; d_s, dimensionless grain size; θ, Shields parameter; ν, curvature ratio; λ, wavenumber; s_r, sinuosity.

Channel	source	B_0^* (m)	D_0^* (m)	U_0^* (m/s)	u_* (m/s)	R_0^* (m)	L^* (m)	d_s^* (mm)	β	d_s 10^{-3}	θ	ν 10^{-2}	λ	s_r	k_{n1}
Copper Creek	1,4,5	9.0	0.37	0.22	0.110	220	1460	7.00	24.3	1.89	1.07	4.1	0.04	2.53	0.237^a
Green-Duwamish	2,4,5	20.0	1.10	0.27	0.049	481	1170	0.20	18.2	0.18	0.74	4.2	0.11	1.59	0.424^a
Lesser Slave	3,5	25.4	3.10	0.50	0.055	590	1680	0.20	8.2	0.064	0.93	4.3	0.10	1.42	0.33^b
Missori	3,5	95.3	2.93	1.73	0.076	5180	12100	0.20	32.5	0.68	1.78	1.8	0.05	1.48	2.20^a
Poweell	2,4,5	18.5	0.88	0.16	0.052	600	2800	0.15	21.0	0.17	1.11	3.1	0.04	2.37	0.265^a
Miljacka	6	11.3	0.28	0.34	0.055	285	878	5.00	40.4	6.67	0.02	4.0	0.08	1.18	0.042^a

[a] Deng et al. [2002], [b] Engmann and Kellerhals [1974]

6.2   Transverse mixing coefficient

Longitudinal dispersion in meandering river is also influenced by the intensity of tranverse mixing coefficient. As mentioned previously (see section 4.2) it is assumed the transverse mixing coefficient is estimated through the relation [Deng et al., 2001]

$$k_{n0} = 0.145 + \frac{1}{3520} \left(\frac{U_0^*}{\sqrt{gD_0^*S}} \right) \left(\frac{2B^*}{D_0^*} \right)^{1.38} \tag{6.1}$$

We can then account for the effects of the local flow depth following the suggestion of Deng et al. [2002], defining the transverse mixing coefficient as

$$k_{n1} = k_{n0} d_0^{\frac{3}{2}} \tag{6.2}$$

where d_0 is local dimensionless flow depth.

6.3 Comparison with the theory
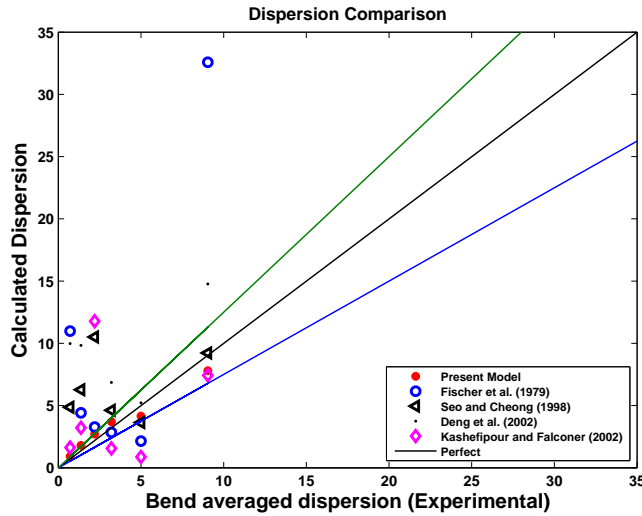
Figure 6.6: Bend averaged Longitudinal dispersion coefficient comparison with the experimental data in meander river.
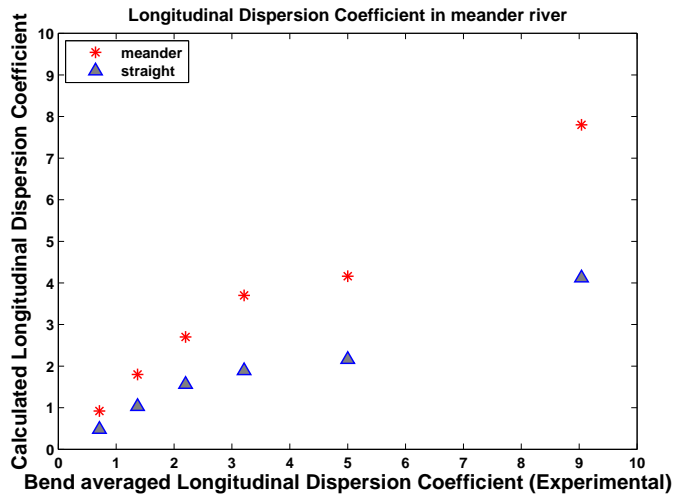
Figure 6.7: Longitudinal dispersion coefficient of both bend averaged and straight alluvial channel, comparison with the experimental data (the star symbols are for bend averaged and triangle symbols are for straight river longitudinsal dispersion coefficient).

Table 6.2: Comparison between observed ($\mathcal{K}_{exp}$) and predicted $\mathcal{K}$ (equation 2.36) longitudinal dispersion coefficients. The values attained by the discrepancy ratio d_r are also reported.

River	$\mathcal{K}_{exp}^*(m^2/s)$	$\mathcal{K}_{exp}^*$	$\mathcal{K}$	d_r
Copper Creek	9.9	5.00	4.16	-0.1839
Green-Duwamish	7.4	1.37	1.8	0.2730
Lesser Slave	27.9	2.20	2.7	0.2048
Missouri	1490	9.04	7.8	-0.1475
Powell	9.5	3.21	3.7	0.1421
Miljacka	2.7	0.71	0.92	-0.2591

Table 6.3: Comparison between observed ($\mathcal{K}_{exp}$) and predicted $\mathcal{K}$ (equation 2.36) longitudinal dispersion coefficients with present model and other model available in literature. [1] Present model; [2] Fischer et al.[1979]; [3] Seo and Cheong [1998]; [4] Deng et al. [2001]; [5] Kashefipour; and Falconer [2002].

River	$\mathcal{K}_{exp}$	[1]	[2]	[3]	[4]	[5]
Copper Creek	5.00	4.16	2.14	3.63	5.21	0.87
Green-Duwamish	1.37	1.8	4.40	6.26	9.83	3.21
Lesser Slave	2.20	2.7	3.27	10.51	11.45	11.77
Missouri	9.04	7.8	32.57	9.22	14.76	7.42
Powell	3.21	3.7	2.84	4.62	6.85	1.55
Miljacka	0.71	0.92	10.97	4.86	9.97	1.62

The comparison between the longitudinal dispersion coefficients observed experimentally and those predicted by the relationship (2.55), is pursued in Table (6.3) and in Figure (6.6). The latter also reports the longitudinal dispersion coeffficients estimated through the semi-empirical and empirical relationships of Table (6.1). To evaluate the difference between measured and predicted dispersion coefficients more quantitatively, the discrepancy ratio d_r ($= log(\mathcal{K}_{calc}/\mathcal{K}_{exp})$) is introduced as measure of the error. This ratio vanishes if predicted and measured values coincide while

positive (negative) values of d_r indicate that the predicted longitudinal dispersion coeffcient is overestimated (underestimated) [White et al., 1973], shown in Table 6.2. The lines beside perfect agreement line reported in figure (6.6) identify the range corresponding to a $\pm 25\%$ error usually adopted [Seo and Cheong, 1998; Kashefipour and Falconer, 2002; Deng et al., 2002] to quantify the maximum acceptable error. Present model shows a better agreement then any of the either models so far presented in literature (see also table 6.3). On the other hand Figure (6.7) shows that accounting for the effects of river meandering on the flow field leads to a general improvement of the estimate provided by the relation developed for a straight river.

Bibliography

[1] Allen, J.R.L. (1970), *Physical processes of sedimentation: an introduction.* Allen & Unwin.

[2] Ames, H., and Contributor eHow, *Factors Affecting a River's Velocity.* http://www.ehow.com/ info_ 8223150 _ factors- affecting- rivers- velocity.html

[3] Bansal, M.K. (1971), Dispersion in Natural Streams. *Journal of the Hydraulics Division,* 97, 1867−1886.

[4] De Barros, F.P.J., Mills, W.B., and Cotta, R.M. (2006), Integral transform solution of a two-dimensional model for contaminant dispersion in rivers and channels with spatially variable coefficients. *Environmental Modelling & Software,* 21, 699−709.

[5] Batchelor, G.K. (1999), *An introduction to fluid dynamics.* Cambridge University Press.

[6] Bartlett, R.A. (1995). *Troubled waters: Champion International and the Pigeon River Controversy.* Knoxville: University of Tennessee Press.

[7] Beltaos, S., and Day, T.J. (1978), A field study of longitudinal dispersion. *Can. J. Civ. Eng.,* 5, 572−585.

[8] Bencala, K.E. (1983), Simulation of solute transport in a mountain pool-and-riffle stream with a kinetic mass transfer model for sorption. *Water Resources Research*, 19, 732−738.

[9] Blanckaert, K., and de Vriend, H.J. (2003), Nonlinear modeling of mean flow redistribution in curved open channels. *Water Resources Research*, 39, 1375.

[10] Blondeaux, P., and Seminara, G. (1985), A unified bar−bend theory of river meanders. *Journal of Fluid Mechanics*, 157, 449−470.

[11] Bogle, G. (1997), Stream velocity profiles and longitudinal dispersion. *Journal of Hydraulic Engineering* 123, 816−820.

[12] Boxall, J.B., and Guymer, I. (2003), Analysis and prediction of transverse mixing coefficients in natural channels. *Journal of Hydraulic Engineering*, 129, 129−139.

[13] Boxall, J.B., and Guymer, I. (2007), Longitudinal mixing in meandering channels: new experimental data set and verification of a predictive technique. *Water Res*, 41, 341−354.

[14] Boxall, J.B., Guymer, I., and Marion, A. (2003), Transverse mixing in sinuous natural open channel flows. *Journal of Hydraulic Research*, 41, 153−165.

[15] Bridge, J.S. (2009), *Rivers and Floodplains: Forms, Processes, and Sedimentary Record*, John Wiley & Sons.

[16] Chang, Y.C. (1971), *Lateral mixing in meandering channels*. University of Iowa.

[17] Chitale, S., Mosselman, E., and Laursen, E. (2000), River width adjustment. I: Processes and Mechanisms. *Journal of Hydraulic Engineering*, 126, 159−162.

[18] Colby, B.R.D. (1961), *Effect of depth of flow on discharge of bed materials*. U.S. Department of the Interior.

[19] Davies, R.J. (2007), *Seismic Geomorphology: Applications to Hydrocarbon Exploration and Production.* Geological Society of London.

[20] Day, T.J. (1977), Longitudinal dispersion of fluid particles in mountain stream's: theory and field evidence. *Journal of Hydrology (N.Z)*, 16, 7−25.

[21] Dean, R.B. (1974), *Reynolds Number Dependence of Skin Friction in Two-dimensional Rectangular Duct Flow and a Discussion of the law of the Wake.* National Aeronautics and Space Administration.

[22] Deng, Z., Singh, V., and Bengtsson, L. (2001), Longitudinal Dispersion Coefficient in Straight Rivers. *Journal of Hydraulic Engineering*, 127, 919−927.

[23] Deng, Z., Bengtsson, L., Singh, V., and Adrian, D. (2002), Longitudinal Dispersion Coefficient in Single-Channel Streams. *Journal of Hydraulic Engineering* 128, 901−916.

[24] Dobran, B.H. (1983), Dispersion in Mountainous Natural Streams. *Journal of Environmental Engineering* , 109, 970−973.

[25] Elder, J.W. (1959), The dispersion of marked fluid in turbulent shear flow. *Journal of Fluid Mechanics*, 5, 544−560.

[26] Engelund, F. (1964), *A Practical Approach to Self-preserving Turbulent Flows.* Danish Acad. of Technical Sciences.

[27] Falcon, M.A. (1979), *Analysis of flow in alluvial channel bends.* University of Iowa.

[28] Ferguson, R.I. (1977), Meander sinuosity and direction variance. *Geological Society of America Bulletin*, 88, 212.

[29] Finnegan, N.J., Roe, G., Montgomery, D.R., and Hallet, B. (2005), Controls on the channel width of rivers: Implications for modeling fluvial incision of bedrock. *Geology*, 33, 229−232.

[30] Fischer, H.B. (1968), *Methods for predicting dispersion coefficient in natural streams, with application to lower reaches of the Green and Duwamish Rivers.* U.S. Geological Survey Professional Paper, 582−A, 27 pp.

[31] Fischer, H. (1975), Discussion on simple method for predicting dispersion in streams by R.S. Mc Quiveyand T.N Keefer. *J Environ Eng Div ASCE*, 101, 453−455.

[32] Fischer, H.B. (1967), The Mechanics of Dispersion in Natural Streams. American Society of Civil Engineers.

[33] Fischer, H.B. (1968), Dispersion Predictions in Natural Streams. *Journal of the Sanitary Engineering Division*, 94, 927−944.

[34] Fischer, H.B. (1969), The effect of bends on dispersion in streams. *Water Resources Research*, 5.

[35] Fischer, H.B. (1973), Longitudinal Dispersion and Turbulent Mixing in Open-Channel Flow. *Annual Review of Fluid Mechanics*, 5, 59−78.

[36] Fischer, H.B., E, J.L., Robert, Y.C.K., and Imberger, J. (1979), *Mixing in inland and coastal waters.* New York: Academic Press.

[37] Forsman, K.J. (2001), *Contaminant transport in non-uniform streams and streambeds.* Uppsala University.

[38] Frascati, A., and Lanzoni, S. (2009), Morphodynamic regime and long-term evolution of meandering rivers. *Journal of Geophysical Research: Earth Surface*, 114, F02002.

[39] Frascati, A., and Lanzoni, S. (2013), A mathematical model for meandering rivers with varying width. *Journal of Geophysical Research: Earth Surface*, 118, 1641−1657.

[40] Godfrey, R.G., and Frederick, B.J. (1970), *Stream dispersion at selected sites.* United States Geological Survey.

[41] Gore, J.A. (1985), *Restoration of rivers and streams.* U.S Department of Energy.

[42] Gupta, A. (2011), *Tropical Geomorphology.* Cambridge University Press.

[43] Hart, J., Guymer, I., Jones, A., and Stovin, V. (2013), Longitudinal Dispersion Coefficients Within Turbulent and Transitional Pipe Flow. *In Experimental and Computational Solutions of Hydraulic Problems, Springer Berlin Heidelberg*, 133−145.

[44] Ho, D.T., Schlosser, P., and Caplow, T. (2002), Determination of longitudinal dispersion coefficient and net advection in the tidal hudson river with a large-scale, high resolution SF6 tracer release experiment. *Environ. Sci. Technol*, 36, 3234−3241.

[45] Howard, A.D. (1980), Threshold in river regims. *In Threshold in Geomorphology, Allen & Unwin, Concord, Mass.*, 227−258.

[46] Howard, A.D. (1987). Modeling fluvial systems: Rock, gravel and sand bed channel. *In River Channels, Blcakwell, Malden, Mass.*

[47] Howard, A.D. (2013). Long Profile Development of Bedrock Channels: Inter-action of Weathering, Mass Wasting, Bed Erosion, and Sediment Transport. *In Rivers Over Rock: Fluvial Processes in Bedrock Channels, American Geophysical Union.* 297−319.

[48] Howard, A.D., Dietrich, W.E., and Seidl, M.A. (1994), Modeling fluvial erosion on regional to continental scales. *Journal of Geophysical Research: Solid Earth*, 99, 13971−13986.

[49] Howard, A. (1992), Modelling channel migration and floodplain development in meandering streams. In *Lowland Floodplain Rivers: Geomorphological Perspectives*. John Wiley & Sons.

[50] Ikeda, S., Parker, G., and Sawai, K. (1981), Bend theory of river meanders. Part 1. Linear development. *Journal of Fluid Mechanics*, 112, 363−377.

[51] Iwasa, Y., and Aya, S. (1991), Predicting Longitudinal Dispersion Coefficient in Open-Channel Flows. *In Proceedings of the International Symposium on Environ. Hydr., Hong Kong*, 505−510.

[52] Jamali, M., Lawrence, G., and Maloney, K. (2005), Dispersion in Varying-Geometry Rivers with Application to Methanol Releases. *Journal of Hydraulic Engineering*, 131, 390−396.

[53] Johannesson, H., and Parker, G. (1989a), Secondary Flow in Mildly Sinuous Channel. *Journal of Hydraulic Engineering*, 115, 289−308.

[54] Johannesson, H., and Parker, G. (1989b), Linear theory of river meanders. *Water Resources Monograph*, American Geophysical Union, 181−213.

[55] Kalkwijk, J.P.T., and De Vriend, H.J. (1980a), Computation of the Flow in Shallow River Bends. *Journal of Hydraulic Research*, 18, 327−342.

[56] Kashefipour, S.M., and Falconer, R.A. (2002), Longitudinal dispersion coefficients in natural channels. *Water Research*, 36, 1596−1608.

[57] Langbain, W.B., and Iseri, K.T. (1995), Manual of Hydrology: Part 1. General Surface-Water Techniques. *Geological Survey Water Supply Paper 1541-A Methods and practices of the Geological Survey.*

[58] Lee, H.J., and DeLisa, J.A. (2007), *Manual of nerve conduction study and surface anatomy for needle electomyography.* Fourth ed. Lippincott Williams and Wilkins.

[59] Leopold, L.B., Wolman, M.G., and Miller, John P (1995), *Fluvial processes in geomorphology.* New York: Dover Publications.

[60] Liu, H. (1977), Predicting Dispersion Coefficient of Streams. *Journal of the Environmental Engineering Division*, 103, 59−69.

[61] Marani, M., Lanzoni, S., Zandolin, D., Seminara, G., and Rinaldo, A. (2002), Tidal meanders. *Water Resources Research*, 38(11), 1225.

[62] Marion, A., and Zaramella, M. (2006), Effects of Velocity Gradients and Secondary Flow on the Dispersion of Solutes in a Meandering Channel. *Journal of Hydraulic Engineering*, 132, 1295−1302.

[63] Marivoet, J.L., and Van Craenenbroeck, W. (1986), Longitudinal dispersion in ship-canals. *Journal of Hydraulic Research*, 24, 123−132.

[64] McQuivey, R.S., and Keefer, T.N. (1976), Convective Model of Longitudinal Dispersion. *Journal of the Hydraulics Division*, 102, 1409−1424.

[65] Morse, P.M., and Feshbach, H. (1953), *Methods of Theoretical Physics, Part I.* McGraw-Hill: New York.

[66] Mueller, J.E. (1968), An Introduction to the Hydraulic and Topographic Sinuosity Indexes. *Annals of the Association of American Geographers*, 58, 371−385.

[67] Nayfeh, A.H. (2007), *Perturbation methods*. Weinheim: Wiley.

[68] NC Division of Water Quality (2010), *Methodology for Identification of Intermittent and Perennial Streams and their Origins*.

[69] Odgaard, A.J. (1981), Transverse Bed Slope in Alluvial Channel Bends. *Journal of the Hydraulics Division*, 107, 1677−1694.

[70] Odgaard, A.J., and Bergs, M.A. (1988), Flow processes in a curved alluvial channel. *Water Resources Research*, 24, 45−56.

[71] Perez, J., Halterman, D., Hodory, L., and White, D. (1997), *A Guide to Developing Local Watershed Action Plans in Ohio*.

[72] Piasecki, M., and Katopodes, N. (1999), Identification of Stream Dispersion Coefficients by Adjoint Sensitivity Method. *Journal of Hydraulic Engineering*, 125, 714−724.

[73] Putnam, W.C., Birkeland, P.W., and Larson, E.E. (1989), *Putnam's geology*. New York: Oxford University Press.

[74] Repetto, M.T. (2002), Planimetric instability of channels with variable width. *Journal of Fluid Mechanics*, 457, 79−109.

[75] Van Rijn, L. (1984), Sediment Transport, Part III: Bed forms and Alluvial Roughness. *Journal of Hydraulic Engineering*, 110, 1733−1754.

[76] Rozovski, I.L. (1957), *Flow of water in bends of open channels*, Academy of Sciences of the Ukrainian SSR.

[77] Rutherford, J.C. (1994), *River mixing*. New York: Wiley.

[78] Seminara, G. (2006), Meanders. *Journal of Fluid Mechanics*, 554, 271−297.

[79] Seminara, G., and Tubino, M. (1992), Weakly nonlinear theory of regular meanders. *Journal of Fluid Mechanics*, 244, 257−288.

[80] Seo, I., and Baek, K. (2004), Estimation of the Longitudinal Dispersion Coefficient Using the Velocity Profile in Natural Streams. *Journal of Hydraulic Engineering*, 130, 227−236.

[81] Seo, I., and Cheong, T. (1998), Predicting Longitudinal Dispersion Coefficient in Natural Streams. *Journal of Hydraulic Engineering*, 124, 25−32.

[82] Shelby, B. (1990), *Resource Values and Instream Flow Recommendations: Gulkana National Wild River, Alaska*. U.S. Department of the Interior, Bureau of Land Management.

[83] Shen, H.W., Harrison, A.S., and Mellema, W.J. (1978), Temperature and Missouri River Stages near Omaha. *Journal of the Hydraulics Division* 104, 1−20.

[84] Da Silva, A.M.F., and Ebrahimi, M. (2013), Bank erosion and planimetric evolution of alluvial meandering streams. *River Basin Management VII*, 277−288.

[85] Smith, R. (1983), Longitudinal dispersion coefficients for varying channels. *Journal of Fluid Mechanics*, 130, 299−314.

[86] Smith, J.D., and Mclean, S.R. (1984), A Model for Flow in Meandering Streams. *Water Resources Research*, 20, 1301−1315.

[87] Sooky, A.A. (1969), Longitudinal dispersion in open channels. *J. Hydraul. Div., Am. Soc. Civ. Eng.*, 95, 1327−1346.

[88] Sun, T., Meakin, P., Jssang, T., and Schwarz, K. (1996), A Simulation Model for Meandering Rivers. *Water Resources Research*, 32, 2937−2954.

[89] Taylor, G. (1954), The Dispersion of Matter in Turbulent Flow through a Pipe. *Proc. R. Soc. Lond. A* ,223, 446−468.

[90] Tennekes, H., and Lumley, J.L. (1972), *A First Course in Turbulence*. MIT Press.

[91] Tubino, M., and Colombini, M. (1992), Correnti uniformi a superficie libera e sezione lentamente variabile. *In XXIII Convegno Di Idraulica E Costruzioni Idrauliche, Florence.*

[92] Vigilar Jr., G.G., and Diplas, P. (1997), Stable Channels with Mobile Bed: Formulation and Numerical Solution. *Journal of Hydraulic Engineering*, 123, 189−199.

[93] Wallis, S.G., and Manson, J.R. (2004), Methods for predicting dispersion coefficients in rivers. *Proceedings of the ICE - Water Management*, 157, 131−141.

[94] Wei, Z. (2011), *Longitudinal Solution Transport in Open -Channel Flow*. Temple University.

[95] Whipple, K.X. (2002), Implication of sediment-flux-dependent river incision models for landscape evolution. *Journal of Geophysical Research*, 107, EGT−3.

[96] Yotsukura, N. et al G. (1970), *Measurement of mixing characteristics of the Missouri river between Siouxcity Iowa and Plattsmouth Nebraska*. U.S. Government Printing Office.

[97] Zhang, W. (2011). *Longitudinal solute transport in open channel flow*. Temple University.

[98] Zolezzi, G., and Seminara, G. (2001), Downstream and upstream influence in river meandering. Part 1. General theory and application to overdeepening. *Journal of Fluid Mechanics*, 438, 183−211.

List of Figures

List of Tables